The Samphire Project: A distal IOCG and evidence for Mesoarchean crust in the Gawler Craton

Thesis submitted in accordance with the requirements of the University of Adelaide for an Honours Degree in Geology

Samuel David Goldsmith

November 2014

THE UNIVERSITY of ADELAIDE

THE SAMPHIRE PROJECT: A DISTAL IOCG AND EVIDENCE FOR MESOARCHEAN CRUST IN THE GAWLER CRATON

THE SAMPHIRE PROJECT: A DISTAL IOCG

ABSTRACT

The Samphire project on the north eastern Eyre Peninsula contains proven uranium resources. These are in paleochannel-like deposits hosted within saprolite that has a granite origin. This granite forms the bedrock of the area and is of a batholith scale termed the Samphire batholith. Alteration takes the form of hematite, quartz and fluorite, forming vein assemblages that display cross cutting relationships. Characterization of this alteration by scanning electron microscope and geochemical analysis suggests this alteration strongly resembles iron oxide-copper-gold alteration that is seen through out the Gawler Craton. U-Pb dating of zircon, thorite and hematite is used to provide reconnaissance geochronology for age of the host granite and also stages of alteration. The summation of results from these techniques, creates a genetic model with the suggestion of the origin of the uranium in the overlying cover from the bedrock granite.

SAMPHIRE, GAWLER CRATON, BEDROCK, MESOARCHEAN, IOCG, U-PB GEOCHRONOLOGY

TABLE OF CONTENTS

LIST OF FIGURES

LIST OF TABLES

INTRODUCTION

The Gawler Craton contains a significant record of Archean to Proterozoic crustal evolution and tectonic processes. Continued study of the region, particularly with respect to geochronology, contributes to an understanding of Precambrian tectonic cycles and how these relate to regional metallogeny. U-Pb dating of zircon or monazite is a well-established method for obtaining ages of crystallization of igneous rocks but does not, necessarily provide accurate ages for associated mineralization. Recent work by Ciobanu *et al.* (2013) has used the trace amount of uranium in the common Fe-oxide hematite to establish a new geochronometer for dating iron-oxide copper-gold (IOCG) style mineralization. This study showed geologically reasonable ages of ~1590 Ma for the super-giant (>9000 Mt) Olympic Dam deposit, the archetypal IOCG deposit for the Gawler Craton, demonstrating the potential for application to analogous Fe-oxide-bearing mineralization elsewhere. Geochemical analysis of hematite and fluorite trace elements showed an enrichment in rare earth elements (REE), Y and High Field Strength Elements (HFSE) that is a recognised trend of IOCG type alteration and deposits within the Gawler Craton (Oreskes & Einaudi 1992; Agangi *et al.* 2010; Kontonikas-Charos *et al.* 2014).

Mineral exploration across the Gawler Craton is hindered by the thickness of the overlying cover sequence (Skirrow *et al.* 2002; Drummond *et al.* 2006; Direen & Lyons 2007). The lack of bedrock outcrop hampers geological mapping and has meant that the tectonic evolution of the region is less well understood than in other better exposed parts of the world. The recent expansion of mineral exploration in South Australia and particularly, the diamond drilling of prospects in parts of the Craton in which negligible data was previously available, has however, provided valuable windows to the bedrock geology. Such is the case of Samphire, a uranium project on the eastern Eyre Peninsula largely concentrated in the cover sequence but likely rooted in the underlying granite bedrock.

This paper provides a description of the granite bedrock at Samphire (Figure 1a, b), and of associated alteration and crosscutting fluorite veins that carry modest amounts of sulphides, Fe-oxides and REE-bearing minerals. The hypothesis offered is that this 'bedrock mineralization' represents a distal IOCG-type mineralization related to the ~ 1590 Ma event. This hypothesis was put forward based on the visual similarity of the host granite to Hiltaba Suite granites elsewhere in the region, observed alteration, mineralogy and the apparent enrichment in U, Th, REE, Y, and various granitophile elements (Sn+W+Mo). The mineralogical-petrographic work is complemented by trace element analysis and reconnaissance geochronology to test this hypothesis, and thus contribute to a genetic model for the Samphire mineralization as well as a better understanding of regional geology.

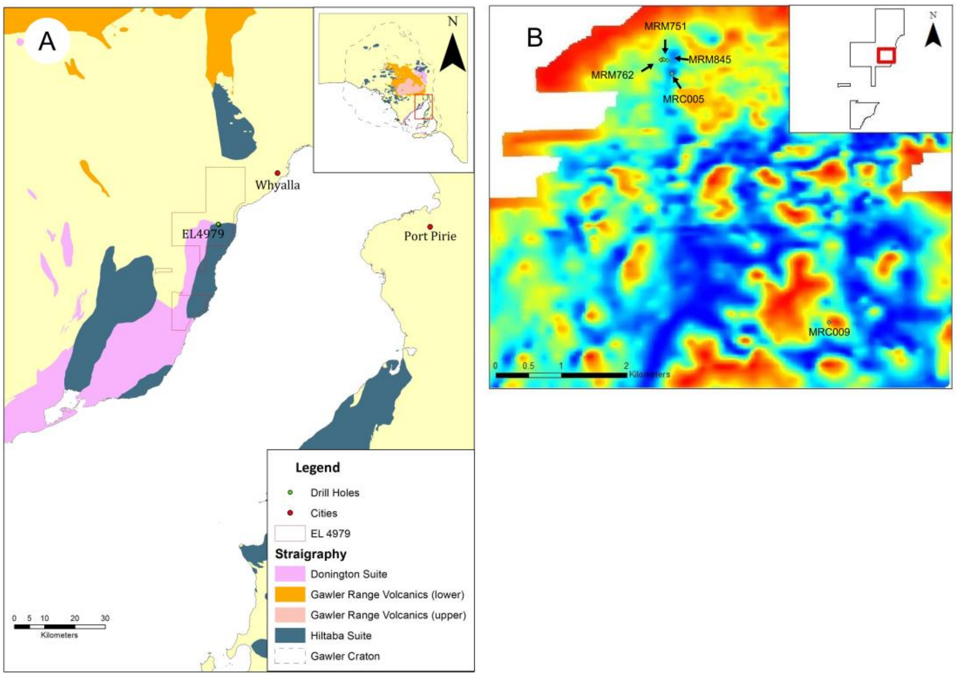

Figure 1 a) Location map of EL4979 within South Australia and relavant lithologies. Inset map provides extent of crystalline basement of the Gawler Craton. b) Bouguer anomaly removed gravity map of prospect area with drillhole locations. Data compiled in ESRI's ARCgis using data sets from SARIG with drillhole location and gravity map provided by Uranium SA.

GEOLOGICAL BACKGROUND

GEOLOGICAL SETTING

The Gawler Craton, South Australia (Figure 1a), is dominated by two phases of tectonic activity – Late Archean and late Paleoproterozoic-early Mesoproterozoic (Hand *et al.* 2007; Betts *et al.* 1998). The stratigraphy and tectonic evolution of the Gawler Craton are covered in depth by Daly *et al.* (1998) and Hand *et al*. (2007) and are only briefly summarised here. It is widely acknowledged that the Gawler Craton consists of an Archean nucleus with a Paleoproterozoic arcuate belt wrapped around (Daly *et al.* 1998; Betts *et al.* 2002), however Fraser *et al*. (2010) suggest extending the timeline of the Gawler Craton back ~500 million years into the Mesoarchean. Fraser *et al*. (2010) dated the Cooyerdoo granite at ~3150 Ma suggesting that parts of the Gawler Craton contain a Mesoarchean basement (see also McAveney 2012). Gneisses of the Late Archean

Sleaford and Mulgathing Complexes display granulite facies metamorphism in many areas that has been attributed to the ~2500-2400 Sleaford Orogeny (Betts *et al.* 2002; Swain *et al.* 2005). The Proterozoic period is split by Hand *et al*. (2007) by the 1730-1690 Ma Kimban orogeny, before which sedimentation was the primary rock-forming process, and after which the main rock forming process was magmatism. Time before the Kimban Orogen was dominated by rift-basin formations and includes deposition of the ~1780 Ma Hutchison group (Parker & Lemon 1982; Szpunar *et al.* 2011). The formation of the arc-related St Peters Suite between 1620 Ma and 1615 Ma, places the Gawler Craton in close proximity to an active plate margin (Hand *et al.* 2007; Swain *et al.* 2008).

The Gawler Range Volcanics (GRV) cover an area greater than 25 000 km^2 with a preserved thickness of 1.5 km (Hand *et al.* 2007; Agangi *et al.* 2012) and outcrop as rhyolites, dacites, andesites, rhyodacites and minor basalts. These GRV are divided into a small- to moderate-volume lower, and a highly-voluminous upper sequence interpreted to represent a siliceous felsic large igneous province (SLIP; Allen *et al*. 2008). The GRV-Hiltaba event is a product of a major tectonic-tectonothermal metallogenic event that also led to widespread greenschist to upper amphibolite facies metamorphism in some parts of the craton (Hand *et al.* 2007). The Hiltaba Suite granites locally intrude the GRV, and occur as oxidized, silicic I- and A- type, metaluminous granitoids of plutonic extent (Ferris *et al.* 2002; Hayward & Skirrow 2010). These Hiltaba Suite granitoids are strongly enriched in uranium, fluorine and other HFSE (Hayward & Skirrow 2010). In the eastern Gawler Craton, Hiltaba Suite plutons are more oxidized and evolved with average εNd_{1595} of -5.9 indicating a greater crustal contribution compared to those of the central and western Gawler Craton (Hand *et al.* 2007; Hayward & Skirrow 2010). Emplacement of Hiltaba Suite granites occurred over a period of approximately 25 million years and is interpreted to have formed via extensive fractionation and crustal contamination of mantle-derived mafic magmas, mixed with silicic crustal melts (Hayward & Skirrow 2010).

Multiple geodynamic models have been proposed for the Late Paleoproterzoic and Mesoproterozoic evolution of the Gawler Craton in an attempt to account for the vast magmatism of the 1595-1575 Ma Gawler Range Volcanics-Hiltaba event. These include anorogenic or intracontinental rift setting, plume-modified back-arc, foreland basin and lithospheric delamination (Giles 1988; Wade *et al.* 2006; Hand *et al.* 2007). This wide spread event coincides with a shift towards a continental interior regime (Hand *et al.* 2007).

IOCG MINERALIZATION WITHIN THE GALWER CRATON

The IOCG deposit clan form a continuum in which the largest examples occur in Early- to Mid-proterozoic regions in intraplate environments (Hitzman *et al.* 1992; Williams *et al.* 2005). IOCG mineralization is, however, not restricted to just these regions (e.g. Corriveau 2007; Groves *et al*. 2010) and can be found in Archean, Mesozoic or Cenozoic terranes (Barton 2014). Mineralisation of this style is defined based upon geochemical features, without a specific tectonic setting, geologic environment or source of ore-forming fluids and metals (Williams *et al.* 2005).

The intrusive Hiltaba Suite and GRV package displays a strong spatial and temporal association with IOCG mineralisation within the Gawler Craton (Williams *et al.* 2005). A domain extending over 700 km on the eastern margin of the Gawler Craton show in Figure 1a, is recognised as the Olympic Cu-Au Province which contains the majority of IOCG deposits and prospects discovered within the Gawler Craton to date (Ferris *et al.*

2002; Skirrow *et al.* 2002; Hayward & Skirrow 2010). The deposits of IOCG-style mineralisation within this province include Olympic Dam, Prominent Hill, Carrapateena, Hillside (Pine Point), Punt Hill and Cairn Hill (Belperio *et al.* 2007; Conor *et al.* 2010; Ismail *et al.* 2014). These deposits display a variety of mineralization and alteration styles consistent with formation at different crustal depths, in different local geological settings, and with different proportions of lithological and structural control. Given the thickness of the overlying cover, recent studies (e.g Ismail *et al*. 2014; Kontonikas-Charos *et al*. 2014; Nikolakopoulos *et al.* in press) have investigated the potential of using trace element concentrations of REE and Y in a range of different minerals as a vectoring tool towards prospective mineralisation in an attempt to overcome this.

THE SAMPHIRE PROJECT

The Samphire Project (Figure 1a) is on the north-eastern Eyre Peninsula, approximately 20 km southwest of Whyalla. The project is wholly owned by Uranium SA Limited and contains two proven sediment (paleochannel)-hosted uranium deposits, Blackbush and Plumbush. The deposits contain a total estimated inferred resource of 86.3 million tonnes of mineralisation (Uranium SA 2014). This uranium mineralization is hosted in sediments of Eocene age, referred to as the Kanaka Beds (Hou *et al.* 2012). The Samphire granite was intersected below the uranium mineralization by diamond drillholes aimed at delineating the extent of uranium mineralisation. Granite basement was found below 100-120 m below an extensive saprolite. Petrographic studies and geochemical (REE + U) data collected on behalf of Uranium SA suggest that the granite resembles the Hiltaba-aged Roxby Downs Granite.

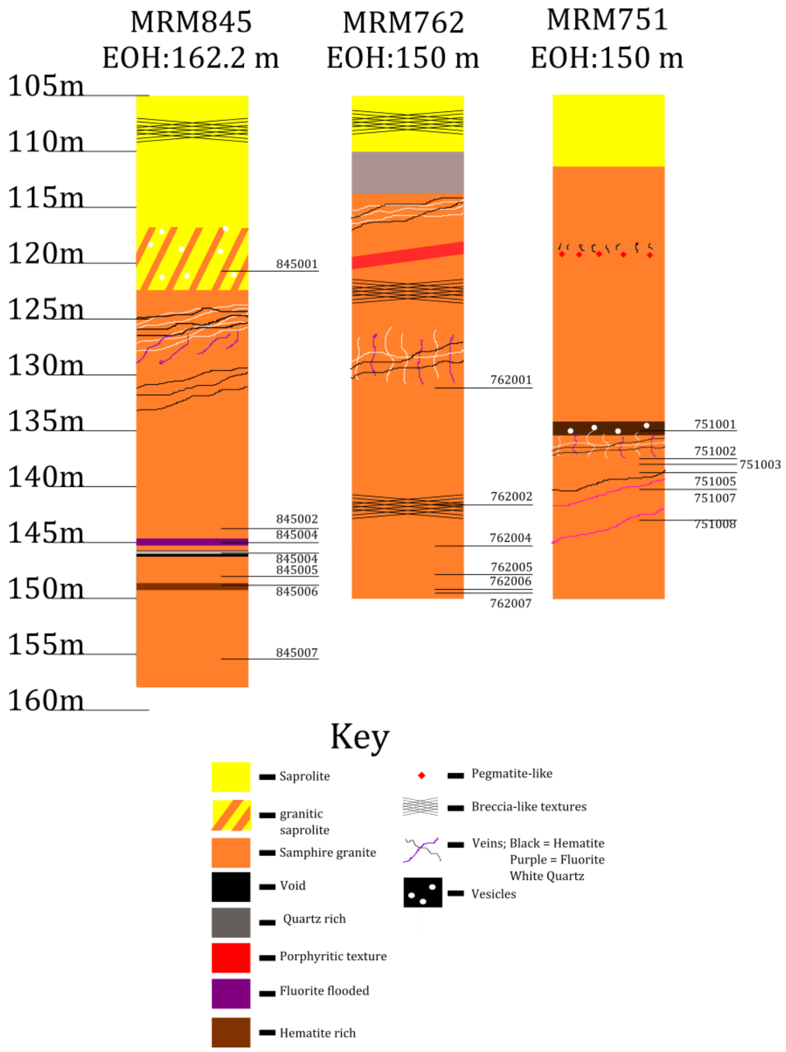

Figure 2 Schematic diagram showing drillcore lithologies and alteration with depth (m) and sample locations. Above 105 m is undifferentiated saprolite and cover sequence.

METHODS

Approach and Sampling

3 diamond drillhole cores (Figure 2) were logged below the saprolite-granite boundary with 20 samples selected for further microanalysis. The samples were chosen to target vein relationships, vein mineralisation, brecciation, clay alteration and compositional variations within the granite and are considered to be representative of the alteration within the drill core. Uranium SA has supplied detailed logs for 6 of the diamond drill holes in the project area which have been used to supplement the logging exercise. The

chosen samples were prepared as 1 inch epoxy-resin mounted blocks by Adelaide Petrographics and are detailed in Table 1. Microanalytical observations were used to supplement macroscale observations and provide more semi-quantitative data at a greater degree of accuracy. Traditional petrographic techniques can identify minerals at the grain scale but defining compositional zonation and trace element concentrations within mineral grains requires more advanced, higher-resolution techniques such as scanning electron microscopy (SEM) and laser ablation inductively coupled plasma mass spectrometry (LA-ICP-MS). The latter offers sub-ppm sensitivity coupled with micron-scale resolution and permits a quantitative understanding of trace element distribution at the scale of single grains.

Analytical

An FEI Quanta 450 scanning electron microscope (SEM) with energy dispersive X-ray spectrometry and back-scatter electron (BSE) imaging capabilities (Adelaide Microscopy) was used. BSE imaging (accelerating voltage, 20 kV, spot size of 4 and beam current of 10 nA) allowed for characterisation of each polished block sample in terms of significant textures and mineralogical relationships.

LA-ICP-MS was used to quantitatively analyse trace elements as spot analysis, element maps from suitable samples and for *in situ* U-Pb dating. The minerals targeting for trace element analysis were hematite and fluorite. This was performed on a Resonetics M-50-LR 193-nm Excimer laser microprobe coupled to an Agilent 7700cx Quadrupole ICP-MS (Adelaide Microscopy). Full details of analytical methods including spot sizes and beam transmission for all LA-ICP-MS methods are given in Appendix A.

OBSERVATIONS AND RESULTS

Petrography

The petrographic-mineralogical study was conducted on granites, their altered equivalent and on cross-cutting veins. The objective was to provide insights into the variation within the host lithologies, as well as the (hydrothermal) mineralogy and textures in the veins. Lithology, alteration stages and mineralogy are summarised in Table 1. Key textures and mineral relationships are illustrated in Figures 3-8.

SAMPHIRE GRANITE

The Samphire granite is a large homogeneous, undeformed, medium-grained granite that contains quartz and K-feldspar as main minerals with lesser amounts of plagioclase feldspar. Mafic minerals are broadly absent as phenocrysts but biotite forms up to 10% of the groundmass. Very small amounts of hornblende were also noted. The granite ranges from pink to purple to grey in colour which relates directly to the proportions of K-feldspar, quartz and fluorite, respectively. Small vesicles, ~2 mm in size, are noted in some intervals of the granite. The groundmass is made up of equigranular, 5-8 mm-sized K-feldspar-quartz-plagioclase with minor biotite and may contain phenocrysts of K-feldspar.

Textures are complex with porphyritic or pegmatite-like packages interspersed in short cm-scale intervals of drillcore within the more common medium-grained texture (Figure 3a, c). Within these porphyritic or pegmatitic varieties, K-feldspar forms 30-50 mm-sized phenocrysts and the groundmass is composed of finer quartz-K-feldspar-plagioclase. There is sufficient compositional variation within the drillcore for small intervals to be recognised as quartz syenite, alkali feldspar granite or monzogranite.

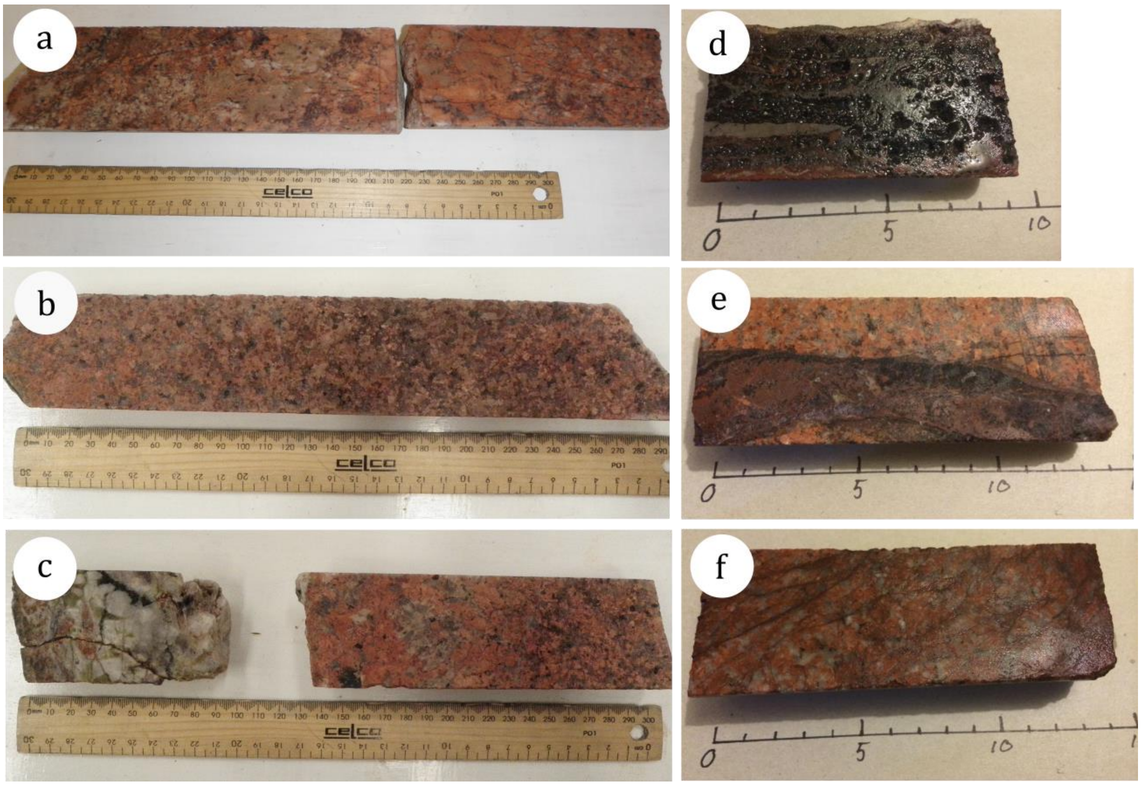

Figure 3 Photos of drill core samples showing textural and compositional variations within Samphire granite. a) 37 cm section from MRM751 with porphyritic texture. b) Fluorite 'flooding' texture towards right hand side with distinct purple colour compared to the left hand section. c) Quartz rich vein containing wall rock clasts with chlorite alteration. Gap between sections is a cavity that is 5 cm in size. Below cavity is a 8-10 cm section of porphyritic texture. d) A hydrothermal 'boiling' texture with very dominant hematite alteration and prominent vugs intersected for 20 cm. e) 4 cm thick fluorite vein with earth hematite overprint. f) hematite vein-let swam imparting breccia-like texture. Scale for e, d and f is in cm.

A series of 'flooded' textures are observed where the K-feldspar content is reduced and quartz or fluorite become almost as abundant as K-feldspar or, more rarely, even greater (Figure 3b). In 'fluorite flooded' intervals, the fluorite content approaches 30% and imparts a distinct purple colouration to the granite. The fluorite is of the non-fluorescent variety.

K-feldspar content ranges from 60-80%. In the groundmass, plagioclase grains are 4-8 mm in length and content is up to 15% of the groundmass and is difficult to distinguish from K-feldspar due to hematite staining. Quartz grains are consistently medium 3-8 mm in size and form 25-50% of the ground mass.

Biotite forms aggregates of grains amounting up to 15% however, is primarily found to make up <10% of the main mineral assemblage.

Hydrothermal alteration is present through much of the Samphire granite and is manifested as clay alteration of primary minerals and crosscutting hydrothermal veins. At the granite-saprolite contact, chlorite and kaolinite replace both plagioclase and potassium feldspar, leaving grains of slightly altered quartz resulting in a rock with low competency (somewhere between a granite and saprolite). Quartz shows little signs of alteration but has a gritty/granular appearance in the clay-rich sections. Plagioclase displays an irregular clouding of grains with sericite and hematite. K-feldspar shows degrees of sericite alteration, overprinting by hematite overprinting and small exsolved lamella of plagioclase giving a perthitic texture. Biotite tends to be greener in altered parts of the drillcore and often with a lustrous sheen that can be attributed to alteration to fine-grained mixtures of chlorite and sericite.

Veins, veinlets and vein swarms are present within the Samphire granite. These contain quartz, fluorite and hematite as dominant minerals and this assemblage defines vein-stage alteration. The veins are infrequent and tend to occur in the deepest 20-30 m of the drill core (i.e., ~20 m below the saprolite). The thickest veins are quartz-fluorite veins, up to 4 cm thick and display selvages of fluorite including coarse (~1 cm), euhedral fluorite grains that grow into to the quartz-fluorite vein centres. These quartz-fluorite veins are generally sub-vertical and do not display significant deformation. Macroscopic pyrite grains, approximately 3 mm in size, are accessory to quartz-fluorite veins. Veins of specular hematite run near-vertical and are <2 cm thick but can be relatively long (~30 cm), with respect to other veins observed. They also show short branches extending into the surrounding granite. Vein swarms of earthy hematite are sub-horizontal and consist of swarms of 5-15 veinlets ~1 mm in thickness giving a brecciated appearance to the granite. Vertical veins of earthy hematite are 1 cm thick and display crosscutting relationships with the thick quartz-fluorite veins, indicating they are later. Thin 2 mm-sized quartz veins are sub-horizontal and crosscut by specular hematite veins and quartz-fluorite veins and earthy hematite veins. A 5-10 cm thick vein is noted in one drill core (MRM845) that contains wall rock clasts displaying chlorite-kaolinite alteration. This vein displays ‘dog tooth’ quartz grains that project downwards into a 5-8 cm cavity (Figure 3c). Thicker (cm-scale) veins are observed to contain fragments of wall rock and can be described as small-scale hydrothermal breccias. No carbonate veins were noted in hand specimen, however when viewed under the SEM, very thin calcite veins with chlorite-kaolinite selvedges were observed.

Mineralogy

ROCK FORMING MINERALS

As briefly described above, the feldspars display alteration to assemblages of sericite-chlorite-kaolinite. This alteration imparts a dusty appearance to the K-feldspar. Some grains display inclusions among this dusty texture that are the result of hematite overprinting and possibly fine-grained REE-minerals (synchysite, monazite and thorite). SEM observation also revealed varying degrees of albitisation of K-feldspar.

Small decussate grains of biotite showing distinct parallel cleavage orientations display various stages of alteration and contain inclusions of rutile within cleavage domains but generally retain their lath-like appearance. Advanced stages of alteration of biotite include replacement by chlorite and sericite along cleavage planes and some fraying of grain boundaries.

Table 1 Index of sample suite

ID	Hole	Depth (m)	Lithology	Mineralogy			
				Early Hem	Hydrothermal Hem	Sulphides	Accessory
751001	751	135.8	Hem. Vein		X	gl	Syn, Bst
751002	751	137.9	Granite	X	x		Zrc, Thr, Rt, Ilm, Mt
751003	751	139.2	Granite		xX	PY	Thr, Sny, Ap, Zrc
751004	751	139.5	Granite		x	PY, cp	Zrc, Rt, Ilm
751005	751	140.1	Granite		x	PY	
751007	751	143.5	Granite		x		Zrc, Ap, Thr, Rt, Ilm
751008	751	145.5	Granite	X	xX	cp	Mt, Rt, Ilm, Syn, Cof
762001	762	133.7	Granite		x	PY	Ap, Rt, Ilm, Zrc, Thr
762003	762	141.1	Granite		x		
762004	762	146.6	Granite		x	PY, Moly, CP	Ap, Rt, Zrc, Mnz, Cof
762005	762	148	Granite		x	SP	Ap, Zrc,Thr, Syn, Mnz
762006	762	149.6	Quartz vein		x	PY, py, CP, GL	Thr, Rt, Syn, Bst, Zrc
762007	762	149.6	Granite				Thr, Rt, Syn, Bst, Zrc, Cof
845001	845	124.5	Saprolite				Zrc, Thr, Syn, Ba, Rst
845002	845	144.8	Granite		x		Rt, Syn,
845003	845	145.5	Granite		x		Thr, Zrc, Ap, Syn, Rt, Cof
845004	845	146.2	Granite		S, x	cp	Thr
845005	845	148.5	Granite			PY, GL	Thr, Zrc, Syn, Bst, Rt, Ap, Cof
845006	845	148.9	Granite	x	x	PY, Moly	Mnz, Rt, Cof
845007	845	155.8	Granite	X			Thr, Syn, Bst, Zrc, Ap, Cof

Abbreviations: Hem – hematite, py – pyrite, cp – chalcopyrite, gl – galena, moly – molybdenite, sp – sphalerite, syn – synchysite, bst – bastnäsite, zrc – zircon, thr – thorite, cof, - coffinite, mnz – monazite, ap - apatite, rt – rutile, ilm – ilmenite, mt – magnetite, qtz – quartz, bt – biotite, chl – chlorite, cal – calcite, K-feld – K-feldspar, alb – albite. Note: x, X, py and PY are used to convey the difference in grain sizes in each sample. Capital letters denote coarser grains and lower case denotes finer grains.

FE-(TI)-OXIDES (HEMATITE, MAGNETITE AND ILMENITE)

The oxide minerals are found in the majority of samples and the most common is hematite. There are four distinct textural varieties of hematite occurring within both the granite groundmass and hydrothermal vein alteration. The first of these is porous, anhedral blebs of hematite (Figure 4g-j) that occur clustered together with the space between grains filled with chlorite-kaolinite (?) alteration of albite or K-feldspar. These porous grains can contain microscopic inclusions, predominantly of quartz but also K-feldspar or a mineral, heavily enriched in Nb and Y (pyrochlore) (Figure 4h). Although blebby and anhedral, this hematite is generally not fractured and appears compositionally homogeneous.

Acicular hematite within veins (Figure 4a-c), shows two size groups: a coarse 100-300 µm-sized population and a distinctly finer population <60 µm in size. These acicular grains form radial rosette-shaped aggregates. The coarser population can be seen bridging across veins and vugs in the samples and contain minor fractures and pores but otherwise appear homogeneous. This coarse type does not appear to replace or be associated with magnetite.

Fine grains of magnetite were discerned in reflected light (Figure 4j) occurring in porous, blebby hematite grains with the appearance of hematite rims on magnetite cores. The hematite rim is not a universal feature of magnetite grains with several grains displaying no hematite directly in contact however, most of the grains found did exhibit such a rim. Fine, anhedral minor ilmenite (Figure 4l) are observed forming symplectites with rutile.

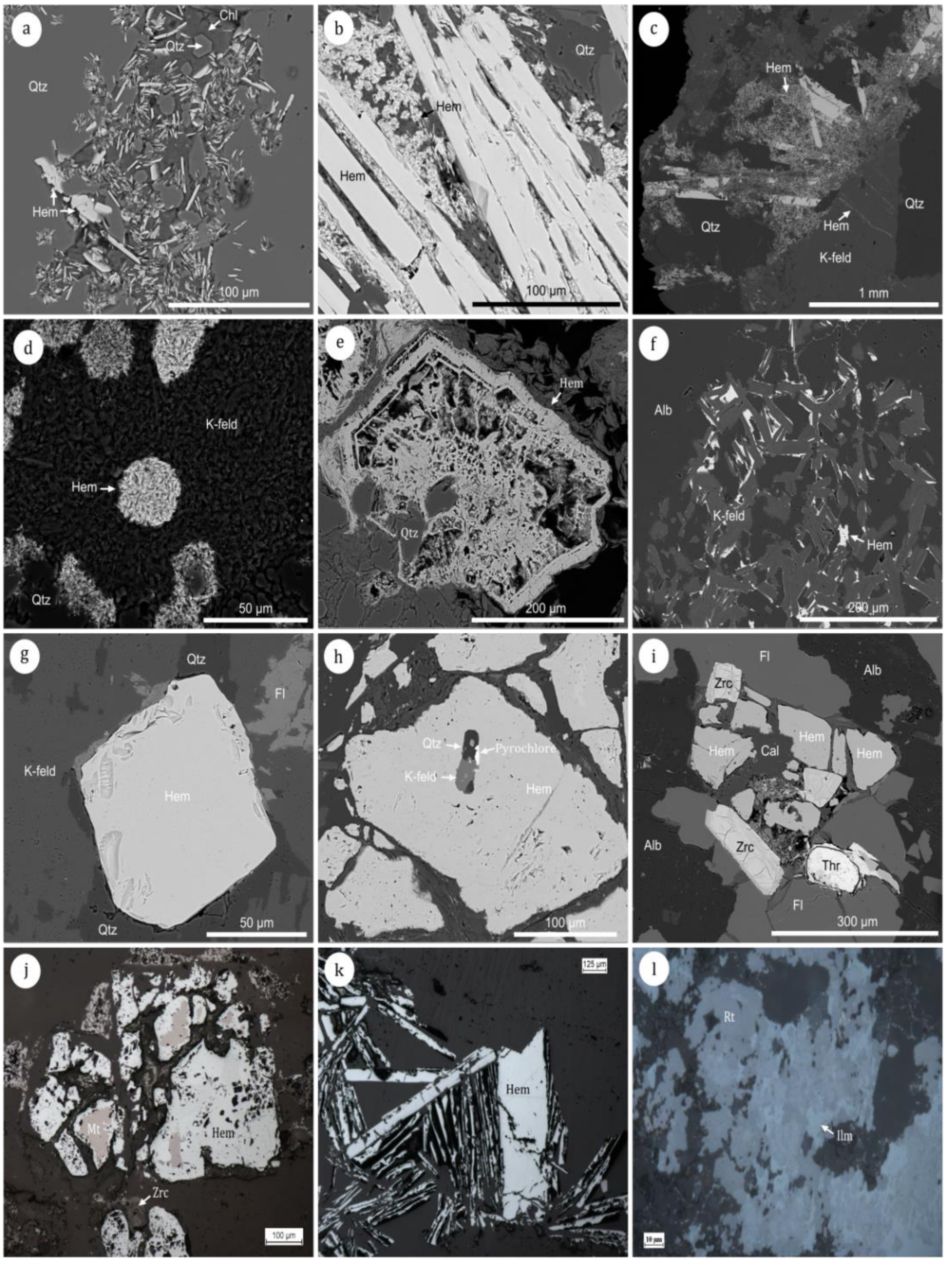

Figure 4 BSE images (a-i) showing hematite textures. Reflected light images (j-l) allow distinction hematite from magnetite. a) Fine-grained aggregates of acicular hematite in quartz groundmass displaying no preferred orientation with quartz grains and clay infilling fracture space. b) Coarse, acicular hematite in a vein with fine hematite in between. c) Small quartz-bearing vein with coarse acicular hematite displaying fractures. Finer-grained hematite is also growing within the vein and in veinlets in K-feldspar. d) Fine-grained aggregates of hematite with a fibrous texture in K-feldspar showing a similar fibrous texture surrounded by homogenous quartz. e) Skeletal hematite with quartz in a clay-rich sample displaying voids. f) Hematite as rims on K-feldspar-albite intergrowths. g) Isolated hematite grain with a very slightly vuggy texture in a quartz vein crosscutting K-feldspar with fluorite on rim. h) Porous, blebby, clustered hematite with K-feldspar-quartz inclusions. The bright patch is pyrochlore. i) Hematite grains clustered with zircons and thorite in fluorite and albite. Calcite fills the space between these grains and as veins in the lower fluorite. j) Porous, blebby hematite showing magnetite cores with fine-grained, interstitial hematite. Metamict zircon is present at the bottom of the image. k) Coarse acicular, homogeneous hematite. l) Rutile-ilmenite symplectite.

A fourth sub-type of hematite displays a skeletal-like texture with a distinct hematite rim surrounding void-space and containing small dendritic hematite attached to the rim. This texture was only seen in one same sample (Figure 4e).

SULPHIDES

Sulphides (pyrite, molybdenite, galena, chalcopyrite and sphalerite in order of abundance) occur as disseminated, commonly isolated, grains either alone or in multi-component assemblages. Pyrite occurs as coarse, subhedral to anhedral grains up to 500 µm in size (Figure 5d, e). These grains form small clusters which are either homogenous or contain vugs and fractures. In some cases, pyrite is clearly altered or replaced, causing destruction of the euhedral morphology to give rounded grain margins (Figure 5d). One unusual texture in pyrite comprises rims on coarse grains of thorite (Figure 5c). Fine grains of euhedral pyrite are found within cavities in K-feldspar and albite. These grain aggregates (Figure 5e) are ~10 µm in size.

Coarse grains of disseminated molybdenite up to 2 mm across were observed in several samples. Molybdenite contains few to no inclusions and maintains a visible cleavage as evident by the ribbon-like appearance (Figure 6b).

Galena grains are scattered through the sample suite the most significant textures occurred as coarse, euhedral to anhedral grains. Euhedral galena up to 100 µm, and a finer-grained variety were noted. Anhedral galena is strongly associated with chalcopyrite (Figure 6c) where the galena forms rims on chalcopyrite with small pyrite inclusions.

Chalcopyrite is a relatively uncommon sulphide and is found only in samples that contain pyrite or pyrite-galena assemblages. Chalcopyrite is highly anhedral and commonly infills finely brecciated pyrite (Figure 6d). Small grains of sphalerite were noted filling voids however these are uncommon. Only one sample (762005) contained significant amounts of sphalerite (Figure 6a). Such sphalerite displays a variety of grain sizes from ~10 µm up to 200 µm, typically disseminated within a calcite groundmass. Sphalerite is anhedral and occupies voids within the calcite.

ACCESSORY MINERALS

Accessory zircons are variable in size with the coarsest being ~300 µm while the smallest are 20 µm. All display strongly metamict textures with internal zonation and fracturing. Some zoned zircons contain a core that is fractured overgrown by a fracture-free rim (Figure 4i). SEM-EDS study revealed no systematic trend of light cores with darker rims compared to darker cores with lighter rims on the back-scatter electron images.

Thorite is abundant and can be quite coarse (grains up to 250 µm: Figure 5c, d). Thorite grains show some zonation and appear strongly altered under reflected light. Coffinite was detected in 7 samples (Table 1) and displays two dissimilar textures. The majority of coffinite was found as thin veins that appear to infill fractures within host phases (Figure 8b, e) with a possible replacement component (Figure 8c, d). Coffinite also occurs as rims on the margins of pyrite (Figure 8a). Synchysite is also a common accessory mineral throughout much of the sample suite; EDS analysis confirmed this as synchysite-(Ce). Synchysite grains are anhedral and can form large (~200-300 µm-sized) aggregates (Figure 7c, d). The mineral also appears to form within veins (Figure

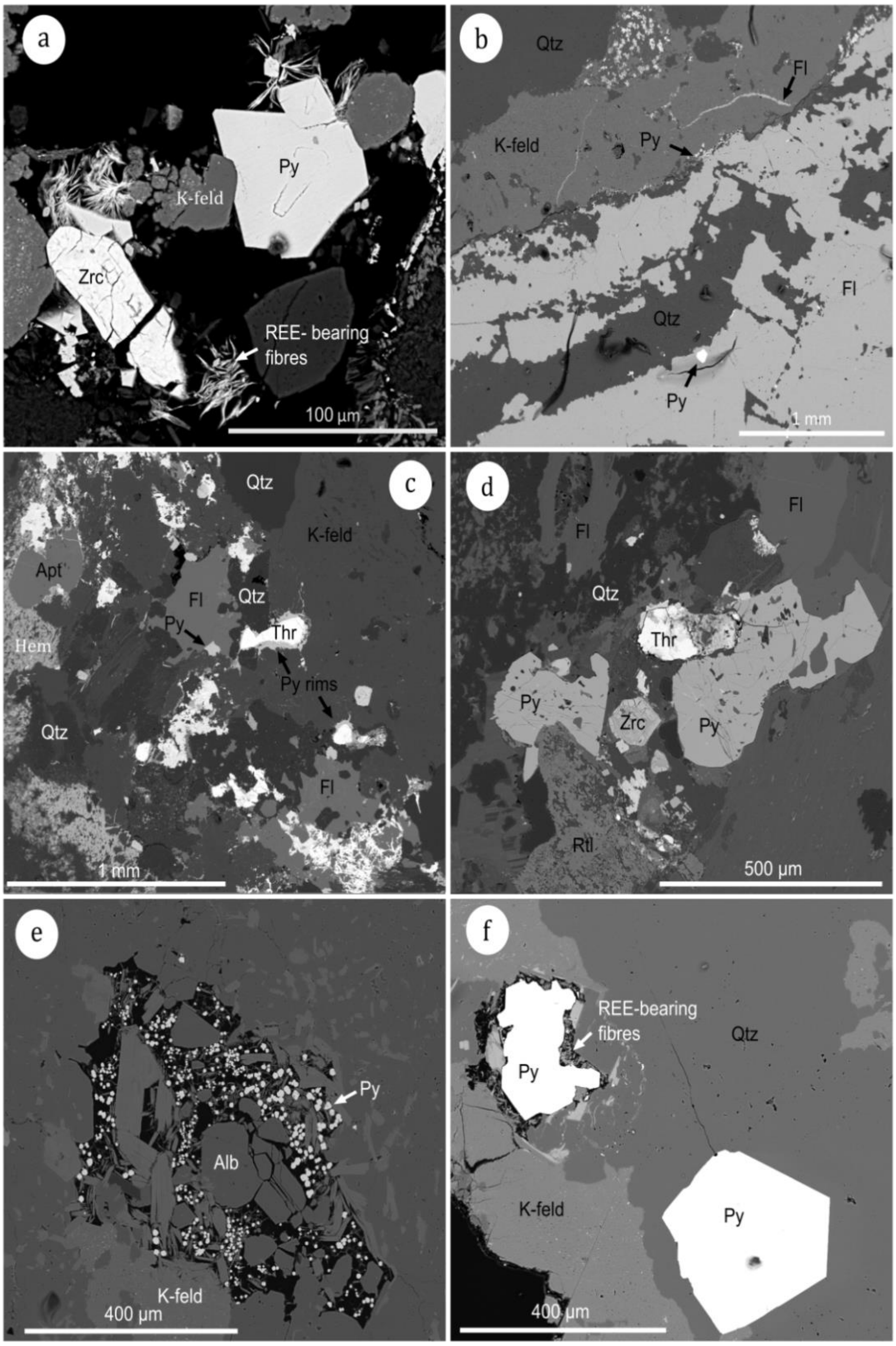

Figure 5 a) Euhedral pyrite within a vug on fluorite-quartz vein margin. Heavily metamict and fracture zircon is present; co--existing K-feldspar has a dusty appearance. Small aggregates of fine, REE-Th-(U)-enriched minerals can be seen growing in the vug. b) Quartz-fluorite vein with coarse and fine pyrite growing close to phase boundaries. K-feldspar has dusty appearance and fluorite veins. c) Pyrite forming rims on thorite grains in a quartz-fluorite vein containing fine-grained hematite. d) Coarse, fractured pyrite containing inclusions of fluorite. e) Fine-grained pyrite clusters in a void within K-feldspar-albite. K-feldspar has dusty appearance at the bottom of the image but the grains within the void are lath- shaped and not dusty. f) Coarse-grained pyrites in a quartz vein. Top pyrite grain is anhedral and has is surrounded by void space into which fine, acicular REE-Th-U-minerals are growing. K-feldspar displays a dusty appearance.

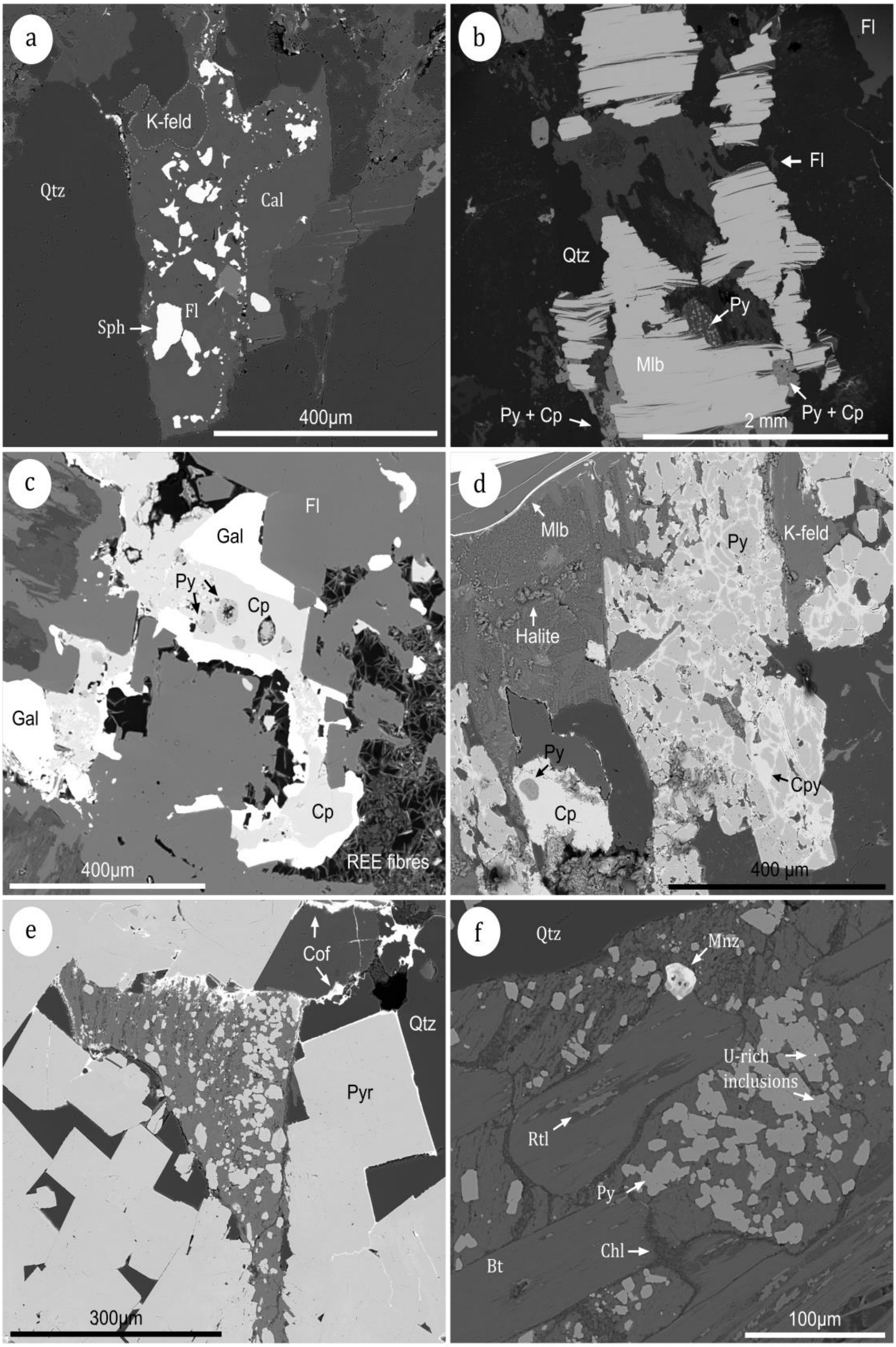
a
K-feld
Qtz
Cal
Fl
Sph
400μm
b
Fl
Fl
Qtz
Py
Mlb
Py + Cp
2 mm
Py + Cp
c
Fl
Gal
Py
Cp
Gal
Cp
400μm
REE fibres
d
Mlb
Py
K-feld
Halite
Py
Cp
Cpy
400 μm
e
Cof
Qtz
Pyr
300μm
f
Qtz
Mnz
U-rich
inclusions
Rtl
Py
Chl
Bt
100μm

Figure 6 a) Anhedral sphalerite within vuggy calcite with an inclusion of euhedral fluorite, hosted in a quartz-K-feldspar groundmass. This sample displays a high proportion of calcite compared with many other samples, and also features abundant synchysite. b) Coarse-grained molybdenite with rims of pyrite-chalcopyrite symplectites (shown in detail in [d]). c) Galena rims forming on elongate chalcopyrite with cores of pyrite. Voids are found close to the pyrite cores and one pyrite is within a void. This assemblage contains significant void space hosting fibrous REE-minerals. The assemblage is hosted in a fluorite-bearing vein. d) Anhedral pyrites with chalcopyrite infill forming a symplectite close to molybdenite. Halite grains can be seen above feldspar (K-feldspar?) that displays a 'wormy' texture. e) Coarse euhdral pyrite with fine anhedral pyrite present between grains with some clay alteration. Coffinite veins form rims and inside voids in the coarse pyrite. Coffinite also surrounds fine-grained pyrite. Quartz fills void space in this assemblage. f) Fine-grained pyrite with uranium-bearing inclusions (coffinite?) in a clay-bearing vein that contains thin laths of biotite with rutile inclusions. A small monazite displaying some internal zonation represents an uncommon accessory component within the sample.

7c, d). Bastnäsite forms aggregates of thin acicular-like grains within synchysite (Figure 7a, b).

Apatite displays two distinct textures. In the first, apatite is heavily altered resulting in extensive fracturing (Figure 7 (g), whereas the other shows apatite displaying internal compositional zoning (Figure 7h). The compositional zoning could not be resolved by EDS analysis but this commonly reflects variation in REE content. The fractured apatite is typically coarse-grained and contains inclusions of thorite; the zoned grains are less altered. Monazite (Figure 6f and Figure 7f) is an uncommon accessory mineral within the system and only a few small (<50 µm) grains were observed.

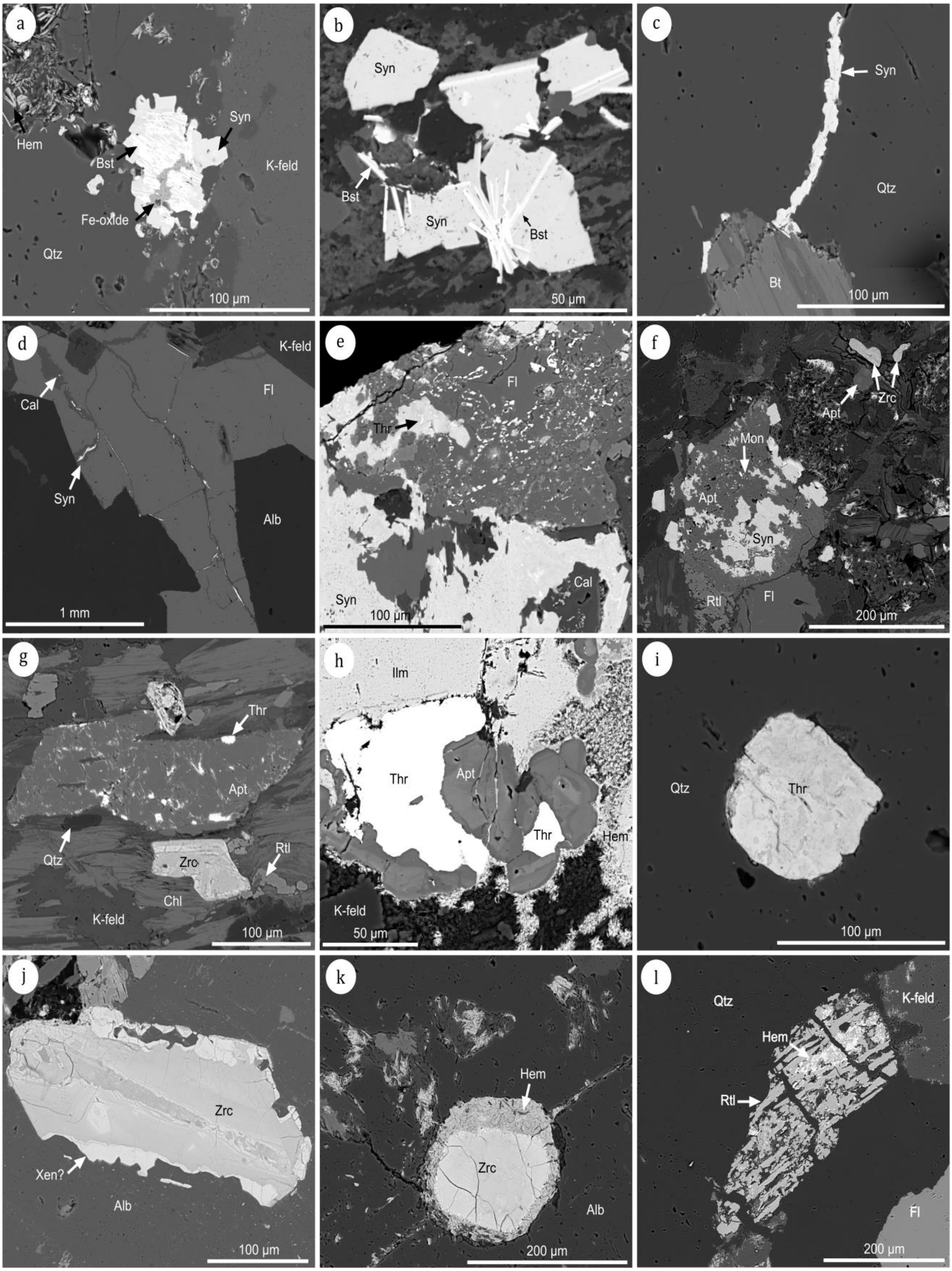
a
Hem
Bst
Syn
K-feld
Fe-oxide
Qtz
100 µm
b
Syn
Bst
Syn
Bst
50 µm
c
Syn
Qtz
Bt
100 µm
d
K-feld
Cal
Fl
Syn
Alb
1 mm
e
Fl
Thr
Syn
100 µm
Cal
f
Zrc
Apt
Mon
Apt
Syn
Rtl
Fl
200 µm
g
Thr
Apt
Qtz
Rtl
Zrc
Chl
K-feld
100 µm
h
Ilm
Thr
Apt
Thr
Hem
K-feld
50 µm
i
Qtz
Thr
100 µm
j
Zrc
Xen?
Alb
100 µm
k
Hem
Zrc
Alb
200 µm
l
Qtz
K-feld
Hem
Rtl
Fl
200 µm

Figure 7 a) Coarse, anhedral synchysite displaying thin lamella of bastnäsite. An inclusion within this grain contains a silica-bearing Fe-oxide signature – probably an intergrowth of quartz and hematite/magnetite. The grain is located on the contact of porous quartz with acicular, vein hematite and dusty K-feldspar. b) Fragmented synchysite grains containing lamella/aggregates of bastnäsite within rich zone of clay alteration. Bastnäsite displays a thin acicular crystal habit and does occur outside of synchysite grains. c) Synchysite vein in quartz. d) Calcite veins in fluorite containing synchysite. e) Coarse and porous synchysite with fine-grained thorite-monazite in a calcite-fluorite groundmass. From previous images there is a possibility of some bastnäsite within the synchysite although the acicular habit is not prominent. g) Heavily altered apatite with synchysite inclusions and minor monazite. Area is heavily altered with void space, REE fibres, metamict zircon and clay alteration. h) Thorite-apatite assemblage with clear zonation within the apatite. Thorite also displays some zonation the reason for this zonation in apatite and thorite was not discernible via EDS analysis. Porous ilmenite can be seen in the top of the frame sharing a transitional boundary with fine grained hematite. i) Heavily altered apatite with thorite. A K-feldspar grain displays small voids imparting a porous texture. Several rutile grains in a clay groundmass. j) Heavily altered ilmenite containing both rutile and fine-grained hematite. Quartz has fractured this mineral but morphology is maintained. k) Coarse zircon in dusty albite, displaying strongly metamict texture including internal zonation and fracturing. l) Fractured zircon with some zonation with a rim of fine-grained hematite located in a fracture within porous albite.

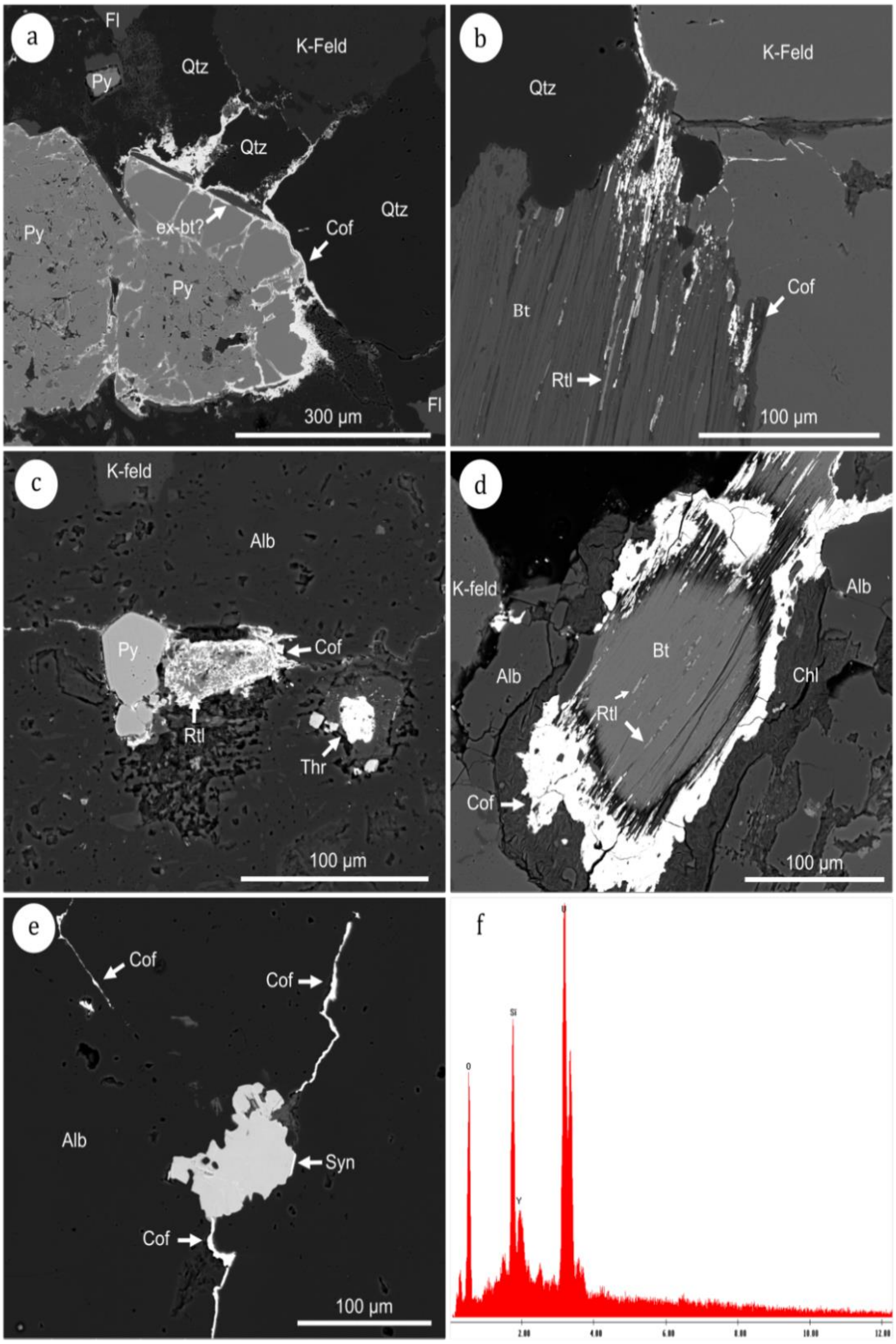

Figure 8 a) Back scatter electron images showing aspects of REE- and U- mineralogy. (a) Coarse pyrite (Pyr) with significant fracturing and pore space filled with coffinite (Cof). Coffinite veins also fill fractures in quartz (Qtz). b) Fine coffinite and coexisting rutile (Rtl) at grain boundary between quartz and K-feldspar. Coffinite is also present within cleavage planes in biotite. c) Strongly-altered rutile displaying coffinite replacement/infill in a very porous albite (Alb) groundmass. Pyrite displays some alteration but is not strongly affected by coffinite. d) Intense alteration of a biotite lath with rutile developed along grain boundaries. Coffinite forms a thick rim about this mineral and breaches into the grain along fracture/cleavage. e) Coffinite veins in an albite groundmass. Synchysite (Syn) also occurs within this vein but does not contain coffinite. f) EDS spectrum for coffinite in (d).

Mineral Relationships

Mineral relationships can be summarised as follows. Common sulphides (pyrite, molybdenite, galena and chalcopyrite), are closely associated with quartz-fluorite veins and vugs. The less common sphalerite is only associated with calcite. Acicular hematite is wholly related to veining whereas blebby hematite shows an association with magnetite (which it replaces), ilmenite, zircon and thorite within the K-feldspar-plagioclase (albite) groundmass. Skeletal hematite is associated with clay-quartz alteration. Apatite and monazite display a weak spatial association but apatite and thorite are always closely related. Bastnäsite is very strongly associated with synchysite which in turn shows an association with fluorite and calcite.

The very fine-grained, earthy hematite between blades of the acicular hematite appears to be very late stage in the mineral sequence and can be seen cross cutting quartz-fluorite bearing veins.

LA-ICP-MS trace element data

IRON-OXIDES

Trace element data for hematite are given in Table 2. Chondrite-normalised REE-fractionation trends are shown in Figure 9a-b. Key geochemical trends are shown as Figure 10. Two types of hematite are present: these can be distinguished both texturally (Figure 10e-f), and in terms of mineral chemistry.

Table 2 LA-ICP-MS data for hematite and other Fe-(Ti)-oxides

Hematite (hydrotherma	Mg	Al	Si	P	Ca	Sc	Ti	V	Cr	Mn	Co	Ni	Cu	Zn
751003-1	69	660	976	<14	<116	2.5	5615	97	<0.76	10	<0.063	0.41	<0.80	1.2
751003-2	198	1970	22337	19	<107	2.1	2565	234	<1.25	17	<0.105	<0.00	0.95	4.6
751003-3	126	3667	10886	<14	<111	5.0	6321	820	<0.46	16	0.16	<0.34	1.1	3.0
751003-4	956	6807	37941	21	<136	6.9	6037	274	<1.23	15	0.21	0.93	<0.77	1.9
751003-5	32	234	397	<17.10	<102	2.4	4758	81	<1.27	14	0.13	<0.54	<0.56	0.6
751003-6	140	1286	1722	<16.20	136	3.1	6140	155	1.5	14	<0.116	0.7	1.09	2.7
751003-7	103	1643	1616	<15.85	<129	8.4	1040	483	0.67	18	0.40	0.34	1.00	2.6
751003-8	304	2661	3974	<13.02	<103	15.7	4874	1559	<0.65	26	0.25	<0.28	<0.52	3.9
751003-9	101	803	8131	16	<94.74	2.6	6483	570	<0.90	23	0.15	0.6	<0.85	4.2
751003-10	302	2489	3221	<14.61	<97.15	12.9	4512	1097	0.51	24	0.25	1.18	0.92	4.1
751003-11	555	3788	6994	<12.87	121	5.6	5154	405	1.19	47	0.44	0.7	1.19	31
751003-12	363	3113	4005	<14	<84.77	12.8	6945	980	<0.74	41	0.47	0.63	0.58	3.1
751003-13	1192	7790	12015	<17.46	<80.14	8.5	1827	344	<1.14	75	0.99	1.2	2.7	15
751003-14	366	4731	11184	<14.80	201	10.0	1762	419	3.1	32	0.36	0.82	1.38	5.7
751003-15	510	4026	6015	<15.32	<92.77	13.9	4002	1268	<0.94	59	0.69	0.81	<0.85	14
751003-16	1118	9551	13541	<14	135	23.5	4312	1088	<0.76	53	0.95	0.79	1.79	14
751003-17	1599	10195	16771	<18.11	173	8.6	10044	126	2.96	160	1.04	0.41	2.24	19
751003-18	1278	7621	13470	<15.53	152	5.8	5857	147	3.03	64	1.03	1.14	2.3	19
751003-19	508	4135	8866	<14	<90.81	10.4	1542	434	1.32	30	0.177	0.34	0.4	5.1
Mean (n=19)	**517**	**4062**	**9688**	**19**	**153**	**8.5**	**4726**	**557**	**1.8**	**39**	**0.48**	**0.73**	**1.4**	**8.1**
S.D.	**476**	**3006**	**9031**	**2.4**	**29**	**5.6**	**2250**	**446**	**1.1**	**35**	**0.34**	**0.29**	**0.70**	**8.1**
Maximum	**1599**	**10195**	**37941**	**21**	**201**	**24**	**10044**	**1559**	**3.1**	**160**	**1.0**	**1.2**	**2.7**	**31**
Minimum	**32**	**234**	**397**	**16**	**121**	**2.1**	**1040**	**81**	**0.51**	**10**	**0.13**	**0.34**	**0.40**	**0.64**
751008-1	10	173	223	18	154	0.25	1197	60	1.0	8	0.36	0.44	0.91	0.97
751008-2	1.7	599	11670	18	118	1.2	891	42	1.1	11	0.19	0.71	0.77	1.08
751008-3	543	6237	8040	19	120	3.4	4425	253	1.1	17	3.95	0.97	2.6	6.19
751008-4	6.2	100	200	27	251	1.1	9922	74	1.3	10	0.53	0.67	1.7	1.77
751008-5	11	490	251	23	204	0.59	906	93	1.1	14	1.9	0.62	1.1	1.49
751008-6	52	715	1221	22	174	1.7	1111	93	1.0	22	3.1	0.39	1.3	1.77
751008-7	0.7	212	146	17	93	1.2	571	258	1.4	3.1	0.09	0.11	0.9	1.23
751008-8	0.7	198	203	19	149	0.97	564	283	1.3	3.5	0.09	0.45	0.61	0.97
751008-9	0.5	206	133	19	163	1.7	623	399	1.3	4.5	0.09	0.00	1.0	1.52
751008-10	10.8	392	354	19	151	1.1	622	93	1.2	22	2.74	0.2	0.7	1.12
Mean (n=10)	**64**	**932**	**2244**	**20**	**158**	**1.3**	**2083**	**165**	**1.2**	**11**	**1.3**	**0.46**	**1.2**	**1.8**
S.D.	**169**	**1875**	**4114**	**3.0**	**45**	**0.85**	**2988**	**122**	**0.15**	**7.1**	**1.5**	**0.30**	**0.59**	**1.6**
Maximum	**543**	**6237**	**11670**	**27**	**251**	**3.4**	**9922**	**399**	**1.4**	**22**	**4.0**	**1.0**	**2.6**	**6.2**
Minimum	**0.49**	**100**	**133**	**17**	**93**	**0.25**	**564**	**42**	**1.0**	**3.1**	**0.09**	**0.00**	**0.61**	**1.0**
Hematite (early)														
751008-1	47	741	733	16	127	19	9436	681	11.1	136	13	6.19	0.85	5.4
751008-2	214	3929	4025	16	94	5.9	5384	457	3.0	295	22	13.17	0.52	17.3
751008-3	59	1896	28124	16	99	3.5	1616	688	26	147	21	6.23	0.97	7.1
751008-4	282	3034	1745	15	95	7.5	2087	787	6.8	258	14	6.48	0.84	12.6
751008-5	3	1575	497	19	117	4.5	2489	691	25	77	12	8.2	0.88	4.3
751008-6	504	5894	8067	18	127	6.2	2842	684	40	181	20	7.8	0.87	16.5
751008-7	541	5396	8717	15	190	2.8	982	570	48	169	13	5.33	0.71	13.8
751008-8	95	2098	7031	15	114	3.3	1859	630	36	166	13	7.27	0.84	4.6
Mean (n=8)	**218**	**3070**	**7367**	**16**	**120**	**6.6**	**3337**	**649**	**25**	**178**	**16**	**7.6**	**0.81**	**10**
S.D.	**209**	**1856**	**9002**	**1.4**	**31**	**5.4**	**2793**	**99**	**16**	**69**	**4.2**	**2.4**	**0.14**	**5.5**
Maximum	**541**	**5894**	**28124**	**19**	**190**	**19**	**9436**	**787**	**48**	**295**	**22**	**13**	**0.97**	**17**
Minimum	**2.66**	**741**	**497**	**15**	**94**	**2.8**	**982**	**457**	**2.95**	**77.25**	**11.74**	**5.33**	**0.52**	**4.27**
84500-1	92	1565	486	<15.37	<130	4.3	1310	722	57	57	5.1	7.5	<0.85	19
84500-2	114	1372	551	<10.96	<73	5.5	1083	680	63	59	5.9	6.3	0.77	16
84500-3	347	1482	1401	<14.53	2398	10	1379	661	63	64	5.9	7.7	5.8	17
84500-4	541	2270	1399	<10.59	224	5.7	1023	713	66	71	5.8	9.2	1.4	16
84500-5	8695	12573	14304	<15.73	44570	11	987	756	98	148	8.0	9.4	4.0	23
84500-6	4360	6114	7517	<15.73	2544	13	15896	782	74	128	9.0	8.7	5.4	28
84500-7	3154	6252	9330	70.99	301	42	2251	797	76	117	13	5.5	20	47
84500-8	122	1628	562	<14.06	<82	6.5	1614	746	64	68	6.0	7.9	<0.78	17
84500-9	262	2420	818	<13.20	169	6.0	892	744	66	56	6.2	8.5	1.7	16
84500-10	58	2304	477	<15.37	225	5.9	1174	725	50	55	6.0	8.0	2.6	20
84500-11	88	2437	358	<13.90	<67	6.2	1728	764	41	57	6.9	7.7	<0.62	30
84500-12	239	1408	739	<13.13	<93	4.5	1120	693	47	60	5.2	6.6	0.97	17
84500-13	292	1742	2321	<14.89	<97	10	1922	681	48	56	5.4	7.1	3.5	25
84500-14	9385	15068	16677	<18.57	22919	21	5467	758	191	208	13	11	10.0	59
84500-15	2255	5493	5683	<21.83	>50000	80	2087	736	139	1721	6.5	7.1	3.2	32
84500-16	10015	26485	45721	32.3	3933	52	17232	851	191	224	13.9	10.3	6.9	57
84500-17	197	2039	1368	<14.21	799	5.8	937	756	51	59	6.3	8.5	4.7	24
84500-18	291	1340	846	<13.52	150	4.9	879	692	50	57	5.9	6.5	<0.69	10
Mean (n=18)	**2251**	**5222**	**6142**	**52**	**7112**	**16**	**3277**	**736**	**80**	**181**	**7.4**	**8.0**	**5.0**	**26**
S.D.	**3495**	**6619**	**11073**	**27**	**14085**	**21**	**4952**	**47**	**46**	**388**	**2.8**	**1.5**	**4.9**	**14**
Maximum	**10015**	**26485**	**45721**	**71**	**44570**	**80**	**17232**	**851**	**191**	**1721**	**14**	**11**	**20**	**59**
Minimum	**58**	**1340**	**358**	**32**	**150**	**4.3**	**879**	**661**	**41**	**55**	**5.1**	**5.5**	**0.77**	**10**
Magnetite														
751008Mt-1	26	2000	704	13.04	77	4.66	1901	702	29	100	18.89	6.4	0.49	8.7
751008Mt-2	29	2180	563	12.27	103	4.53	1781	688	26	181	16.98	4.25	0.69	6.3
Ilmenite														
751003 Ilm/mix-1	2186	37122	#####	147	#####	159		308	7.1	390	2.9	1.6	18	58
751003 Ilm/mix-2	221	2173	88680	29	46989	72		249	4.1	178	1.3	1.5	3.1	17
751003 Ilm/mix-3	131	1451	<551	<23	1237	142		229	2.6	228	2.4	1.7	4.3	11

Ga	As	Sr	Y	Zr	Nb	Mo	Sn	Sb	Ba	La	Ce	Pr	Nd	Sm	Eu	Gd
8.8	0.88	0.25	0.43	1.32	244	0.49	484	0.78	1.0	0.53	0.81	0.06	0.14	<0.05	<0.01	0.09
9.0	<0.60	0.69	0.68	2.73	237	0.17	513	3.5	1.6	0.37	0.6	0.07	0.26	0.13	<0.01	<0.063
10.9	0.48	0.47	0.58	1.95	297	27	487	4.7	22	0.55	0.84	0.09	0.18	0.13	0.01	0.10
14.7	<0.75	0.91	0.59	2.02	228	0.29	932	4.5	1.2	0.76	1.058	0.08	0.34	<0.07	0.01	<0.061
9.6	0.81	0.26	0.95	2.46	871	1.5	1203	5.8	1.1	0.54	1.157	0.09	0.17	0.18	<0.01	0.08
8.3	<0.73	0.31	1.37	7.09	357	0.92	370	1.8	0.6	0.38	0.89	0.10	0.25	0.08	0.01	0.10
13	<0.64	0.41	0.94	2.53	429	4.0	1957	7.6	3.7	0.98	1.9	0.21	0.60	0.11	<0.01	0.18
15	<0.51	0.66	1.252	4.12	389	1.7	1112	16	5.9	1.2	2.2	0.25	0.61	0.16	0.02	0.19
11	0.77	0.79	1.52	3.56	414	1.8	483	10	1.3	1.9	2.2	0.25	0.62	0.26	0.02	0.12
14	0.96	0.65	1.59	5.46	283	1.8	1186	12	4.7	1.2	2.5	0.22	0.83	0.28	0.02	0.21
17	0.87	0.94	2.18	12.65	276	2.3	1004	23	7.7	1.4	2.9	0.29	0.47	0.16	<0.01	0.24
12	<0.61	1.09	2.68	8.54	428	3.2	1400	28	6.5	2.3	3.9	0.40	1.17	0.43	0.04	0.40
19	1.09	1.4	2.63	6.11	323	5.0	1022	22	22	2.8	5.0	0.56	1.38	0.39	0.02	0.46
16	5.06	0.628	4.96	6.3	309	2.0	1304	11	7.5	2.7	4.9	0.43	1.09	0.62	0.04	0.60
14	1.86	1.42	2.62	7.6	273	4.6	1232	48	7.1	4.4	6.9	0.54	1.35	0.30	0.06	0.156
19	1.23	1.69	5.05	17.98	389	6.4	1271	31	15	2.8	5.9	0.58	1.86	0.60	0.03	0.59
15	1.44	2.68	5.27	19.29	312	9.4	260	39	35	5.0	8.9	0.83	2.94	0.66	0.05	0.85
18	0.86	3.04	8.07	24.09	498	7.2	409	21	17	4.3	9.1	0.88	2.74	0.96	0.09	1.11
15	<0.51	0.705	0.833	1.86	287	0.72	1627	8.5	26	1.6	1.8	0.21	0.63	0.19	0.01	0.21
14	**1.4**	**1.0**	**2.3**	**7.2**	**360**	**4.2**	**961**	**16**	**10**	**1.9**	**3.3**	**0.32**	**0.93**	**0.33**	**0.03**	**0.33**
3.4	**1.2**	**0.77**	**2.1**	**6.6**	**145**	**6.0**	**476**	**13**	**10**	**1.4**	**2.7**	**0.25**	**0.83**	**0.25**	**0.02**	**0.30**
19	**5.1**	**3.0**	**8.1**	**24**	**871**	**27**	**1957**	**48**	**35**	**5.0**	**9.1**	**0.88**	**2.9**	**0.96**	**0.09**	**1.1**
8.3	**0.48**	**0.25**	**0.43**	**1.3**	**228**	**0.17**	**260**	**0.78**	**0.62**	**0.37**	**0.60**	**0.06**	**0.14**	**0.08**	**0.01**	**0.08**
9	<0.97	0	0.02	0.24	677	0.00	1133	0.42	0.30	0.01	0.05	0.01	0.05	0.02	0.01	0.04
9	2.3	0.05	0.07	0.15	369	0.15	1529	2.60	0.33	0.17	0.36	0.02	0.10	0.05	0.02	0.10
13	<0.83	0.59	0.29	0.80	308	171	1075	0.76	2.02	0.28	0.52	0.04	0.09	0.03	0.00	0.10
9	<1.52	0.07	0.06	0.06	351	6.5	801	0.74	0.71	0.06	0.07	0.02	0.08	0.04	0.02	0.03
12	<1.15	0.20	0.14	0.41	354	2.0	1251	1.85	0.29	0.15	0.32	0.03	0.13	0.06	0.02	0.11
10	1.1	0.13	0.44	0.95	337	0.16	1445	0.57	0.76	0.46	1.17	0.08	0.11	0.11	0.03	0.08
14	<0.98	0	0.05	0.12	461	0.04	594	0.17	0.46	0.01	0.01	0.02	0.00	0.05	0.01	0.05
14	<0.93	0	0.01	0.08	456	0.09	623	0.46	0.00	0.02	0.01	0.01	0.06	0.06	0.00	0.04
12	<0.82	0.263	0.65	0.31	244	0.54	533	0.62	0.00	0.11	0.34	0.06	0.24	0.17	0.01	0.19
9.7	<0.91	0.243	0.39	1.4	260	0.27	1570	1.13	0.29	0.23	0.42	0.05	0.18	0.07	0.01	0.01
11	**1.7**	**0.16**	**0.21**	**0.45**	**382**	**18**	**1055**	**0.93**	**0.52**	**0.15**	**0.33**	**0.03**	**0.10**	**0.06**	**0.01**	**0.08**
2	**0.83**	**0.18**	**0.22**	**0.45**	**126**	**54**	**398**	**0.75**	**0.58**	**0.14**	**0.35**	**0.02**	**0.07**	**0.04**	**0.01**	**0.05**
14	**2.3**	**0.59**	**0.65**	**1.4**	**677**	**171**	**1570**	**2.6**	**2.02**	**0.46**	**1.17**	**0.08**	**0.24**	**0.17**	**0.03**	**0.19**
9.0	**1.1**	**0.00**	**0.01**	**0.06**	**244**	**0.00**	**533**	**0.17**	**0.00**	**0.01**	**0.01**	**0.01**	**0.00**	**0.02**	**0.00**	**0.01**
12	4.7	3.2	19.2	7.7	113	3.64	174	5.3	3.81	36.08	52.13	4.38	11.28	2.48	0.22	2.66
12	2.9	3.3	18.5	1.9	89	72	134	4.7	13.64	16.83	26.9	2.23	6.3	1.51	0.18	1.5
16	2.0	1.0	4.3	3.4	15	7.55	49	2.2	2.3	2.47	4.55	0.376	1.29	0.383	0.07	0.7
34	0.89	1.1	10.0	0.11	10	3.71	88	2.5	1.16	7.55	15.96	1.58	5.37	1.22	0.11	1.3
22	<0.70	0.15	0.81	5.2	9	4.12	52	0.47	0.28	0.54	0.91	0.11	0.44	0.07	0.03	0.21
24	1.25	1.01	6.5	6.1	27	3.96	62	1.4	4.13	5.63	9.42	0.803	1.77	0.397	0.06	0.63
12	1.1	0.82	34	112	34	3.05	23	0.64	3.64	4.36	8.12	0.62	2.4	0.74	0.11	1.53
16	2.1	1.01	6.7	14	27	4.3	48	1.3	0.84	2.65	5.29	0.44	1.69	0.337	0.05	0.47
18	**2**	**1.4**	**13**	**19**	**40**	**13**	**79**	**2**	**4**	**10**	**15**	**1**	**3.8**	**0.9**	**0.1**	**1.1**
7.7	**1.3**	**1.1**	**11**	**38**	**39**	**24**	**51**	**2**	**4**	**12**	**17**	**1**	**3.6**	**0.8**	**0.1**	**0.8**
34	**4.7**	**3.3**	**34**	**112**	**113**	**72**	**174**	**5**	**14**	**36**	**52**	**4**	**11.3**	**2.5**	**0.2**	**2.7**
11.61	**0.89**	**0.15**	**0.81**	**0.11**	**9.18**	**3.05**	**23.40**	**0.47**	**0.28**	**0.54**	**0.91**	**0.11**	**0.44**	**0.07**	**0.03**	**0.21**
124	<0.70	0.81	11	60	7	1.4	30	<0.35	<0.49	0.32	0.89	0.10	0.21	0.22	0.03	0.41
116	<0.56	0.52	33	160	68	1.4	23	<0.34	<0.27	0.28	1.6	0.25	1.0	0.36	0.02	1.1
100	2.1	24	712	638	1013	1.7	25	<0.42	0.49	113.2	371	51	219	93	4.1	116
100	<0.53	5.1	130	115	448	1.2	25	0.44	0.43	20	72.3	10	40	15	0.68	18
106	1.1	3.3	252	564	117	0.43	23	<0.38	0.28	3.4	11	1.6	7.6	3.64	0.18	6.4
108	1.0	3.9	46	179	407	1.0	33	0.53	0.57	1.8	6.0	0.92	3.0	1.24	0.07	1.9
84	4.2	10	773	3997	329	2.2	49	<0.40	0.55	1.3	7.6	1.2	6.6	5.96	0.36	18
120	<0.52	0.43	20	105	32	1.1	39	<0.27	<0.00	1.1	5.1	0.06	0.59	0.21	0.00	0.78
142	<0.49	0.24	12	53	21	0.79	36	<0.53	0.43	1.7	1.5	0.17	0.48	0.39	0.02	0.76
128	0.61	2.2	60	53	36	1.1	37	<0.41	<0.00	11	33	4.7	23	8.79	0.43	12
155	<0.70	0.13	3.0	5.5	9.4	1.2	50	<0.39	<0.00	0.49	4.6	0.30	0.54	0.30	0.01	0.30
118	<0.54	0.48	3.1	6.7	36	0.77	27	<0.57	<0.00	2.5	7.4	0.63	2.1	0.63	0.01	1.1
60	0.54	8.9	36	41	584	1.1	36	0.98	0.52	5.5	21	2.8	10	4.31	0.21	5.9
96	1.6	3.4	110	94	178	1.7	28	0.4	0.21	2.2	4.2	0.61	4.0	2.11	0.03	2.7
66	1.5	49	145	75	69	1.5	35	0.88	0.52	20	52	6.7	28	12.30	0.50	16
91	1.4	8.5	20	107	380	0.92	41	<0.86	2.0	2.1	5.9	0.70	2.7	0.84	0.08	1.2
114	0.77	8.7	222	94	106	6.4	34	1.24	0.65	41	136	20	74	34	1.4	46
100	0.92	0.31	14	33	13	0.30	22	<0.50	0.27	1.5	18	0.23	0.73	0.25	<0.0103	0.71
107	**1.4**	**7.2**	**145**	**355**	**214**	**1.4**	**33**	**0.75**	**0.58**	**13**	**42**	**5.7**	**24**	**10**	**0.48**	**14**
24	**1.0**	**12**	**230**	**926**	**269**	**1.3**	**8.3**	**0.34**	**0.47**	**27**	**89**	**12**	**52**	**22**	**1.00**	**28**
155	**4.2**	**49**	**773**	**3997**	**1013**	**6.4**	**50**	**1.2**	**2.0**	**113**	**371**	**51**	**219**	**93**	**4.1**	**116**
60	**0.54**	**0.13**	**3.0**	**5.5**	**7.1**	**0.30**	**22.10**	**0.40**	**0.21**	**0.28**	**0.89**	**0.06**	**0.21**	**0.21**	**0.00**	**0.30**
25	<0.58	0.011	0.504	2.03	1.3	4.0	43	0.17	0.11	0.08	0.25	0.01	0.05	0.03	0.01	0.06
24	<0.60	0.096	0.982	3.68	2.7	3.61	46	0.3	0.32	0.49	0.88	0.06	0.16	0.04	0.01	0.12
19	106	101	617	277	17915	27	189	137	282	327	744	72	207	55	4.0	55
3.9	65	60	349	49	8439	12	133	44	59	203	388	40	114	31	2.0	33
2.6	45	35	216	51	6227	7.2	222	34	35	124	255	28	94	26	1.8	29

Tb	Dy	Ho	Er	Tm	Yb	Lu	Σ REY	Hf	Ta	W	^{206}Pb	^{207}Pb	^{208}Pb	Th	U
<0.01	0.08	0.02	0.07	0.02	0.14	0.04	2.4	0.07	46	4082	2.9	0.86	1.2	2.5	1.7
0.03	0.16	0.06	0.13	0.02	0.18	0.03	2.7	0.15	16	2676	3.7	0.87	1.8	4.0	2.0
0.01	0.18	0.04	0.12	0.02	0.13	0.01	3.0	0.08	34	341	5.2	2.21	2.7	3.8	2.7
0.01	0.17	0.02	0.06	0.02	0.14	0.03	3.3	0.10	45	1332	5.1	1.5	2.2	3.3	2.3
0.03	0.36	0.03	0.17	0.04	0.23	0.04	4.0	0.11	54	2810	5.4	1.9	2.9	4.8	2.9
0.02	0.22	0.04	0.19	0.06	0.34	0.07	4.1	0.09	76	2223	3.7	1.3	1.8	2.6	3.0
0.03	0.20	0.06	0.21	0.04	0.30	0.02	5.8	0.15	8.7	4061	7.0	2.3	3.1	7.9	4.5
0.06	0.28	0.08	0.29	0.04	0.36	0.05	7.1	0.23	37	395	11	3.0	4.7	7.5	7.3
0.05	0.25	0.06	0.23	0.05	0.40	0.06	8.0	0.12	92	1362	13	7.3	7.9	6.4	6.8
0.08	0.34	0.08	0.25	0.07	0.41	0.06	8.2	0.24	54	3209	13	3.1	4.6	6.9	8.4
0.07	0.34	0.10	0.38	0.11	0.58	0.11	9.4	0.32	23	605	17	5.5	7.6	8.9	8.4
0.08	0.61	0.11	0.43	0.10	0.73	0.11	13	0.24	102	2566	18	5.3	7.3	11	12
0.11	0.61	0.15	0.37	0.10	0.49	0.11	15	0.34	9.5	2475	24	6.5	10	17	17
0.12	0.74	0.16	0.57	0.11	0.75	0.12	18	0.26	11	3381	24	7.9	10	15	17
0.08	0.70	0.10	0.55	0.07	0.72	0.12	19	0.21	45	2202	42	20	21	10	21
0.11	1.1	0.20	0.87	0.18	1.2	0.22	21	0.59	44	1524	28	6.3	10	20	21
0.18	1.5	0.21	0.79	0.19	1.2	0.19	29	0.43	28	150	37	8.8	14	34	26
0.26	1.6	0.37	1.1	0.27	2.0	0.34	33	0.80	34	1152	34	9.1	16	41	22
0.02	0.23	0.03	0.11	0.03	0.24	0.05	6.2	0.15	10	4022	10	3.0	4.2	5.7	8.0
0.08	**0.50**	**0.10**	**0.37**	**0.08**	**0.55**	**0.09**	**11**	**0.25**	**40**	**2135**	**16**	**5.1**	**7.0**	**11**	**10**
0.06	**0.43**	**0.09**	**0.30**	**0.07**	**0.48**	**0.08**	**9.1**	**0.19**	**27**	**1290**	**12**	**4.5**	**5.5**	**10**	**8.0**
0.26	**1.6**	**0.37**	**1.1**	**0.27**	**2.0**	**0.34**	**33**	**0.80**	**102**	**4082**	**42**	**20**	**21**	**41**	**26**
0.01	**0.08**	**0.02**	**0.06**	**0.02**	**0.13**	**0.01**	**2.4**	**0.07**	**8.7**	**150**	**2.9**	**0.86**	**1.2**	**2.5**	**1.7**
0.01	0.03	0.00	0.03	0.01	0.03	0.00	0.32	0.04	14.0	5942	0.35	0.16	0.16	0.10	0.10
0.01	0.03	0.01	0.02	0.01	0.04	0.01	1.01	0.10	7.3	5603	1.41	0.83	0.81	0.17	0.66
0.01	0.04	0.01	0.07	0.01	0.06	0.01	1.56	0.15	24.7	280	2.43	0.87	1.04	0.43	0.54
0.00	0.00	0.00	0.02	0.01	0.04	0.00	0.46	0.00	47.8	880	0.41	0.20	0.25	0.08	0.08
0.05	0.05	0.01	0.02	0.00	0.04	0.02	1.16	0.04	5.6	2268	1.15	0.31	0.53	0.48	0.22
0.01	0.09	0.02	0.09	0.01	0.10	0.03	2.82	0.05	6.5	2798	3.62	1.82	2.02	1.97	0.65
0.01	0.04	0.01	0.01	0.01	0.03	0.01	0.31	0.06	1.9	180	0.09	0.18	0.08	0.01	0.01
0.00	0.02	0.01	0.02	0.00	0.03	0.00	0.29	0.04	4.6	332	1.49	0.05	0.05	0.01	0.02
0.03	0.09	0.04	0.10	0.01	0.01	0.01	2.05	0.04	2.0	152	1.37	0.30	0.65	2.17	0.06
0.01	0.09	0.01	0.05	0.02	0.12	0.01	1.67	0.06	5.1	4986	3.02	1.25	1.49	2.28	0.37
0.01	**0.05**	**0.01**	**0.04**	**0.01**	**0.05**	**0.01**	**1.16**	**0.06**	**12**	**2342**	**1.5**	**0.60**	**0.71**	**0.77**	**0.27**
0.02	**0.03**	**0.01**	**0.03**	**0.01**	**0.03**	**0.01**	**0.86**	**0.04**	**14**	**2373**	**1.2**	**0.58**	**0.65**	**0.96**	**0.26**
0.05	**0.09**	**0.04**	**0.10**	**0.02**	**0.12**	**0.03**	**2.82**	**0.15**	**48**	**5942**	**3.6**	**1.8**	**2.0**	**2.3**	**0.66**
0.00	**0.00**	**0.00**	**0.01**	**0.00**	**0.01**	**0.00**	**0.29**	**0.00**	**1.9**	**152**	**0.09**	**0.05**	**0.05**	**0.01**	**0.01**
0.52	3.51	0.76	3.16	0.75	6.43	1.23	145	0.35	16.71	45	65.8	33.4	32.9	7.9	20
0.31	2.86	0.71	2.94	0.66	5.96	1.16	89	0.08	2.56	283	98.7	41.8	41.3	3.0	36
0.12	0.673	0.17	0.58	0.13	0.91	0.207	17	0.25	1.66	11	25.5	13.3	15.1	9.5	5.62
0.24	1.7	0.34	1.40	0.29	2.30	0.445	50	0.04	0.174	15	23.1	12.8	12.9	0.2	1.45
0.02	0.249	0.04	0.21	0.04	0.29	0.052	4	0.15	0.78	0.45	4.0	0.9	2.3	15.3	0.46
0.16	1.15	0.30	0.96	0.28	1.98	0.468	30	0.29	3.53	3.7	23.5	11.8	14.6	11.2	4.84
0.48	4.72	1.33	5.05	1.08	9.35	1.82	76	5.11	8.01	2.1	21.5	10.3	13.4	30.5	7.20
0.13	1.1	0.20	0.83	0.18	1.35	0.258	22	0.50	1.91	12	17.2	7.3	9.2	15.8	3.17
0.2	**2.0**	**0.5**	**1.9**	**0.4**	**3.6**	**0.7**	**54**	**0.8**	**4.4**	**47**	**35**	**16**	**18**	**12**	**10**
0.2	**1.6**	**0.4**	**1.7**	**0.4**	**3.3**	**0.6**	**47**	**1.7**	**5.5**	**97**	**31**	**14**	**13**	**9**	**12**
0.5	**4.7**	**1.3**	**5.1**	**1.1**	**9.4**	**1.8**	**145**	**5.1**	**17**	**283**	**99**	**42**	**41**	**30**	**36**
0.02	**0.25**	**0.04**	**0.21**	**0.04**	**0.29**	**0.05**	**4.01**	**0.04**	**0.17**	**0.45**	**4.03**	**0.9**	**2.33**	**0.23**	**0.46**
0.20	1.8	0.51	2.5	0.52	5.1	0.79	25	2.4	0.7	0.04	7.1	1.0	1.9	27	13
0.43	4.6	1.4	6.7	1.3	12	1.60	66	7.1	2.2	0.11	12	2.1	3.0	56	22
19	110	20	57	8.7	57	8.9	1962	20	9.8	1.15	57	9.2	14	1981	42
2.7	18	4.1	11	1.6	11	1.5	355	3.4	2.9	0.52	25	4.4	6.1	307	16
1.6	16	4.5	20	4.3	39	6.4	378	19	3.3	1.2	27	3.6	8.7	163	49
0.6	4.7	1.5	6.2	1.3	12	1.9	89	9.3	21	7.2	66	8.4	14	96	25
7.8	79	24	118	27	221	35	1326	125	21	2.1	93	13.2	22	886	401
0.34	3.4	0.96	4.1	0.79	7.70	1.3	46	5.6	1.0	0.16	7.8	1.1	2.1	36	17
0.13	1.4	0.36	2.0	0.44	5.72	0.53	27	3.3	0.78	0.11	3.1	1.1	1.0	20	11
1.96	11	2.3	6.2	0.86	6.35	0.88	183	2.2	1.2	0.08	15	2.6	3.7	260	5.9
0.14	0.27	0.09	0.40	0.07	0.70	0.10	11	0.30	0.09	0.11	1.5	0.3	0.43	6	1.3
0.11	0.84	0.09	0.41	0.14	0.54	0.09	20	<0.209	1.2	0.10	5.6	0.8	1.6	10	1.6
1.02	6.4	1.2	3.3	0.45	3.09	0.46	102	1.6	63	0.67	94	14	17	215	8.9
0.68	5.0	1.2	5.4	1.07	9.39	1.6	150	4.7	7.4	6.8	33	5	10	28	23
3.15	23	4.8	17	2.43	20	3.3	354	2.9	3.2	1.3	26	5.25	8.8	140	11
0.27	2.2	0.47	2.46	0.44	4.4	0.63	44	4.0	17	20	79	11	23	48	64
6.87	37	7.1	17	2.20	13	1.9	659	3.6	2.0	0.10	48	8.7	14	772	7.6
0.19	2.1	0.32	1.60	0.49	4.4	0.71	44	2.7	0.65	0.27	5.9	0.81	1.5	16	6.8
2.6	**18**	**4.2**	**16**	**3.0**	**24**	**3.7**	**325**	**13**	**8.8**	**2.36**	**34**	**5.1**	**8.5**	**282**	**40**
4.8	**30**	**6.9**	**29**	**6.2**	**51**	**8.1**	**522**	**29**	**15**	**5.0**	**31**	**4.5**	**7.4**	**494**	**92**
19	**110**	**24**	**118**	**27**	**221**	**35**	**1962**	**125**	**63**	**20**	**94**	**14**	**23**	**1981**	**401**
0.11	**0.27**	**0.09**	**0.40**	**0.07**	**0.54**	**0.09**	**11.36**	**0.30**	**0.09**	**0.04**	**1.53**	**0.33**	**0.43**	**6.43**	**1.30**
0.01	0.04	0.01	0.07	0.02	0.13	0.027	1.3	0.19	0.18	0.23	1.06	0.567	0.81	0.77	0.25
0.02	0.14	0.05	0.13	0.08	0.26	0.066	3.5	0.09	0.37	1.5	3.0	1.7	1.8	1.0	0.60
14	105	25	96	19	127	19	2487	10.24	2681	1236	1141	432	446	381	826
8.2	62	16	58	11	73	11	1399	2.1	1267	601	357	152	167	181	203
7.0	52	12	42	7.7	47	7.2	948	2.6	910	174	266	113	140	247	133

Early hematite (analysed in samples 845007 and 751008) replaces accessory magnetite and is characterised by strong enrichment in REE and Y (hereafter REY). The chondrite-normalised REE-fractionation trend (Figure 9a) is distinct, with a convex trend and a particularly strong negative Eu-anomaly (albeit somewhat smaller in sample 751008).

A second, later hematite generation occurs along veinlets and has a bladed appearance. This generation contains much lower ΣREY, and features a flatter chondrite-normalised REY-fractionation trend (Figure 9b), as well as a smaller, negative Eu-anomaly and negative Y-anomaly. The trends for sample 751008 appear relatively noisy due to the very low absolute REY concentrations. The Y-anomaly can readily be explained by the co-existence with hydrothermal fluorite (see below), as well as xenotime and other hydrothermal REY-bearing minerals into which Y will preferentially partition.

The two generations of hematite contain very different concentrations of other common, minor constituents. Figure 10a and b shows how the two generations may be

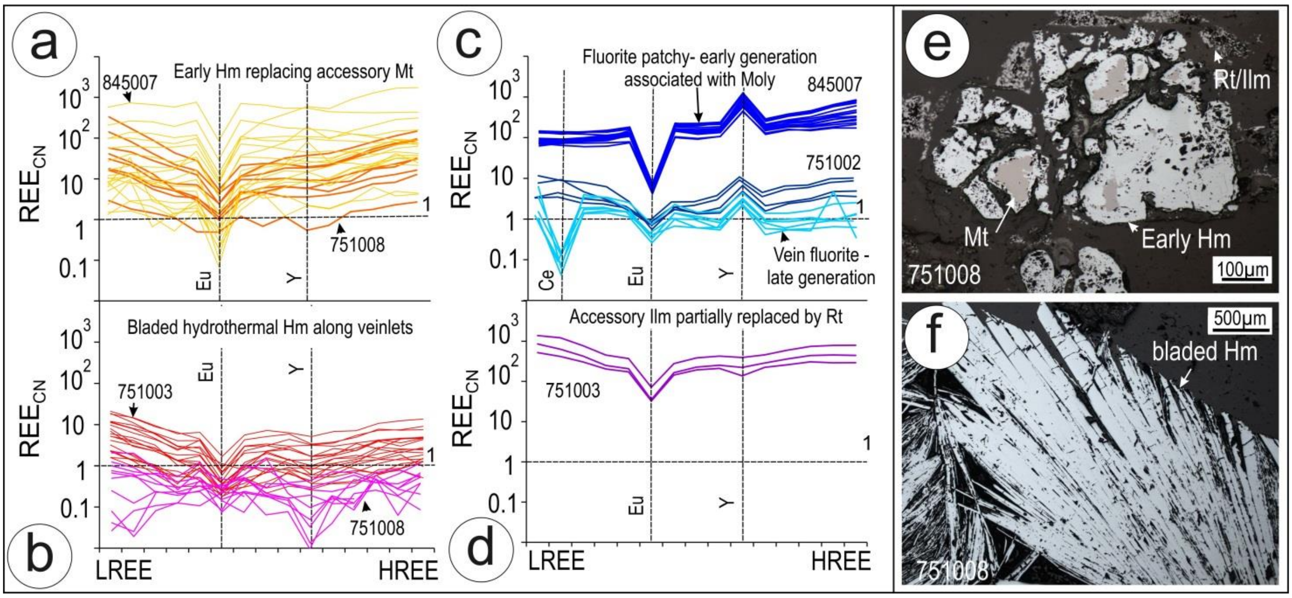

Figure 9 REY Fractionation trends for hematite and fluorite (a-d) and BSE images (e-f) showing the two textural types of hematite. See text for further details.

discriminated in terms of (Th+U) and U vs. (W+Sn+Mo). Note that Th concentrations are particularly high in this generation. The early generation has much higher (Th+U) but the second generation is characterised by enrichment of the granitophile elements by several orders of magnitude. The excellent correlation between (Th+U) and REY is depicted in Figure 10c. The much lower U and Th concentrations in the second generation hematite also relates to the presence of minerals such as coffinite into which Th and U will preferentially partition. Excellent discriminations between the two groups are seen on the plots of Ni vs. Cr (Figure 10d), V vs. Nb (Figure 10e), Mn vs. Co (Figure 10f) and Cr vs. Ti (Figure 10g). These differences are efficiently summarised in a final plot (Figure 10h), in which the relative enrichment in granitophile elements (U+Th+Sn+W+Mo) in the second generation contrasts with enrichment in transition elements (Co, Ni, Mn, Zn) in the early magnetite.

LA-ICP-MS element maps of the second generation of hematite typically occurring along veins (Figure 11) confirm the presence of elements of interest within the hematite, notably Sn, W, Nb, Ta, U and Th, as well as other elements more common in hematite such as Ti and V. The maps also show zonation with sets of zones perpendicular to the long axis of each lamella with respect to W, Sn, Nb, Ta, V. In contrast, other elements show heterogeneity relative to the overall aggregate of hematite, i.e., marked depletion in REY (Ce and Y shown), U and Th in the coarser lamellae. The two types of element distribution can be attributed to (i) primary growth and (ii) superimposed overprint, respectively. Potassium feldspar at the top of the map contains some albite which is seen to be a carrier of Sr and Ga; Ba is present in both types of feldspar.

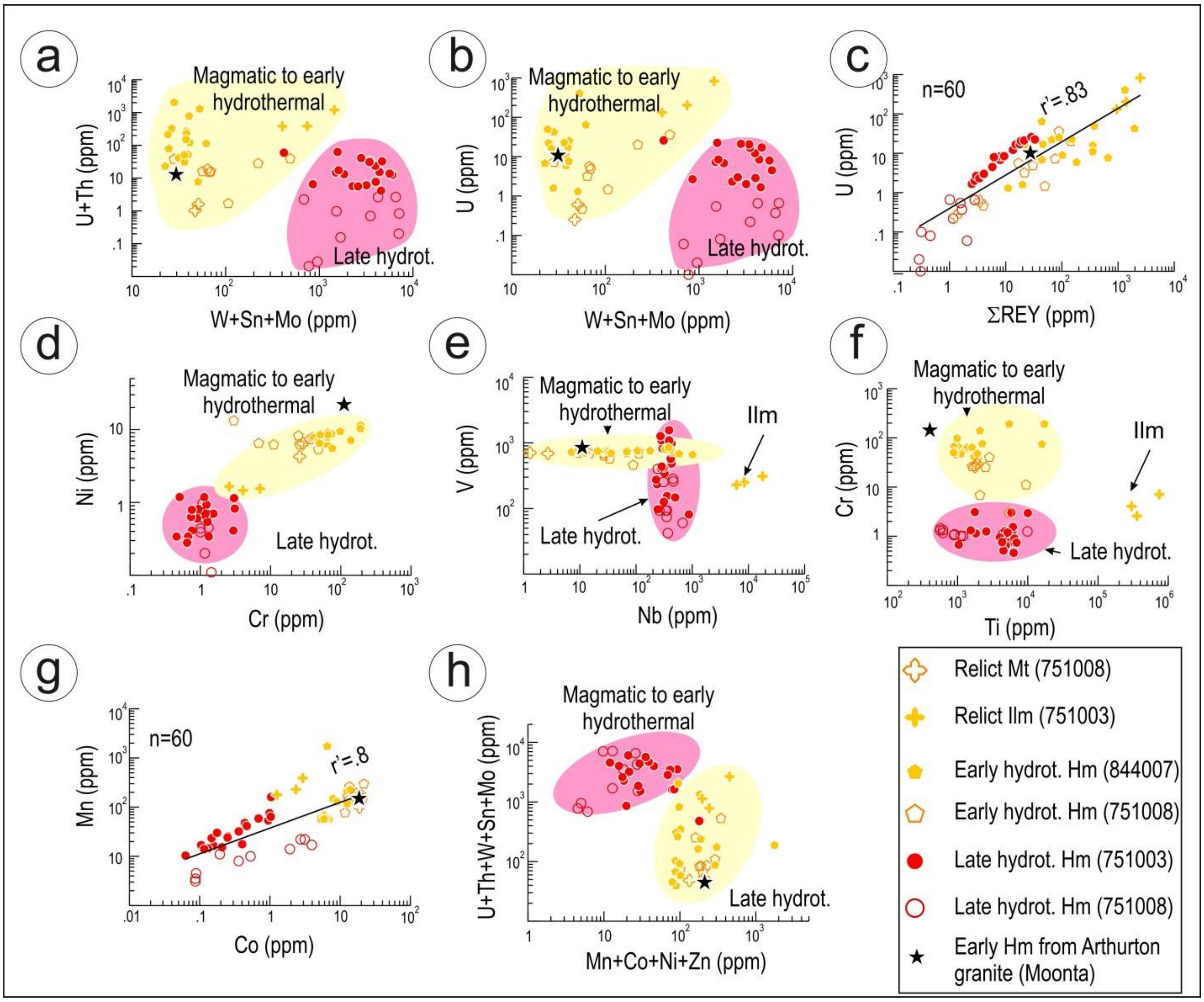

Figure 10 Geochemical discriminant diagrams for different types of hematite. See text for further details.

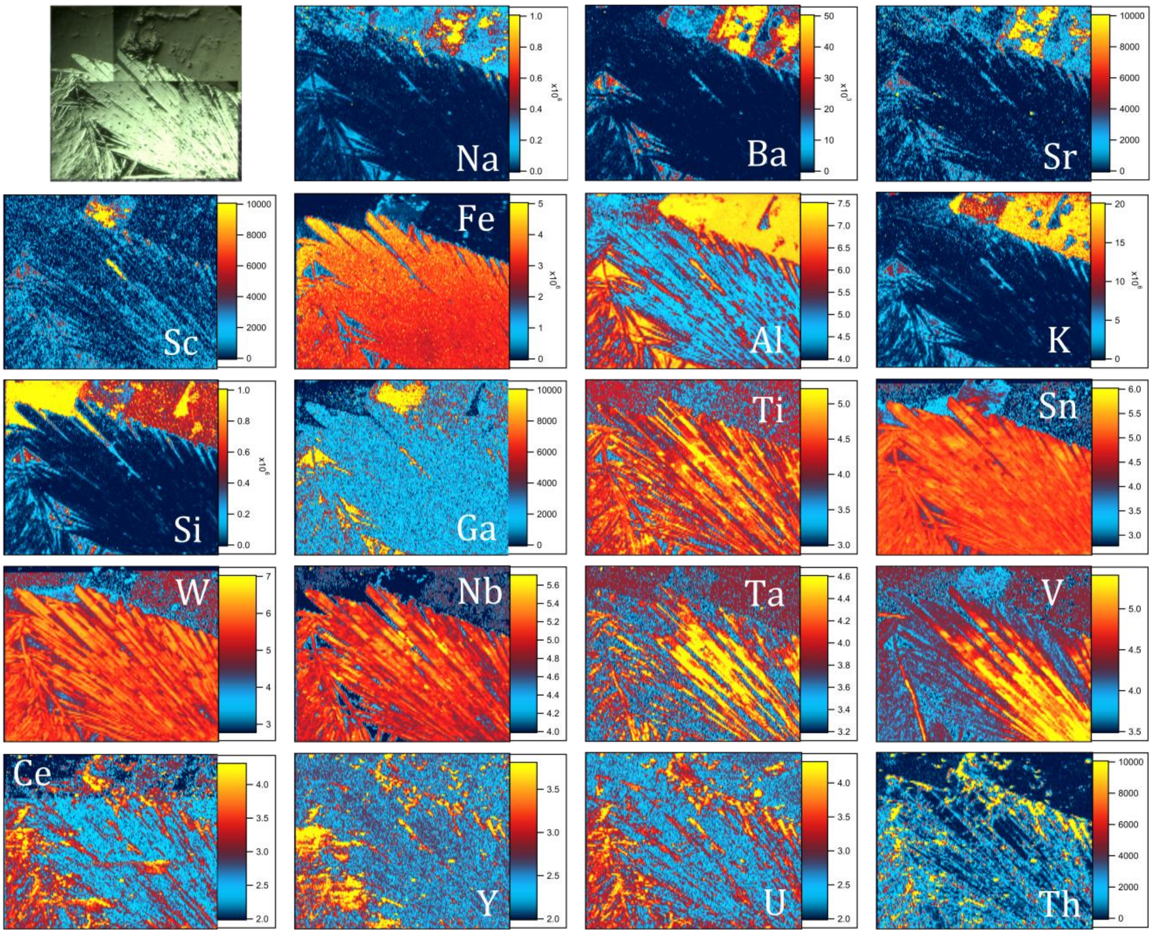

Figure 11 LA-ICP-MS element maps of bladed hematite (sample 751008). Note internal compositional zonation (sets of zones perpendicular to the long axis of each lamellae) with respect to Ti, Sn, W, Nb, Ta and V. Note that part of the aggregate is depleted in Ce, Y, U and Th. Note also partial replacement of Ba-bearing K-Feldspar (at the top) by albite. Scale bars are counts per second. Log scale bars are used for elements; Al, Nb, Sn, Ta, Ti, U V, W and Y. The log scale bars are 10^{n} where *n* is the number on the scale bar.

MAGNETITE AND ILMENITE

Trace element patterns for accessory magnetite are distinct, and broadly reflect partitioning with co-existing ilmenite. Analysed ilmenite is present as relicts undergoing decomposition to rutile. The mineral carries high concentrations of REY (Table 2). Chondrite-normalised REY-fractionation trends (Figure 9d) are flat with a strong negative Eu-anomaly.

Table 3 LA-ICP-MS data for rock fluorite.

	Mg	Al	Si	P	Sc	Ti	V	Cr	Mn	Fe	Co	Ni	Cu	Zn	Ga	As	Sr	Y	Zr	Nb	Mo	Sn	Sb
845007Fluor-1	24	<0.43	194	<15	<0.14	<4.1	<0.09	<0.92	19	485	5.6	0.11	<0.85	<1.2	<0.00	<0.82	5.9	688	<0.07	0.05	0.73	<0.08	<0.10
845007Fluor-2	28	0.97	197	<17	<0.17	<4.8	<0.11	<0.45	16	638	<0.15	0.32	1.9	<2.5	<0.09	1.3	6.9	710	<0.00	0.18	0.14	0.39	<0.17
845007Fluor-3	27	4.5	325	<12	0.21	12	<0.07	<0.55	19	659	1.8	0.59	1.2	46	<0.00	0.67	5.5	909	6.3	10	0.21	0.19	<0.06
845007Fluor-4	19	33	<127	<12	<0.15	<3.8	<0.12	<1.0	17	514	1.5	<0.37	<0.62	<1.1	<0.00	<0.85	5.4	936	<0.25	0.20	7.0	<0.07	0.10
845007Fluor-5	2385	3743	5013	13	3.6	29	4.7	0.42	49	6770	0.78	1.0	4.7	5.3	4.3	<0.62	7.2	892	2.8	13	6.7	0.44	<0.11
845007Fluor-6	17	0.99	<134	<15	0.20	4.0	<0.13	<0.90	15	540	0.16	0.50	<0.87	<1.5	<0.12	<0.80	5.1	1036	<0.00	0.03	0.30	0.09	<0.12
845007Fluor-7	17	<0.38	174	<13	<0.18	4.1	0.27	0.48	18	484	2.3	<0.45	<1.1	1.4	<0.00	<0.72	4.9	1070	0.02	0.13	0.18	0.07	<0.06
845007Fluor-8	6261	8102	10502	<19	2.7	9.1	15	<0.71	89	15947	27	1.4	2.31	8.4	12	1.3	11	1157	<2.6	2.0	0.11	0.86	<0.14
845007Fluor-9	14	2.8	204	<19	0.28	<5.2	<0.11	<0.74	15	539	1.2	<0.46	3.5	22	<0.07	<0.85	7.1	1248	<0.00	0.08	0.15	<0.09	<0.14
845007Fluor-10	12	89	533	<13	0.32	4.7	<0.07	<0.53	13	452	0.27	0.08	1.2	<1.2	0.08	0.84	12	1330	2.3	0.50	8.7	0.07	0.06
845007Fluor-11	210	311	909	14	0.54	<3.4	0.35	<0.40	24	1024	0.51	0.50	<0.69	<1.4	0.65	1.1	5.2	1303	<0.06	0.53	0.31	0.11	<0.06
845007Fluor-12	28	8332	18304	<19	0.55	<4.1	0.37	<1.2	13	775	0.45	0.33	<1.3	2.3	2.4	<0.87	12.7	1437	22	3.9	0.09	0.19	<0.18
845007Fluor-13	415	474	630	<14	0.43	<3.0	1.1	<0.64	19	1532	0.64	0.25	1.5	2.6	1.1	0.71	7.4	1619	0.14	0.20	0.02	0.10	<0.13
845007Fluor-14	23	<0.53	144	<17	0.30	<3.6	0.05	0.75	20	617	<0.17	0.50	<0.84	<1.5	<0.08	<0.78	7.0	1836	<0.00	0.10	0.11	<0.07	<0.12
845007Fluor-15	17	<0.56	<155	23	<0.21	<4.4	<0.05	<1.1	15	592	15	0.39	<1.3	6.0	<0.00	<0.94	8.1	1898	0.02	0.09	0.12	<0.09	<0.11
845007Fluor-16	14	0.82	180	<15	0.15	5.9	<0.09	<0.84	14	547	0.08	0.43	3.2	<1.8	<0.08	<0.70	8.3	1945	1.5	0.09	0.10	<0.09	<0.09
845007Fluor-17	13	<0.42	<135	<16	0.33	<3.7	<0.09	<0.59	14	551	2.0	0.29	<0.83	<1.7	<0.06	1.4	9.1	1993	<0.05	0.15	0.04	<0.08	<0.11
Mean (n=17)	**560**	**1758**	**2870**	**17**	**0.80**	**9.8**	**3.1**	**0.55**	**23**	**1922**	**4.0**	**0.48**	**2.4**	**12**	**3.4**	**1.1**	**7.6**	**1295**	**4.4**	**1.8**	**1.5**	**0.25**	**0.08**
S.D.	**1577**	**3196**	**5517**	**5.4**	**1.1**	**9.0**	**5.3**	**0.18**	**19**	**3914**	**7.5**	**0.35**	**1.3**	**15**	**4.5**	**0.32**	**2.3**	**432**	**7.6**	**3.8**	**2.9**	**0.25**	**0.03**
Maximum	**6261**	**8332**	**18304**	**23**	**3.6**	**29**	**15**	**0.75**	**89**	**15947**	**27**	**1.4**	**4.7**	**46**	**12**	**1.4**	**13**	**1993**	**22**	**13**	**8.7**	**0.86**	**0.10**
Minimum	**12**	**0.82**	**144**	**13**	**0.15**	**4.0**	**0.05**	**0.42**	**13**	**452**	**0.08**	**0.08**	**1.2**	**1.4**	**0.08**	**0.67**	**4.9**	**688**	**0.02**	**0.03**	**0.02**	**0.07**	**0.06**

	Ba	La	Ce	Pr	Nd	Sm	Eu	Gd	Tb	Dy	Ho	Er	Tm	Yb	Lu	Σ REY	Hf	Ta	W	^{206}Pb	^{207}Pb	^{208}Pb	Th	U
845007Fluor-1	0.14	17	40	5.6	28	11	0.23	21	3.4	26	7.1	26	3.7	28	4.3	**909**	<0.04	0.01	23	0.32	<0.03	0.07	0.24	0.28
845007Fluor-2	0.13	15	45	6.8	34	12	0.28	20	3.3	27	6.6	25	3.9	30	5.2	**943**	0.03	<0.00	16	0.38	0.06	0.09	0.21	0.31
845007Fluor-3	<0.00	20	54	8.4	42	16	0.26	29	4.5	34	8.2	30	5.0	38	7.0	**1206**	0.30	1.8	17	5.6	0.95	1.5	14	25
845007Fluor-4	<0.00	16	44	7.5	39	17	0.28	29	4.4	33	8.2	29	4.7	37	6.5	**1212**	<0.00	0.01	18	0.34	0.08	0.11	0.22	0.16
845007Fluor-5	2.22	31	77	11	52	20	0.42	32	4.8	35	8.7	31	4.5	34	5.7	**1239**	0.10	1.3	20	6.6	1.2	2.0	34	31
845007Fluor-6	<0.00	18	49	8.1	43	18	0.31	30	4.8	35	9.3	33	5.3	45	8.1	**1342**	0.04	<0.00	17	0.37	0.09	0.08	0.25	0.20
845007Fluor-7	<0.32	19	50	7.9	41	17	0.31	31	5.0	36	9.0	32	5.5	45	7.9	**1375**	<0.04	<0.00	17	0.24	0.10	0.13	0.24	0.15
845007Fluor-8	1.0	17	46	8.2	48	17	0.29	30	4.9	38	10	36	6.1	54	10	**1482**	<0.162	0.52	14	4.2	0.60	1.1	0.59	1.33
845007Fluor-9	<0.41	18	48	8.3	47	18	0.26	29	5.0	38	10	37	6.6	55	10	**1579**	0.04	<0.00	13	<0.06	0.07	0.06	0.18	0.09
845007Fluor-10	0.10	18	45	7.9	45	19	0.38	29	5.0	39	10	36	6.3	55	10	**1656**	<0.00	0.07	13	0.85	0.27	0.39	0.30	1.8
845007Fluor-11	<0.00	23	57	8.3	46	22	0.32	37	6.3	46	11	40	6.2	51	8.3	**1666**	0.04	0.04	21	0.69	0.06	0.11	0.29	1.6
845007Fluor-12	1.1	19	49	8.6	48	19	0.41	33	5.3	41	11	41	7.4	60	12	**1792**	0.63	0.65	12	2.6	0.77	0.90	5.0	4.3
845007Fluor-13	<0.28	22	56	9.3	52	20	0.40	33	5.7	42	12	44	8.2	74	15	**2012**	<0.033	0.01	11	0.60	0.07	0.18	0.19	0.14
845007Fluor-14	<0.48	34	85	13	68	25	0.42	41	7.4	52	14	54	10	93	18	**2351**	<0.00	0.02	17	0.20	0.07	0.12	0.34	0.17
845007Fluor-15	<0.00	33	81	13	69	27	0.39	45	7.3	57	14	57	11	96	19	**2428**	<0.00	<0.00	15	0.15	0.09	0.04	0.33	0.17
845007Fluor-16	<0.00	32	75	13	63	24	0.37	39	7.0	56	15	55	10	99	20	**2453**	<0.05	0.01	12	0.34	0.05	0.13	0.64	0.23
845007Fluor-17	<0.45	35	82	13	69	26	0.36	44	8.1	59	16	61	11	104	21	**2543**	0.01	<0.02	13	0.40	0.14	0.16	0.29	0.17
Mean (n=17)	**0.78**	**23**	**58**	**9.2**	**49**	**19**	**0.34**	**32**	**5.4**	**41**	**11**	**39**	**7**	**59**	**11**	**1658**	**0.15**	**0.40**	**16**	**1.5**	**0.29**	**0.42**	**3.3**	**4.0**
S.D.	**0.84**	**7.2**	**16**	**2.3**	**12**	**4.5**	**0.06**	**7.1**	**1.4**	**10**	**2.8**	**11**	**2.5**	**25**	**5.4**	**530**	**0.21**	**0.62**	**3.2**	**2.1**	**0.37**	**0.59**	**8.5**	**9.2**
Maximum	**2.2**	**35**	**85**	**13**	**69**	**27**	**0.42**	**45**	**8.1**	**59**	**16**	**61**	**11**	**104**	**21**	**2543**	**0.63**	**1.8**	**23**	**6.6**	**1.2**	**2.0**	**34**	**31**
Minimum	**0.10**	**15**	**40**	**5.6**	**28**	**11**	**0.23**	**20**	**3.3**	**26**	**6.6**	**25**	**3.7**	**28**	**4.3**	**909**	**0.01**	**0.01**	**11**	**0.15**	**0.05**	**0.04**	**0.18**	**0.1**

Table 4 LA-ICP-MS data for vein fluorite.

	Mg	Al	Si	P	Sc	Ti	V	Cr	Mn	Fe	Co	Ni	Cu	Zn	Ga	As	Sr	Y	Zr	Nb	Mo	Sn	Sb
751002Flvein-1	2.5	1.9	<175	27	<0.17	5.4	<0.07	<0.99	<0.86	93	0.2	<0.00	1.5	5.2	<0.09	21	10	36	0.31	<0.12	0.23	<0.09	<0.34
751002Flvein-2	4.9	223	837	121	<0.23	<2.1	<0.15	<1.6	17	1416	<0.19	<0.85	56	401	0.12	23	14	57	0.21	<0.00	0.19	<0.13	<0.40
751002Flvein-3	3.9	<0.73	890	<34	<0.23	<3.7	0.25	<1.7	1.3	95	<0.00	<0.98	<1.1	17	<0.11	30	16	45	0.10	0.05	0.10	<0.12	<0.30
751002Flvein-4	4.0	2.1	<126	<20	0.11	1.9	0.08	<1.0	0.73	102	0.2	1.3	1.9	2.4	<0.00	21	15	39	<0.00	9.1	0.23	<0.11	0.31
751002Flvein-5	4.8	4.9	616	46	<0.11	<2.05	<0.08	1.8	0.72	120	0.5	1.2	<0.62	22	<0.06	38	12	51	0.13	<0.00	<0.06	0.68	<0.18
751002Flvein-6	3.5	4.8	431	53	0.66	<3.0	<0.00	<0.59	<0.69	86	0.24	<0.39	<0.90	1.3	<0.11	<0.76	15	134	<0.06	<0.04	0.14	<0.11	0.25
751002Flvein-7	2.0	3.5	131	<18	<0.10	<3.0	<0.06	1.2	0.60	163	<0.06	<0.31	2.7	19	<0.06	0.67	15	234	<0.05	<0.00	0.10	<0.06	<0.16
751002Flvein-8	3.5	9.0	<106	<17	<0.11	<0.99	0.16	0.62	0.51	116	0.25	<0.40	<0.75	12	<0.08	1.8	13	191	<0.00	<0.03	0.28	<0.07	<0.18
751002Flvein-9	4.0	3.0	<148	<22	<0.14	<3.2	<0.06	<0.85	<0.72	97	<0.07	0.49	<1.0	80	<0.11	3.1	22	92	1.2	0.05	<0.07	<0.10	0.17
751002Flvein-1	2.4	5.9	270	81	0.3	<2.2	<0.06	<0.79	1.1	130	0.13	<0.00	1.74	48	<0.08	54	17	84	<0.00	0.07	0.96	0.08	1.1
Mean (n=10)	**3.6**	**29**	**529**	**66**	**0.36**	**3.6**	**0.16**	**1.2**	**3.2**	**242**	**0.25**	**0.98**	**13**	**61**	**0.12**	**21**	**15**	**96**	**0.39**	**2.3**	**0.28**	**0.38**	**0.46**
S.D.	**1.0**	**73**	**306**	**37**	**0.28**	**2.5**	**0.09**	**0.59**	**6.2**	**413**	**0.13**	**0.43**	**24**	**122**		**18**	**3.2**	**69**	**0.47**	**4.5**	**0.28**	**0.42**	**0.43**
Maximum	**4.9**	**223**	**890**	**121**	**0.66**	**5.4**	**0.25**	**1.8**	**17**	**1416**	**0.50**	**1.3**	**56**	**401**	**0.12**	**54**	**22**	**234**	**1.2**	**9.1**	**0.96**	**0.68**	**1.1**
Minimum	**2.0**	**1.9**	**131**	**27**	**0.11**	**1.9**	**0.08**	**0.62**	**0.51**	**86**	**0.13**	**0.49**	**1.5**	**1.3**	**0.12**	**0.67**	**10**	**36**	**0.10**	**0.05**	**0.10**	**0.08**	**0.17**

	Ba	La	Ce	Pr	Nd	Sm	Eu	Gd	Tb	Dy	Ho	Er	Tm	Yb	Lu	Σ REY	Hf	Ta	W	^{206}Pb	^{207}Pb	^{208}Pb	Th	U
751002Flvein-1	<0.00	2.0	0.31	1.3	6.6	1.6	0.11	1.9	0.19	1.4	0.19	0.76	0.11	9.1	0.07	61	0.05	0.01	0.34	0.14	1.0	<0.028	0.02	0.04
751002Flvein-2	7.0	19	0.25	4.4	18	2.7	0.15	2.9	0.41	2.2	0.50	1.5	0.26	1.4	0.33	110	<0.00	<0.00	0.44	1.1	0.61	0.53	0.07	0.71
751002Flvein-3	<0.63	2.8	0.37	1.8	9.4	2.3	0.21	2.0	0.34	1.3	0.42	0.86	0.18	1.4	0.21	68	0.15	<0.02	0.24	0.23	0.51	0.62	0.04	0.25
751002Flvein-4	0.36	3.6	0.56	1.7	8.6	2.2	0.19	1.2	0.20	1.2	0.28	0.77	0.13	0.9	0.14	61	<0.04	0.03	0.14	0.15	0.05	0.04	0.03	0.04
751002Flvein-5	0.43	2.4	0.16	1.3	7.5	2.3	0.15	2.8	0.36	1.9	0.45	1.3	0.23	1.5	0.31	73	0.05	<0.01	0.38	0.49	0.22	0.61	0.03	0.27
751002Flvein-6	<0.00	24	76	5.3	15	2.5	0.36	3.5	0.51	4.9	1.3	4.7	0.91	9.3	1.5	284	<0.00	<0.00	0.04	0.14	0.18	0.06	0.02	0.54
751002Flvein-7	0.86	9.2	33	3.4	15	3.2	0.46	5.8	1.1	11	3.0	13	2.2	21.3	3.4	358	0.05	<0.00	0.35	<0.02	<0.04	0.18	0.03	0.02
751002Flvein-8	<0.00	9.0	25	2.6	12	2.9	0.40	4.1	0.84	8.3	2.3	10	1.9	17	2.8	289	<0.00	<0.02	0.42	0.18	<0.03	0.02	<0.01	0.17
751002Flvein-9	<0.00	38	72	9.7	36	4.4	0.27	4.1	0.49	3.5	0.89	4.2	0.79	7.1	1.0	274	0.06	0.02	0.09	0.93	0.86	0.30	0.04	0.72
751002Flvein-1	<0.00	9.6	0.66	3.7	18	4.1	0.38	4.9	0.54	3.9	0.77	2.3	0.42	4.1	0.69	138	<0.00	0.06	1.5	3.0	1.44	1.75	0.21	2.59
Mean (n=10)	**2.2**	**12**	**21**	**3.5**	**15**	**2.8**	**0.27**	**3.3**	**0.5**	**3.9**	**1.0**	**4.0**	**0.71**	**7.3**	**1.0**	**172**	**0.07**	**0.03**	**0.39**	**0.70**	**0.61**	**0.46**	**0.05**	**0.54**
S.D.	**3.2**	**12**	**31**	**2.6**	**8.6**	**0.88**	**0.12**	**1.4**	**0.3**	**3.3**	**0.93**	**4.4**	**0.75**	**7.0**	**1.2**	**116**	**0.04**	**0.02**	**0.40**	**0.92**	**0.48**	**0.54**	**0.06**	**0.77**
Maximum	**7.0**	**38**	**76**	**9.7**	**36**	**4.4**	**0.46**	**5.8**	**1.1**	**11**	**3.0**	**13**	**2.2**	**21**	**3.4**	**358**	**0.15**	**0.06**	**1.5**	**3.0**	**1.4**	**1.8**	**0.21**	**2.6**
Minimum	**0.36**	**2.0**	**0.16**	**1.3**	**6.6**	**1.6**	**0.11**	**1.2**	**0.2**	**1.2**	**0.19**	**0.76**	**0.11**	**0.94**	**0.07**	**61**	**0.05**	**0.01**	**0.04**	**0.14**	**0.05**	**0.02**	**0.02**	**0.02**

FLUORITE

Two types of fluorite can also be distinguished in terms of REY chemistry. The first type of fluorite (Table 3), occurring as patches and co-existing with molybdenite, is shown to be a significant carrier of REY, with consistent concentrations of ~1000-2000 ppm (ΣREE + Y) in the 17 analytical spots (Table 3a). The chondrite-normalised REY-fractionation trend for fluorite (Figure 9c) is distinct, with a generally flat trend and pronounced negative Eu-anomaly and positive Y-anomaly, consistent with published REY data for fluorite (e.g. Gagnon *et al.* 2003). The second type of fluorite, restricted to the wider veins, is characterised by significantly lower ΣREY. Chondrite-normalised REY-fractionation trends are flat and similar to type I except for a marked negative Ce-anomaly typical for grains along the vein margin. In both types, the measured concentrations of other elements in fluorite are generally low. Minor although inconsistent concentrations of Mg, Fe and Si are noted - possibly attributable to µm-scale mineral inclusions. Based on these marked differences two generations of fluorite can be suggested, where the second type implies REDOX changes in the fluids.

U-Pb geochronology

ZIRCON U-PB

Zircon U-Pb geochronology was conducted on zircon *in-situ* from polished blocks of the samples 751002, 751002, and 845007. SEM images show that zircon grains from all three samples are heavily cracked with obvious visual evidence of crystal damage via metamictisation (Figure 4i and Figure 7j). The grains range in morphology from rounded to acicular. Laser ablation spots were placed on all identifiable zircon grains identified in the polished blocks, two zircon grains in 751002, four in 751003, and four in 845007. Multiple spots were placed on each zircon grain in the hope of forming internal isochrons as poor data quality was predicted given the visual evidence of heavy alteration. Model 1 discordia lines were fit through data for each grain and are displayed in Figure 12. Most zircon display a very poor fit with high scatter and high common lead content (Appendix B1). As such upper intercept ages calculated are to be taken as reconnaissance only. Despite this it is apparent that many of the zircon grains targeted represent an inherited component to the granite samples, each giving different ages outside of error. Samples of Samphire Granite have been previously dated as Hiltaba in age with two interpreted ages of 1584 ± 4 and 1585 ± 6 (Jagodzinski & Reid in press).

Sample 751003

Four separate zircon grains were targeted from this sample. Common lead contents ranged from low to high from grain to grain, and within each grain (Appendix B1). Each grain displays a distinctly different discord albeit with large errors. Grain one gives an upper intercept of 1136 ± 360 Ma, grain two 1480 ± 97 Ma, grain three 2594 ± 91 Ma, and grain four 2391 ± 780 Ma. Little emphasis can be placed on the calculated absolute ages. Despite the very large errors on each discord it is apparent that each forms its own distinct discord line, suggesting differing ages for each grain, and/or different components of common lead addition.

Sample 751002

Two separate zircon grains were targeted from this sample. Common lead contents for all analyses were high (Appendix B1). High scatter of analyses are apparent once plotted on a conventional Concordia diagram (Figure 12). Analyses were separated by grain as per the previous sample. Grain one gives an upper intercept age of 2838 ± 330 Ma, and the three analyses of grain two give a similar upper intercept age of 2480 ± 110 Ma.

Sample 845007

Four separate zircon grains were analysed in this sample, with common lead components ranging from moderate to high. An internal discordia line was only calculated for grain 1 given the small number of analyses conducted on the remaining three grains (Appendix B1). The single grain gives an upper intercept age of 1902 ± 170 Ma, and a weighted average $^{207}Pb/^{206}Pb$ age of 1764 ± 80 Ma.

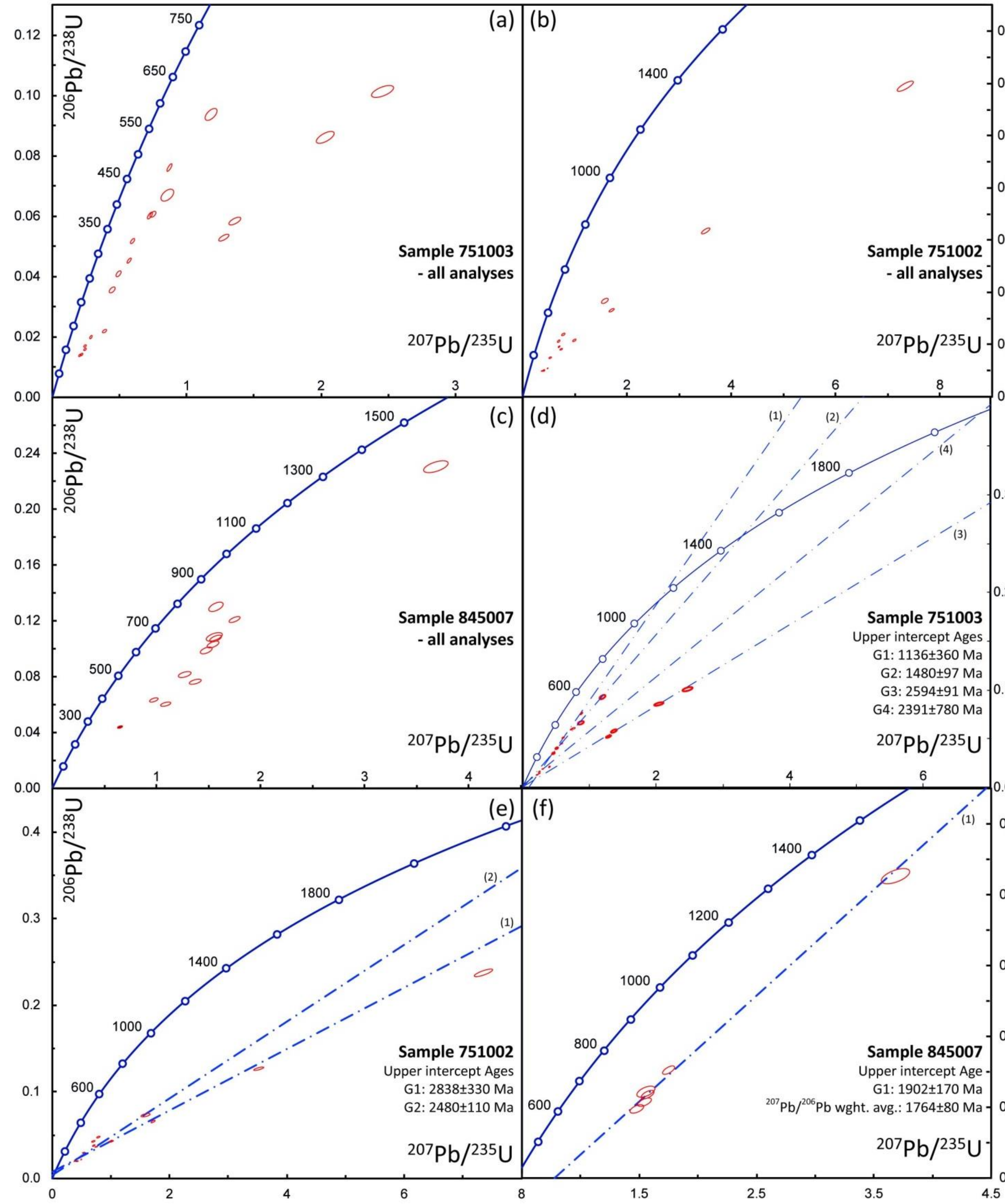

Figure 12 Zircon Concordia. (a) 751003 zircon concordia all spots; (b) 751002 zircon concordia all spots; (c) 845007 zircon concordia grain 1; (d) 751003 zircon concordia separated by grain; (e) 751002 zircon concordia separated by grain; (f) 845007 zircon concordia separated by grain. All ellipses are 68.3% confident

THORITE U-PB

Similar to the zircon analyses, thorite U-Pb analysis was conducted *in-situ* from polished blocks of samples 751002 and 751003. Reflected light images show variable amounts of cracks and changing reflectivity, possibly indicating zonation and variable alteration. Grains were large rounded to oblong in morphology. Multiple analytical spots were placed on two grains from each of the samples. Their large size and the reduced laser spot used allowed many analytical points to be placed on all grains. When plotted on a conventional concordia diagram analytical points from each of the two grains from sample 751003 displayed slightly different discord trends and thus were treated separate. Analytical points from the two grains of sample 751002 also displayed two separate trends, however analytical spots from each “age group” were present in each of the two grains, thus data for 751002 was separated based on their “age group”. Most data displayed moderate to high common Pb contents, and as with zircon the ages display high scatter and are taken as reconnaissance only.

Sample 751003

Two separate thorite grains were targeted from this sample, with common Pb contents ranging from low to high from grain to grain and within each grain (Appendix B2). Grain one gives an upper intercept of 2265 ± 79 Ma with a weighted average $^{207}Pb/^{206}Pb$ age of 2314 ± 25 Ma. Grain two gives an upper intercept of 2452 ± 290 Ma with a weighted average $^{207}Pb/^{206}Pb$ age of 2645 ± 140 Ma.

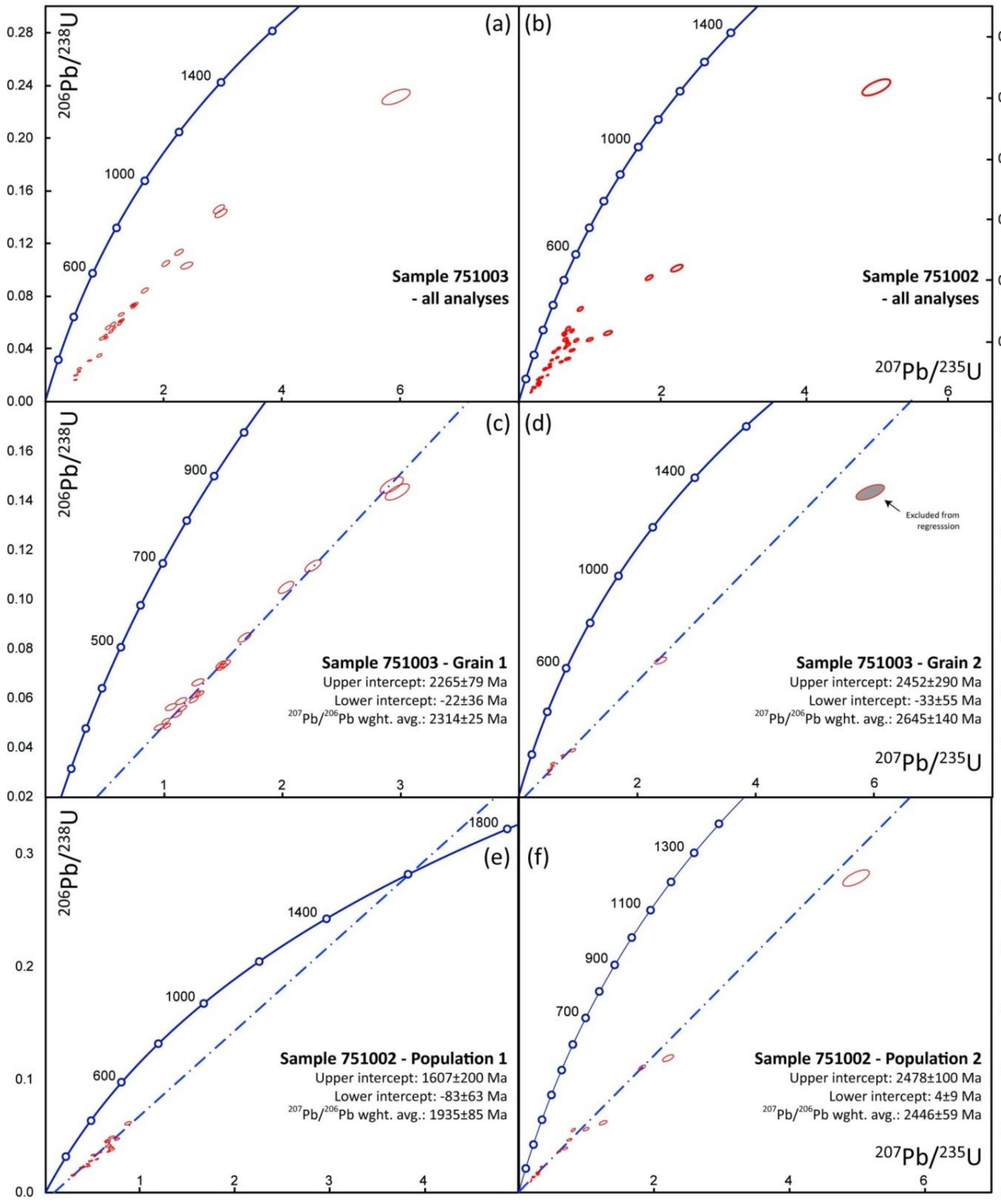

Figure 13 Thorite Concordia. (a) 751003 thorite Concordia all spots; (b) 751002 thorite Concordia all spots; (c) 751003 thorite Concordia grain 1; (d) 751003 thorite Concordia grain 2; (e) 751002 thorite Concordia population 1; (f) 751002 thorite Concordia population 2. All ellipses are 68.3% confidence

Sample 751002

As with the previous sample, two separate thorite grains were targeted from this sample. Common Pb contents for analyses were low to high (Appendix B2). As mentioned above, these data were separated based on their apparent “age groups”, with analyses from each age group present in each grain. High scatter of analyses are apparent once plotted on a conventional Concordia diagram (Figure 13). Population one gives an upper intercept age of 1607 ± 200 Ma with a weighted average $^{207}Pb/^{206}Pb$ age of 1935 ± 85 Ma. Population two give an upper intercept age of 2478 ± 100 Ma and weighted average $^{207}Pb/^{206}Pb$ age of 2446 ± 59 Ma, similar to that of sample 751003.

HEMATITE U-PB

Hematite U-Pb analysis was conducted *in-situ* from polished blocks of samples 751003 and 751008. As discussed above, an early and late phase of hematite was identified and targeted for U-Pb analysis in an effort to determine the age of each phase. Multiple analytical spots were placed on multiple grains from each of the samples. Their large size allowed a large spot size to be utilised on all grains. Due to the same textural relationships between the early and late phase iron oxide, data from both samples were combined. When pooled and plotted on a conventional concordia diagram, analytical display a very large amount of scatter (Figure 14). This is due to the very low level of uranium in the some of the late phase hematite, in addition to the moderate to large amounts of common lead in all analyses. Following the same methods as what was previously successfully employed to hematite dating (Ciobanu *et al.* 2013), data was filtered based on uranium and common lead content. Analyses that returned less than 1000 cps uranium, or a $^{204}Pb/^{206}Pb$ count ratio >0.1, were excluded from age calculations (Appendix B3). In addition grains that were highly reversely discordant were excluded. The remaining data was almost solely from the late hematite phase, and as a result the single point from the early phase was pooled with the late. The resultant data displays a very poor discord line with an upper intercept of 3215 ± 130, and a weighted average $^{207}Pb/^{206}Pb$ age of 3071 ± 90 Ma.

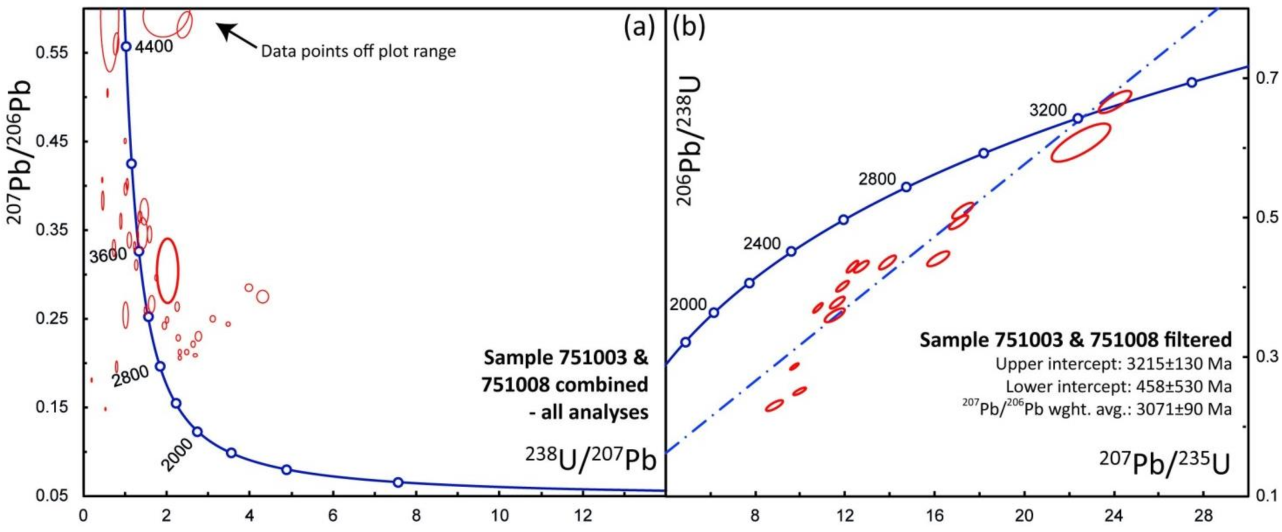

Figure 14 Hematite Concordia. a) 751003 and 751008 all data. Note some spots lie off displayed plot area; b) 751003 and 751008 data filtered as per relevant text. All ellipses are 68.3% confident.

DISCUSSION

A conceptual model for bedrock mineralization within the Samphire project area needs to consider all information, including geological, petrographic, mineralogical and geochronological data. Derivation of a genetic model is dependent on the critical evaluation of all available evidence.

The mineral assemblages observed in altered granite and within the crosscutting 'epithermal' fluorite veins hosted by the granite sampled here closely resemble those identified in IOCG-style mineralization throughout the eastern parts of the Gawler Craton (Conor *et al.* 2010; Hayward & Skirrow 2010). IOCG-style mineralization of Hiltaba-age is known on the Eyre Peninsula as far west as the Middleback Ranges, where it occurs at the Moola and Princess prospects within mining tenements held by Arrium (Feltus et al. in press). Other base and precious metal prospects discovered in the Central Eyre region in recent years (e.g. in the Paris and Menninnie Dam areas), even if not considered as IOCG systems, do show a spatial affinity with 1.6 – 1.575 Ga Hiltaba Suite Granites or Gawler Range Volcanics, and are thus cautiously interpreted as the products of the same metallogenic event.

Alongside fluorite, base metal sulphides (including molybdenite) and hematite, complex mineral associations containing rare earth elements, uranium and thorium, as well as HFSE and other granitophile elements (W, Sn, Mo) have been observed in this study (Figures 4-8). Based on these characteristics it is reasonable to interpret the bedrock mineralization as related to the host granite. However, despite the fact that the petrographic and mineral signatures are broadly comparable with those known from other IOCG deposits and prospects in the Olympic Province, the reconnaissance zircon, thorite and hematite geochronological data shows inherited ages that are older than the ~1.6 Ga age of the Hiltaba Suite.

Petrography and mineral geochemical signatures

The LA-ICP-MS trace element data presented here shows that there are two distinct generations of hematite expressed in both textural and compositional terms: (i) an early generation which replaces accessory magnetite + ilmenite, and is characterised by enrichment in REY and U; and (ii) a clearly later (hydrothermal) generation of hematite (along veinlets, bladed appearance) that is enriched in other granitophile elements (W+Sn+Mo) relative to the first generation (Figure 10a). A known mechanism of alteration within IOCG-type mineralization is hematite replacing magnetite, which is associated with an early, deep to late, shallow trend (Mark *et al.* 2006; Bastrakov *et al.* 2007).

The early alteration of granite comprises mineralogical features (albite lamella in K-feldspar), similar to those reported for Hiltaba granites from the Moonta area during albitization (Kontonikas-Charos *et al.* 2014). The geochemical signature of hematite replacing accessory magnetite in the Arthurton granite (Moonta area; Ciobanu 2013 DET CRC unpublished report) is also comparable to that within the Mullaquana granite here (Figure 10). Zonation patterns and enrichment in W, Sn, Mo in the second generation of hematite is comparable to U-bearing hematite from mineralised breccias at Olympic Dam (Ciobanu *et al.* 2013). The depletion in REY relative to first generation of hematite can be attributed to preferential partitioning into REY-minerals such as thorite, and also fluorite. The relative U-depletion can be attributed to partial remobilisation of this element (Figure 11).

Petrographic data and chondrite-normalised REE fractionation patterns for fluorite also point to the likelihood of two generations of fluorite. This raises the question of what each of these generations represent, and what is their relative timing. Moreover the pronounced negative Ce-anomaly in vein fluorite, as well as the lower REY budget, indicates fluids which are distinct from those related to the earlier phase of alteration and molybdenite deposition.

Figure 15 proposes a sequence of hydrothermal alteration within the Samphire Granite. The presence of calcite and halite suggest some interesting possibilities for evolving fluid compositions and sources within the alteration sequence. IOCG ore fluids have been shown to be variable and contain high salinity with significant volatile (H_2O, CO_2 and F) contents (Kendrick *et al.* 2007; Reid *et al.* 2009; McPhie *et al.* 2011a; McPhie *et al.* 2011b). Fluid mixing models have been proposed (e.g. Haynes *et al.* 1995) between magmatic source fluids and meteoric/surficial brines.

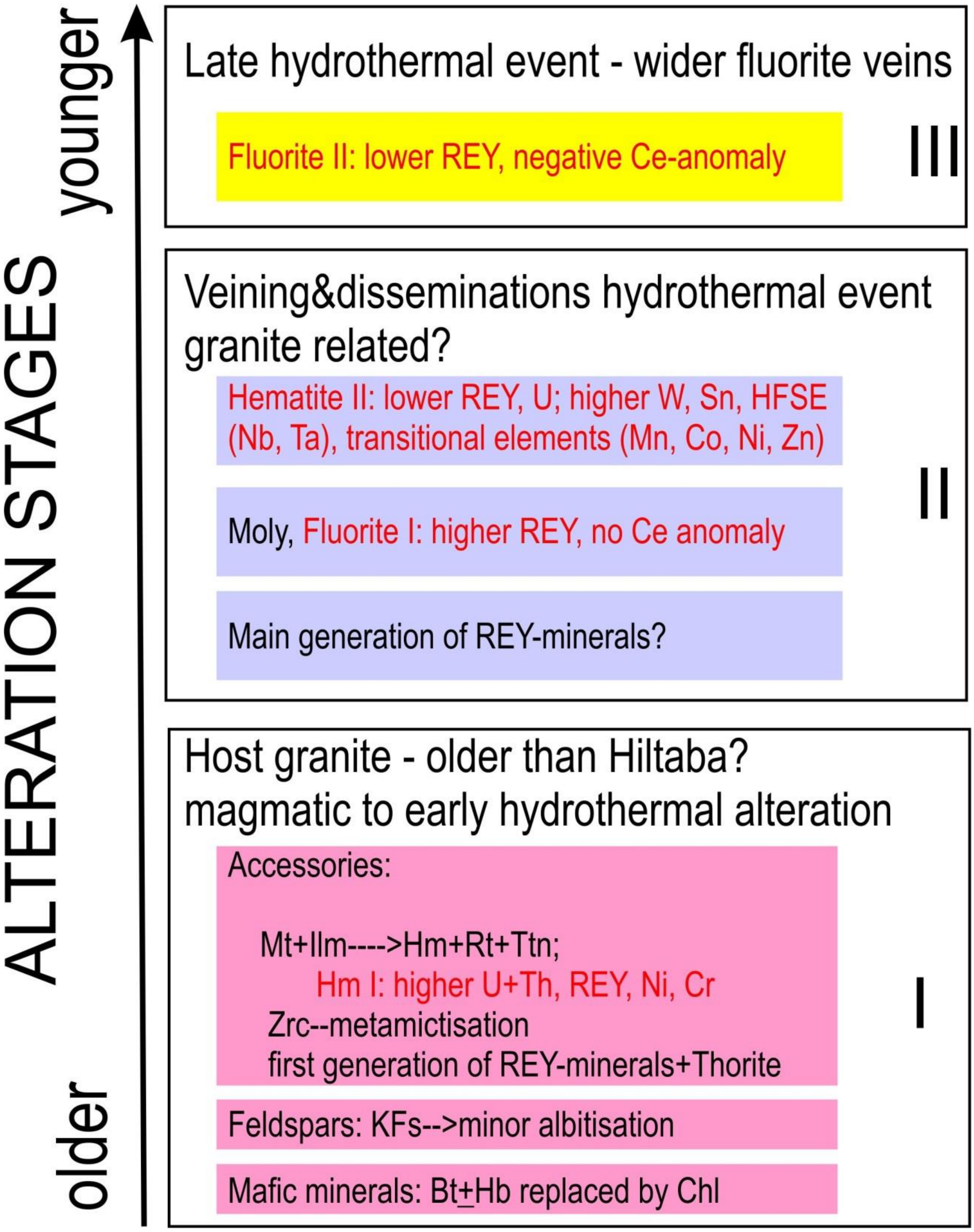

Figure 15 Schematic diagram summarasing results of this study in the context of the propsed geolocial evolution.

Geochronological constraints

Direct evidence for the age of granites underlying the Samphire prospect is available in the form of U-Pb SHRIMP zircon data of samples from drillholes MRC005 and MRC009 (Jagodzinski and Reid, in press) intersecting the Mullaquana granite. These gave interpreted ages of magmatic crystallization of 1584 ± 4 Ma and 1585 ± 6 Ma, respectively. These two drillholes are ~1 and ~10 km SE of the area covered in the present study.

The reconnaissance geochronological data presented here is in poor agreement with the results of Jagodzinski & Reid (in press). The ages determined for thorite (Pb/Pb ages of 2.6-2.3 and 1.935 Ga) and hematite (Pb/Pb ages older than 3.0 Ga?) are all significantly older than expected, which could be interpreted as inherited uranium and thorium. The upper intercept zircon ages and average Pb-Pb ages display a broad range from Archean to later Proterozoic.

These results should be interpreted with caution for a number of reasons: (i) metamictization of the zircons; (ii) use of non-matrix-matched zircon standards for thorite and hematite; (iii) the relatively small number of grains analysed; and (iv) a high proportions of common lead in many of the analysed grains. They are nevertheless sufficiently different and internally consistent to warrant interest. It is also important to note there are no grounds to suspect instrumental problems, given that ‘expected’ ages were determined on other samples using identical methodology during the same LA-ICP-MS runs. Thorite has been shown to be a robust and accurate geochronometer well suited to LA-ICP-MS U-Pb analysis, and without any evidence for isotopic inheritance (Cottle 2014).

One plausible interpretation is that the granite sampled and dated in this study is not the same as that analyzed by Jagodzinski & Reid (in press) and that the bedrock in the vicinity of Samphire (broadly considered as the Samphire batholith) is populated by granites of different ages despite similarity in appearance. The granite body strikes 35 km N-S and is clearly delineated by magnetic imagery. It has, until now, been considered to be a composite body but nevertheless to have a shared age. Interestingly, Uranium SA have shown that certain petrogenetic indicators differ from the Hiltaba average, notably concentrations of high field strength elements, high K/Rb and high Rb/Sr.

A second possibility is that the Samphire granite incorporates fragments or xenoliths of older granites or other felsic igneous rocks. Indirect support for this interpretation comes from the observation (Figure 3) of more porphyritic varieties within an otherwise homogeneous rock.

Further work is required to validate the ages obtained here as they potentially provide tantalising evidence for introduction of U-Th-bearing assemblages during Archean to Paleoproterozoic time into this portion of the Gawler Craton, well before the Hiltaba event at 1.6 Ma. Future work might also attempt to constrain the age of the fluorite veins relative to the host granite. The presence of abundant and relatively coarse-grained molybdenite within those veins opens up the possibility of using Re-Os geochronology to constrain the age of mineralization (Reid *et al.* 2013).

There exists a good precedent for pre-Hiltaba aged granites in the eastern part of the Eyre Peninsula. Fraser *et al.* (2010) have given U–Pb SHRIMP zircon ages and Sm–Nd isotopic evidence for early Mesoarchean (∼3150 Ma) crust which covers an area of at least ∼1500 km^2. The Cooyerdoo Granite sample analysed by Fraser *et al.* (2010) was collected ~50 km NW of the Samphire property.

Towards a genetic model

Several sub-styles of uranium mineralization occur on the Samphire property. The largest tonnage (the Blackbush deposit) occurs in the Eocene-Miocene cover sequence, particularly within Eocene Kanaka beds that lie immediately above the unconformable top of the granite (Figure 16). More recently, higher-grade mineralization has been recognised within the unconformity zone itself. A third type of uranium mineralisation (so-called ‘bedrock mineralization’) is restricted to decompression structures in clay-altered granite and saprolite, with the best grades in shallow-dipping structures within the granite.

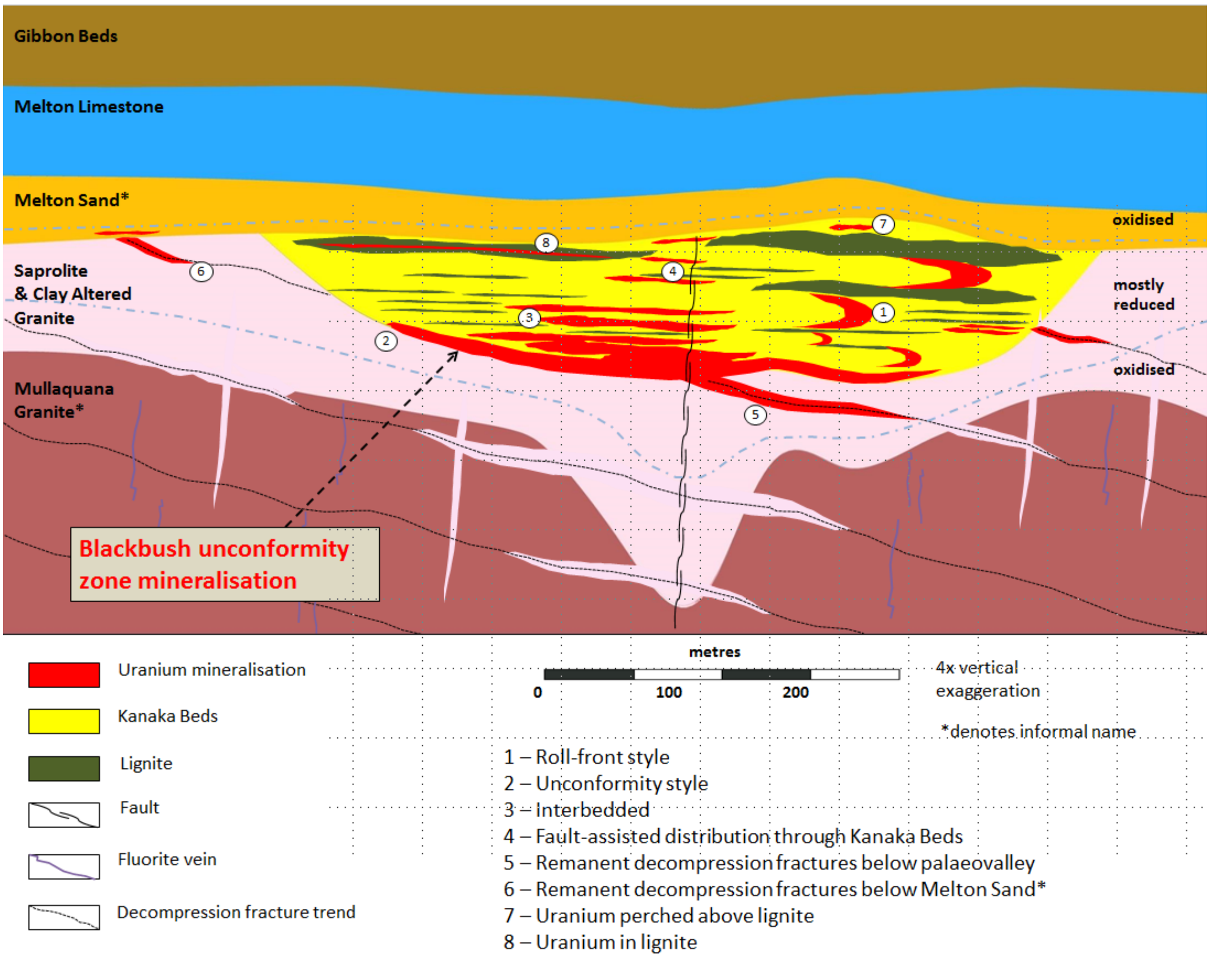

Figure 16 Schematic cross-section showing location of uranium of uranium mineralization in the Samphire project area relative to bedrock (Uranium SA 2013)

In the currently held genetic model to explain all uranium mineralization on the Samphire property, the uranium in the cover sequence, at the granite-cover unconformity, and in clay-altered granite was originally sourced in the underlying granite and was driven into the cover at some time after sedimentation of the latter. According to Uranium SA presentations, and based on the work of Schofield (2010), the granite is considered to hold potential for larger reserves of disseminated magmatic-related uranium. In this model, the fluorite veins are considered to have played a role as conduits for upwards migration of U-bearing fluids.

The present study shows changes in the signatures of key alteration minerals (Fe-oxides, REY-minerals, fluorite) from the basement granite, supporting recycling of U, granitophile elements (W, Sn, Mo) and REY concurrent with the above idea that the granite is host and a potential source for U mineralisation, whether within clay-altered granite or in the cover. The low U content in fluorite relative to other coexisting minerals such as hematite in stage II indicates this is not necessarily the key pathfinder for U pathways. The observed trace element recycling is concurrent with a sequence of superimposed magmatic and tectonic events in this area.

Practical implications

The study suggests that the bedrock geology of the Samphire project area may be more complex than previously considered. This has implications for a conceptual genetic model and also for ongoing exploration of bedrock-hosted mineralization in the Samphire deposit, including the 2014 discovery of mylonite-hosted uranium mineralization (Dragon prospect), 4 km west of Blackbush and likely part of the regional, 1730–1690 Ma Kalinjala Mylonite Zone (Dutch *et al.* 2008).

Geochemical fingerprinting of Fe-oxides is increasingly used in ore geology, not only to discriminate between different deposit types (e.g. Dupuis & Beaudoin 2011) but also to recognise temporally-distinct generations of mineralization with metallogenically complex terranes (e.g. Ciobanu *et al.* 2013), or where mineralization events have been superimposed on one another. The data for hematite presented here represent a valuable contribution to ongoing work aimed at establishing a framework for distribution patterns in Fe-oxides in South Australian IOCG deposits and in other types of iron-bearing ore systems.

CONCLUSIONS

Mineralogy and textural relationships have been determined in altered granite and crosscutting fluorite veins. The assemblages, comprising fluorite, base metal sulphides and hematite, and minerals containing REE, U and Th are comparable with those found in IOCG mineralization across the eastern Gawler Province.

LA-ICP-MS trace element data for hematite and fluorite show geochemically and texturally distinct generations, raising the possibility of multiple mineralization events.

Reconnaissance U-Pb geochronology of zircon, hematite and thorite has given a range of Archean-Paleoproterozoic ages, all of which are significantly older than the anticipated ~1.6 Ga. This raises the possibility that there are older granites, or fragments thereof in the region, and that uranium could have been introduced early in the crustal history of the region.

ACKNOWLEDGMENTS

A big thank you to my supervisor Nigel Cook and co-supervisor Cristi Ciobanu for their support, experience and patience. With a special thanks to Ben Wade from Adelaide Microscopy without whom this wouldn’t have been so exciting. Thanks to Uranium SA, Russel Bluck and Callan Brown for their contribution and providing the project. Adelaide Microscopy, Ken Neubauer, Aoife McFadden, Katie Howard and Ros King for equipment training and support throughout the year get my final thanks. Thank you all.

REFERENCES

AGANGI A., KAMENETSKY V. & MCPHIE J. 2012. Evolution and emplacement of high fluorine rhyolites in the Mesoproterozoic Gawler silicic large igneous province, South Australia. *Precambrian Research* 208-211, 124-144.
AGANGI A., KAMENETSKY V. S. & MCPHIE J. 2010. The role of fluorine in the concentration and transport of lithophile trace elements in felsic magmas: Insights from the Gawler Range Volcanics, South Australia. *Chemical Geology* 273, 314-325.
BARTON M. D. 2014. 13.20 - Iron Oxide(–Cu–Au–REE–P–Ag–U–Co) Systems. *In:* Holland H. D. & Turekian K. K. eds., *Treatise on Geochemistry (Second Edition)*, pp 515-541, Elsevier, Oxford.
BASTRAKOV E. N., SKIRROW R. G. & DAVIDSON G. J. 2007. Fluid Evolution and Origins of Iron Oxide Cu-Au Prospects in the Olympic Dam District, Gawler Craton, South Australia. *Economic Geology* 102, 1415-1440.
BELPERIO A., FLINT R. & FREEMAN H. 2007. Prominent HIll: A Hematite-Dominated, Iron oxide copper-Gold System. *Economic Geology* 102, 1499-1510.
BETTS P. G., GILES D., LISTER G. S. & FRICK L. R. 2002. Evolution of the Australian lithosphere. *Australian Journal of Earth Sciences* 49, 661-695.
CIOBANU C. L., WADE B. P., COOK N. J., SCHMIDT MUMM A. & GILES D. 2013. Uranium-bearing hematite from the Olympic Dam Cu–U–Au deposit, South Australia: A geochemical tracer and reconnaissance Pb–Pb geochronometer. *Precambrian Research* 238, 129-147.
CONOR C., RAYMOND O. L., BAKER T., TEALE G. S., SAY P. & LOWE G. 2010. *Alteration and Mineralisation in the Moonta-Wallaroo Copper-Gold Mining Field Region, Olympic Domain, South Australia.* (Hydrothermal Iron Oxide-Copper-Gold & Related Deposits: A Global Perspective, Vol. 3). PGC Publishing, Adelaide.
COTTLE J. 2014. In-situ U-Th/Pb geochronlogy of (urano)thorite. *American Mineralogist* 99, 1985-1995.
DALY S. J., FANNING C. M. & FAIRCLOUGH M. C. 1998. Tectonic evolution and exploration potential of the Gawler Craton, South Australia. *Journal of Australian Geology and Geophysics* 17, 145-168.
DIREEN N. G. & LYONS P. 2007. Regional Crustal Setting of Iron Oxide Cu-Au Mineral Systems of the Olympic Dam Region, South Australia: Insights from Potentional-Field Modeling. *Economic Geology* 102, 1397 - 1414.
DRUMMOND B., LYONS P., GOLEBY B. & JONES L. 2006. Constraining models of the tectonic setting of the giant Olympic Dam rion oxide-copper-gold deposits, South Australia, using deep seismis reflection data. *Tectonophysics* 420, 91-103.
DUPUIS C. & BEAUDOIN G. 2011. Discriminant diagrams for iron oxide trace element fingerprinting of mineral deposit types. *Mineralium Deposita* 46, 319-335.
DUTCH R., HAND M. & KINNY P. D. 2008. High-grade Paleoproterozoic reworking in the southeastern Gawler Craton, South Australia. *Australian Journal of Earth Sciences* 55, 1063-1081.
FERRIS G., SCHWARZ M. P. & HEITHERSAY P. 2002. *The Geological framework, Distribution and Controls of Fe-Oxide Cu-Au Mineralisation in the Gawler Craton, South Australia. Part 1 - Geological and Tectonic Framework* (Hydrothermal Iron Oxide-Copper-Gold & Related Deposits: A Global Perspective, Vol. 2). PGC Publishing, Adelaide.
GAGNON J., SAMSON I. M., FRYER B. J. & WILLIAMS-JONES A. E. 2003. Compositional heterogeneity in fluorite and the genesis of fluorite deposits: Insights from LA-ICP-MS Analysis. *The Canadian Mineralogist* 41, 356-382.
GILES C. 1988. Petrogenesis of the Proterozoic Gawler Range Volcanics, South Australia. *Precambrian Research* 40/41, 407-427.
HAND M., REID A. & JAGODZINKSKI E. 2007. Tectonic Framework and Evolution of the Gawler Craton, Southern Australia. *Economic Geology* 102, 1377 - 1395.
HAYNES D. W., CROSS K. C., BILLS R. T. & REED M. H. 1995. Olympic Dam Ore Genesis: A Fluid-Mixing Model. *Economic Geology* 90, 281-307.
HAYWARD N. & SKIRROW R. G. 2010. *Geodynamic Setting and Controls on Iron Oxide Cu-Au (±U) Ore in the Gawler Craton, South Australia* (Hydrothermal Iron Oxide-Copper-Gold & Related Deposits: A Global Perspective, Vol. 3). PGC Publishing, Adelaide.
HITZMAN M. W., ORESKES N. & EINAUDI M. T. 1992. Geological characteristics and tectonic setting of proterozoic iron oxide (Cu・U・Au・REE) deposits. *Precambrian Research* 58, 241-287.
HOU B., FABRIS A. J., MICHAELSEN B. H., KATONA L. F., KEELING J. L., STOIAN L., WILSON T. C., FAIRCLOUGH M. C. & COWLEY W. M. 2012. Paleodrainage and Cenozoic coastal barriers of South Australia: new map and GIS dataset. *MESA Journal* 66, 26-32.

ISMAIL R., CIOBANU C. L., COOK N. J., TEALE G. S., GILES D., MUMM A. S. & WADE B. 2014. Rare earths and other trace elements in minerals from skarn assemblages, Hillside iron oxide–copper–gold deposit, Yorke Peninsula, South Australia. *Lithos* 184–187, 456-477.
KENDRICK M. A., MARK G. & PHILLIPS D. 2007. Mid-crustal fluid mixing in a Proterozoic Fe oxide-Cu-Au deposit, Ernest Henry, Australia: Evidence from Ar, Kr, Xe, Cl, Br and I. *Earth and Planetary Science Letters* 256, 328-343.
KONTONIKAS-CHAROS A., CIOBANU C. L. & COOK N. J. 2014. Albitization and redistribution of REE and Y in IOCG systems: Insights from Moonta-Wallaroo, Yorke Peninsula, South Australia. *Lithos* 208–209, 178-201.
MARK G., OLIVER N. H. S. & WILLIAMS P. J. 2006. Mineralogical and chemical evolution of the Ernest Henry Fe oxide-Cu-Au ore system, Cloncurry district, northwest Queensland, Australia. *Mineralium Deposita* 40, 769-801.
MCAVANEY S. 2012. The Cooyerdoo Granite: Paleo- and Mesoachean basement of the Gawler Craton. *MESA Journal* 65, 31-40.
MCPHIE J., KAMENETSKY V., ALLEN S., EHRIG K., AGANGI A. & BATH A. 2011a. The fluorine link between a supergiant ore deposit and a silicic large igneous province. *Geology* 39, 1003 - 1006.
MCPHIE J., KAMENETSKY V., CHAMEFORT I., EHRIG K. & GREEN N. 2011b. Origin of the supergiant Olympic Dam Cu-U-Au-Ag deposit, South Australia: Was a sedimentary basin involved? *Geology* 39, 795-798.
ORESKES N. & EINAUDI M. T. 1992. Origin of Hydrothermal Fluids at Olympic Dam: Preliminary Results from Fluid Inclusions and Stable Isotopes. *Economic Geology* 87, 64-90.
PARKER A. J. & LEMON N. M. 1982. Reconstruction of the early Proterozoic stratigraphy of the Gawler Craton, South Australia. *Journal of the Geolocial Society of Australia: An Internation geosceicne Journal of the Geological Society of Australia* 29, 221-238.
REID A., FLINT R., MAAS R., HOWARD K. & BELOUSOVA E. 2009. Geochronological and isotopic constraints on Palaeoproterozoic skarn base metal mineralisation in the central Gawler Craton, South Australia. *Ore Geology Reviews* 36, 350-362.
REID A., SMITH R. N., BAKER T., JAGODZINKSKI E., SELBY D., GREGORY C. J. & SKIRROW R. G. 2013. Re-Os Dating of Molybdenite within Hematite breccias from the Vulcan Cu-Au Prospect, Olympic Cu-Au Province, South Australia. *Economic Geology* 108, 883-894.
SA U. 2014. *Annual Report*.
SKIRROW R. G., BASTRAKOV E. N., DAVIDSON G. J., RAYMOND O. L. & HEITHERSAY P. 2002. *The Geological Framewor, Distribution and Controls of Fe-Oxide Cu-Au Mineralisation in the Gawler Craton, South Australia. Part II - Alteration and Mineralisation* (Hydrothermal Iron Oxide-Copper-Gold & Related Deposits: A Global Perspective, Vol. 2). PGC Publishing, Adelaide.
SWAIN G., BAROVICH K., HAND M., FERRIS G. & SCHWARZ M. P. 2008. Petrogenesis of the St Peter Suite, southern Australia: Arc magmatism and Proterozoic crustal growth of the South Australian Craton. *Precambrian Research* 166, 283-296.
SWAIN G., WOODHOUSE A., HAND M., BAROVICH K., SCHWARZ M. & FANNING C. M. 2005. Provenance and tectonic development of the late Archaean Gawler Craton, Australia; U-Pb zircon geochemical and Sm-Nd isotopic implications. *Precambrian Research* 141, 103-136.
SZPUNAR M., HAND M., BAROVICH K., JAGODZINKSKI E. & BELOUSOVA E. 2011. Isotopic and geochemical constraints on the Paleoproterozoic Huthison Group, Southern Australia: Implications for paleoproterozoic continental reconstructions. *Precambrian Research* 187, 99-126.
WADE B., BAROVICH K., HAND M., SCIMGEOUS I. R. & CLOSE D. F. 2006. Evidence for Early Mesoproterozoic Arc Magmatism in the Musgrace Block, Central Australia: Implications for Proterozcoid Crustal Growth and Tectonic Reconstruction of Australia. *The Journal of geology* 114, 43-63.
WILLIAMS P. J., BARTON M. D., JOHNSON D. A., FONTBOTE L., DE HALLER A., MARK G., OLIVER N. H. S. & MARSHICK R. 2005. Iron Oxide Copper-Gold Deposits: Geology, Space-Time Distribution, and Possible Modes of Origin. *Economic Geology* 100th Anniversary Volume, 371-405.

APPENDIX A: LA-ICP-MS METHODOLOGY

LA-ICP-MS trace element spot analysis

Sample material consists of 1-inch polished blocks. Samples were investigated using optical and scanning electron microscopes prior to LA-ICP-MS analysis.

Trace element compositions of hematite and fluorite were determined using a Resonetics M-50-LR 193-nm Excimer laser microprobe coupled to an Agilent 7700cx Quadrupole ICP-MS housed at Adelaide Microscopy. The M-50 utilises a two-volume small volume ablation cell designed by Laurin Technic Pty (e.g., Müller et al., 2009). Ablation was performed in an atmosphere of UHP He (0.7 l/min), and upon exiting the cell the aerosol cell is mixed with Ar (0.93 l/min) immediately after the ablation cell, after which the mix is passed through a pulse-homogenizing device or “squid” prior to direct introduction into the torch. The ICPMS was optimized daily to maximize sensitivity on isotopes of the mass range of interest, while keeping production of molecular oxide species (i.e., $^{232}Th^{16}O/^{232}Th$) and doubly charged ion species (i.e., $^{140}Ce^{2+}/^{140}Ce^{+}$) as low as possible, and usually <0.2%. Beam diameter was set at 30 μm, with a repetition rate of 10 Hz and energy set to produce a fluence at the sample of ~8 Jcm^{-2}. Ablation was conducted using identical tune conditions to those mentioned in the mapping section below.

Data were collected using time-resolved data acquisition in fast peak-jumping mode, and calculations were carried out using the data reduction software GLITTER (Van Achterbergh et al., 2001). Total acquisition time per analysis was 80 seconds (s), with 30s background measurement followed by 50s of sample ablation. Calibration was performed against the NIST-601 and BHVO-2G standard glasses using the coefficients of Pearce et al. (1997). Batches of ten analyses were bracketed by repeat analyses of the external standard BHVO-2G, allowing monitoring of, and correction for, instrumental drift. A linear drift correction based on the analysis sequence and on the bracketing analyses of BHVO-2G, was applied to the count rate for each sample. ^{57}Fe and ^{43}Ca were used as the internal standards for hematite and fluorite, respectively, assuming end-member composition. Nadoll and Koenig (2011) reported that silicate glass standards can produce accurate results for trace element LA-ICP-MS analyses of Fe-oxides.

The following basic set of isotopes were monitored: ^{24}Mg, ^{27}Al, ^{29}Si, ^{31}P, ^{43}Ca, ^{45}Sc, ^{49}Ti, ^{51}V, ^{53}Cr, ^{55}Mn, ^{57}Fe, ^{58}Fe, ^{59}Co, ^{60}Ni, ^{65}Cu, ^{66}Zn, ^{69}Ga, ^{75}As, ^{89}Y, ^{90}Zr, ^{93}Nb, ^{95}Mo, ^{118}Sn, ^{121}Sb, $^{137}Ba$$^{139}La$, ^{140}Ce, ^{141}Pr, ^{146}Nd, ^{147}Sm, ^{153}Eu, ^{157}Gd, ^{159}Tb, ^{163}Dy, ^{165}Ho, ^{166}Er, ^{169}Tm, ^{172}Yb, ^{175}Lu, ^{181}Ta, ^{182}W, ^{206}Pb, ^{207}Pb, ^{208}Pb, ^{232}Th and ^{238}U.

LA-ICP-MS element mapping

LA-ICP-MS mapping of hematite was conducted using the same LA-ICP-MS system. Imaging was performed by ablating sets of parallel line rasters in a grid across the sample. A beam size of 24 μm and a scan speed of 15 μm/s were chosen which resulted in the desired sensitivity of elements of interest, and adequate spatial resolution for the study. The spacing between the lines was kept at a constant 24 μm to match the size of the laser beam used. The effect of redeposition during mapping was minimized by preablating each line prior to its main data collection run. A laser repetition of 10 Hz was selected at a constant energy output of 100 mJ, resulting in an energy density of ~6 J/cm2 at the target. Using these beam conditions depth of ablation during mapping was around 5-10 μm. A set of 21 elements were analyzed with dwell time for all masses set to 0.003 s, resulting in a total sweep time of ~0.03 s. A 20 second background acquisition was acquired at the start of every raster, and to allow for cell wash-out, gas stabilization, and computing processing, a delay of 20 s was used after each line. Identical rasters were done on reference glasses NIST-610 and BHVO-2G at the start and end of a mapping run.

Images were compiled and processed using the program Iolite developed by the Melbourne Isotope Group at Melbourne University (e.g., Woodhead et al., 2007). Iolite is an open source software package for processing ICP-MS data, and is an add-in for the data analysis program Igor developed by WaveMetrics. A typical mapping run was analyzed over a 6-7-hour session, in which significant instrument drift could occur. To correct for this, standards were analyzed immediately before and after the run to assess drift and if present, was corrected for by applying a linear fit between the two sets of standards. Following this, for each raster and every element, the average background was subtracted from its corresponding raster, and the rasters were compiled into a 2-D image displaying combined background/drift corrected intensity for each element.

U-Pb dating methodology

In situ U-Pb hematite, zircon, and thorite geochronology was undertaken via Laser Ablation Inductively Coupled Plasma Mass Spectrometry (LA-ICP-MS). U-Pb analyses were carried out on a Resonetics M-50 193nm Excimer laser attached to an Agilent 7700cs ICP-MS. Ablation was conducted in a helium atmosphere after which argon gas added immediately after the cell to aid transport of material. Iron oxide analysis was conducted with a spot size of 33 micron, zircon a spot size of 17 micron, and thorite at a reduced spot size of 10 micron and transmission of 25%, in order to limit the sensitivity of thorium at the mass spectrometer. A laser frequency of 10 Hz was used resulting in a fluence range of 5-8 J/cm^2 at the ablation site for iron oxide, zircon, and thorite. A single analytical spot consisted of a 30s gas blank followed by 30s of data acquisition with the laser firing. Measured isotopes were ^{204}Pb, ^{206}Pb, ^{207}Pb, ^{208}Pb, ^{232}Th, and ^{238}U with dwell times of 10, 30, 60, 20, 20, and 30 ms respectively for both iron oxide and zircon analysis, and 10, 15, 30, 10, 10, and 15ms for thorite analysis. Mass ^{204}Pb was measured as a monitor of common lead content, and due to the unresolvable isobaric interference of ^{204}Hg on ^{204}Pb common lead corrections were not conducted.

Age calculations and corrections for down-hole element fractionation for all three phases dated were corrected in the GLITTER software via the use of the external primary zircon standard GJ-1 (TIMS normalisation data ^{207}Pb/^{206}Pb = 608.3 Ma, ^{206}Pb/^{238}U = 600.7 Ma and ^{207}Pb/^{235}U = 602.2 Ma[S5]). An overestimated uncertainty of 1% was assigned to the TIMS derived normalisation age for GJ-1. Instrument drift was also corrected for in GLITTER via standard bracketing every 15-20 unknowns and application of a linear correction. Accuracy was verified by repeat analysis of the in-house Sri Lankan zircon standard (BJWP-1, ID-TIMS ^{206}Pb/^{238}U = 720.4 Ma). The compiled weighted average ^{206}Pb/^{238}U age for BJWP-1 were 717 ± 10 for (95% confidence; n=13).

Due to the unresolvable ^{204}Hg on ^{204}Pb interference, isotope ratios are presented uncorrected for common lead, with concordia plots generated using Isoplot/Ex 3.71 (Ludwig 2008).

REFERENCES

Ciobanu, C.L., Wade, B., Cook, N.J., Schmidt Mumm, A., Giles, D., 2013. Uranium-bearing hematite from the Olympic Dam Cu-U-Au deposit, South Australia; a geochemical tracer and reconnaissance Pb-Pb geochronometer. Precambrian Research 238, 129-147.
Jackson, S.E., Pearson, N.J., Grifin, W.L., Belousova, E.A., 2004. The application of laser ablation inductively coupled plasma-mass spectrometry to in-situ U-Pb zircon geochronology. Chemical Geology 211, 47-69.
Ludwig, K.R., 2008. A User's Manual for Isoplot 3.6: A Geochronological Toolkit for Microsoft Excel (revision of April 8, 2008). Berkeley Geochronology Center Special Publication No. 4, Berkeley, CA, 77 pp.
Müller, W., Shelley, M., Miller, P., Broude, S., 2009. Initial performance metrics of a new custom-designed ArF excimer LA-ICPMS system coupled to a two-volume laser-ablation cell. Journal of Analytical Atomic Spectrometry 24, 209-214
Nadoll, P., Koenig, A.E., 2011. LA-ICP-MS of magnetite: methods and reference materials. Journal of Analytical Atomic Spectrometry 26, 1872-1877.
Payne, J.L., Hand, M., Barovich, K.M., Wade, B.P., 2008. Temporal constraints on the timing of high-grade metamorphism in the northern Gawler Craton: implications for assembly of the Australian Proterozoic. Australian Journal of Earth Sciences 55, 623–640.
Pearce, N.J.G., Perkins, W.T., Wetgate, J.A., Gorton, M.P., Jackson, S.E., Neal, C.R., Chenery, S.P., 1997. A compilation of new and published data for NIST SRM 610 and NIST SRM 612 glass reference materials. Geostandards Newsletter 21, 115-144.
Van Achterbergh, E., Ryan, C.G., Jackson, S.E., Griffin, W.L., 2001. Data reduction software for LAICP-MS. In: Sylvester, J.P. (Ed.), Laser-ablation-ICPMS in the Earth Sciences; Principles and Applications. Mineralogical Association of Canada, Short Course Series 29, p. 239-243.
Woodhead, J.D., Hellstrom, J., Hergt, J.M., Greig, A., Maas, R., 2007. Isotopic and Elemental Imaging of Geological Materials by Laser Ablation Inductively Coupled Plasma-Mass Spectrometry. Geostandards and Geoanalytical Research 31, 331-343.

APPENDIX B1: U-PB DATING OF ZIRCON

Analysis_#	Grain	$^{207}Pb/^{206}Pb$	1σ	Isotope Ratios $^{206}Pb/^{238}U$	1σ	$^{207}Pb/^{235}U$	1σ	$^{208}Pb/^{232}Th$	1σ	Ages (Ma) $^{207}Pb/^{206}Pb$	1σ
Sample 751003											
751003 - 01	1	0.0829	0.0011	0.0765	0.0008	0.8739	0.0115	0.0076	0.0003	###	26
751003 - 02	1	0.0895	0.0019	0.0609	0.0006	0.7517	0.0142	0.0101	0.0007	###	39
751003 - 03	1	0.0833	0.0013	0.0520	0.0005	0.5972	0.0089	0.0060	0.0003	###	31
751003 - 04	1	0.0871	0.0015	0.0605	0.0008	0.7256	0.0127	0.0036	0.0002	###	33
751003 - 05	1	0.0912	0.0014	0.0456	0.0006	0.5729	0.0092	0.0059	0.0003	###	30
751003 - 06	2	0.0925	0.0035	0.0672	0.0012	0.8574	0.0304	0.0087	0.0006	###	70
751003 - 07	2	0.0913	0.0022	0.0940	0.0013	1.1822	0.0277	0.0059	0.0005	###	45
751003 - 08	2	0.0914	0.0030	0.0359	0.0006	0.4479	0.0140	0.0058	0.0005	###	61
751003 - 09	2	0.0874	0.0025	0.0412	0.0007	0.4934	0.0137	0.0022	0.0001	###	54
751003 - 10	3	0.1754	0.0042	0.1017	0.0014	2.4601	0.0526	0.0071	0.0004	###	40
751003 - 11	3	0.1745	0.0033	0.0533	0.0007	1.2787	0.0248	0.0018	0.0001	###	31
751003 - 12	3	0.1708	0.0037	0.0864	0.0013	2.0321	0.0444	0.0052	0.0004	###	36
751003 - 13	3	0.1685	0.0038	0.0587	0.0009	1.3598	0.0309	0.0023	0.0002	###	37
751003 - 14	4	0.1038	0.0028	0.0201	0.0003	0.2874	0.0075	0.0015	0.0001	###	48
751003 - 15	4	0.1279	0.0037	0.0221	0.0004	0.3897	0.0110	0.0041	0.0004	###	50
751003 - 16	4	0.1039	0.0034	0.0142	0.0003	0.2030	0.0064	0.0010	0.0001	###	59
751003 - 17	4	0.1093	0.0030	0.0161	0.0003	0.2429	0.0065	0.0014	0.0001	###	49
751003 - 18	4	0.1108	0.0034	0.0144	0.0002	0.2198	0.0066	0.0034	0.0004	###	55
751003 - 19	4	0.1027	0.0032	0.0172	0.0003	0.2433	0.0074	0.0026	0.0002	###	56
Sample 751002											
751002 - 01	1	0.1572	0.0025	0.0222	0.0003	0.4810	0.0077	0.0021	0.0001	###	27
751002 - 02	1	0.1478	0.0031	0.0202	0.0003	0.4107	0.0086	0.0021	0.0001	###	35
751002 - 03	1	0.1858	0.0031	0.0667	0.0008	1.7076	0.0278	0.0097	0.0005	###	27
751002 - 04	1	0.1998	0.0031	0.1275	0.0015	3.5108	0.0543	0.0207	0.0009	###	25
751002 - 05	1	0.2235	0.0032	0.2382	0.0026	7.3414	0.1003	0.0842	0.0031	###	22
751002 - 06	1	0.1644	0.0036	0.0438	0.0007	0.9917	0.0218	0.0041	0.0003	###	36
751002 - 07	1	0.1442	0.0028	0.0370	0.0005	0.7354	0.0142	0.0046	0.0003	###	33

751002 - 08	1	0.1316	0.0026	0.0387	0.0005	0.7021	0.0141	0.0033	0.0002	###	34
751002 - 09	1	0.1178	0.0027	0.0481	0.0007	0.7796	0.0180	0.0030	0.0002	###	41
751002 - 10	1	0.1264	0.0038	0.0302	0.0005	0.5265	0.0156	0.0094	0.0009	###	52
751002 - 11	1	0.1159	0.0027	0.0432	0.0006	0.6905	0.0160	0.0063	0.0005	###	41
751002 - 12	2	0.1322	0.0028	0.0203	0.0003	0.3708	0.0079	0.0011	0.0001	###	37
751002 - 13	2	0.1553	0.0048	0.0737	0.0013	1.5780	0.0480	0.0054	0.0005	###	52
751002 - 14	2	0.1416	0.0047	0.0208	0.0004	0.4059	0.0131	0.0019	0.0002	###	56
Sample 845007											
845007 - 01	1	0.1046	0.0020	0.1215	0.0015	1.7517	0.0339	0.0102	0.0006	###	35
845007 - 02	1	0.1080	0.0029	0.0994	0.0015	1.4788	0.0394	0.0090	0.0008	###	49
845007 - 03	1	0.1157	0.0026	0.2311	0.0028	3.6868	0.0778	0.0217	0.0016	###	39
845007 - 04	1	0.1085	0.0028	0.1034	0.0016	1.5453	0.0399	0.0078	0.0006	###	46
845007 - 05	1	0.1058	0.0025	0.1078	0.0016	1.5711	0.0374	0.0093	0.0007	###	43
845007 - 06	1	0.1035	0.0034	0.1092	0.0019	1.5572	0.0506	0.0030	0.0003	###	60
845007 - 07	2	0.1299	0.0037	0.0768	0.0012	1.3744	0.0389	0.0040	0.0004	###	49
845007 - 08	2	0.1309	0.0041	0.0605	0.0010	1.0921	0.0333	0.0051	0.0005	###	53
845007 - 09	3	0.1110	0.0030	0.0638	0.0010	0.9757	0.0264	0.0056	0.0005	###	48
845007 - 10	3	0.1062	0.0028	0.0445	0.0006	0.6511	0.0167	0.0049	0.0004	###	48
845007 - 11	3	0.0871	0.0025	0.1307	0.0021	1.5705	0.0455	0.0107	0.0010	###	55
845007 - 12	4	0.1123	0.0034	0.0822	0.0013	1.2726	0.0382	0.0076	0.0008	###	54

Appendix B2: U-Pb dating of thorite

Analysis_#				**Isotope Ratios**						**Ages (Ma)**	
	Grain	**^{207}Pb/^{206}Pb**	**1σ**	**^{206}Pb/^{238}U**	**1σ**	**^{207}Pb/^{235}U**	**1σ**	**^{208}Pb/^{232}Th**	**1σ**	**^{207}Pb/^{206}Pb**	**1σ**
Sample 751003											
751003 - 01	1	0.1527	0.0029	0.0621	0.0009	1.3067	0.0247	0.0023	0.0001	2376	32
751003 - 02	1	0.1440	0.0029	0.1139	0.0015	2.2637	0.0452	0.0047	0.0003	2276	34
751003 - 03	1	0.1496	0.0026	0.0619	0.0009	1.2769	0.0232	0.0024	0.0001	2342	30
751003 - 04	1	0.1507	0.0031	0.0537	0.0008	1.1157	0.0233	0.0018	0.0001	2354	35
751003 - 05	1	0.1456	0.0031	0.0509	0.0007	1.0213	0.0218	0.0016	0.0001	2295	36
751003 - 06	1	0.1438	0.0039	0.0486	0.0008	0.9630	0.0250	0.0014	0.0001	2273	46
751003 - 07	1	0.1361	0.0041	0.0567	0.0009	1.0639	0.0307	0.0013	0.0001	2178	52
751003 - 08	1	0.1409	0.0038	0.0592	0.0009	1.1510	0.0298	0.0018	0.0001	2238	46
751003 - 09	1	0.1404	0.0036	0.0667	0.0010	1.2915	0.0317	0.0018	0.0001	2232	44
751003 - 10	1	0.1524	0.0030	0.0491	0.0007	1.0311	0.0206	0.0015	0.0001	2373	33
751003 - 11	1	0.1504	0.0028	0.0562	0.0008	1.1649	0.0223	0.0018	0.0001	2350	32
751003 - 12	1	0.1483	0.0027	0.0730	0.0010	1.4918	0.0283	0.0027	0.0001	2327	31

751003 - 13	1	0.1456	0.0027	0.0739	0.0010	1.4829	0.0281	0.0025	0.0001	2295	31
751003 - 14	1	0.1528	0.0030	0.0596	0.0008	1.2559	0.0246	0.0021	0.0001	2377	33
751003 - 15	1	0.1485	0.0032	0.0742	0.0011	1.5193	0.0327	0.0025	0.0002	2329	36
751003 - 16	1	0.1502	0.0032	0.1438	0.0022	2.9777	0.0652	0.0009	0.0001	2348	36
751003 - 17	1	0.1406	0.0030	0.1052	0.0015	2.0402	0.0430	0.0009	0.0001	2235	36
751003 - 18	1	0.1438	0.0032	0.0851	0.0013	1.6863	0.0367	0.0007	0.0000	2273	37
751003 - 19	1	0.1450	0.0032	0.1468	0.0022	2.9345	0.0645	0.0012	0.0001	2288	37
751003 - 20	2	0.1829	0.0079	0.0206	0.0005	0.5188	0.0204	0.0003	0.0000	2679	69
751003 - 21	2	0.2189	0.0088	0.0170	0.0004	0.5120	0.0190	0.0007	0.0001	2973	64
751003 - 22	2	0.1858	0.0050	0.2318	0.0038	5.9370	0.1576	0.0078	0.0007	2705	44
751003 - 23	2	0.1867	0.0067	0.0356	0.0007	0.9157	0.0308	0.0016	0.0002	2713	58
751003 - 24	2	0.1794	0.0056	0.0232	0.0004	0.5741	0.0168	0.0007	0.0001	2648	51
751003 - 25	2	0.1725	0.0052	0.0315	0.0006	0.7497	0.0214	0.0008	0.0001	2582	49
751003 - 26	2	0.1626	0.0073	0.0256	0.0006	0.5734	0.0236	0.0001	0.0000	2483	74
751003 - 27	2	0.1675	0.0047	0.1037	0.0017	2.3943	0.0662	0.0025	0.0002	2533	46
Sample 751002											
751002 - 01	1	0.1551	0.0055	0.0138	0.0003	0.2950	0.0099	0.0006	0.0000	2403	59
751002 - 02	1	0.1749	0.0047	0.2075	0.0037	5.0025	0.1323	0.0083	0.0005	2605	44
751002 - 03	1	0.1729	0.0052	0.0422	0.0008	1.0055	0.0290	0.0011	0.0001	2586	49
751002 - 04	1	0.1036	0.0030	0.0456	0.0008	0.6514	0.0186	0.0005	0.0000	1690	53
751002 - 05	1	0.1606	0.0032	0.0827	0.0011	1.8300	0.0361	0.0014	0.0001	2462	33
751002 - 06	1	0.1244	0.0035	0.0258	0.0004	0.4426	0.0120	0.0004	0.0000	2020	49
751002 - 07	1	0.1297	0.0029	0.0302	0.0005	0.5394	0.0118	0.0007	0.0000	2094	38
751002 - 08	1	0.1303	0.0026	0.0368	0.0005	0.6611	0.0132	0.0006	0.0000	2102	34
751002 - 09	1	0.1001	0.0022	0.0462	0.0007	0.6373	0.0139	0.0006	0.0000	1626	40
751002 - 10	1	0.1814	0.0049	0.0887	0.0015	2.2176	0.0567	0.0043	0.0003	2666	44
751002 - 11	1	0.1412	0.0032	0.0416	0.0006	0.8109	0.0185	0.0008	0.0001	2242	39
751002 - 12	1	0.1228	0.0027	0.0404	0.0006	0.6843	0.0147	0.0008	0.0000	1997	38
751002 - 13	1	0.1136	0.0033	0.0419	0.0007	0.6569	0.0185	0.0006	0.0001	1858	51
751002 - 14	1	0.1137	0.0030	0.0361	0.0006	0.5657	0.0148	0.0007	0.0001	1860	47
751002 - 15	1	0.1192	0.0031	0.0287	0.0005	0.4716	0.0120	0.0006	0.0000	1945	45
751002 - 16	1	0.1552	0.0053	0.0351	0.0007	0.7501	0.0243	0.0005	0.0000	2404	57
751002 - 17	1	0.1583	0.0045	0.0187	0.0003	0.4085	0.0111	0.0005	0.0000	2438	47
751002 - 18	1	0.1300	0.0038	0.0387	0.0007	0.6936	0.0199	0.0006	0.0000	2098	51
751002 - 19	1	0.1012	0.0026	0.0622	0.0010	0.8676	0.0225	0.0009	0.0001	1646	48
751002 - 20	1	0.1139	0.0028	0.0479	0.0008	0.7516	0.0183	0.0006	0.0000	1862	43
751002 - 21	1	0.1021	0.0033	0.0493	0.0009	0.6944	0.0218	0.0003	0.0000	1663	58
751002 - 22	1	0.1355	0.0038	0.0153	0.0003	0.2866	0.0079	0.0005	0.0000	2171	49
751002 - 23	1	0.1447	0.0048	0.0133	0.0003	0.2646	0.0083	0.0002	0.0000	2284	56
751002 - 24	2	0.1583	0.0045	0.0273	0.0005	0.5956	0.0163	0.0008	0.0001	2438	47
751002 - 25	2	0.1302	0.0048	0.0165	0.0003	0.2966	0.0104	0.0002	0.0000	2101	64
751002 - 26	2	0.1267	0.0048	0.0158	0.0003	0.2768	0.0099	0.0003	0.0000	2053	66
751002 - 27	2	0.1345	0.0044	0.0239	0.0004	0.4430	0.0139	0.0005	0.0000	2157	56
751002 - 28	2	0.1421	0.0050	0.0171	0.0003	0.3354	0.0111	0.0003	0.0000	2254	59
751002 - 29	2	0.1582	0.0067	0.0105	0.0002	0.2296	0.0090	0.0002	0.0000	2437	70
751002 - 30	2	0.1506	0.0062	0.0135	0.0003	0.2810	0.0108	0.0002	0.0000	2352	68
751002 - 31	2	0.1250	0.0041	0.0229	0.0004	0.3951	0.0124	0.0003	0.0000	2029	57
751002 - 32	2	0.1064	0.0031	0.0341	0.0006	0.5005	0.0141	0.0007	0.0001	1739	52
751002 - 33	2	0.1742	0.0066	0.0078	0.0002	0.1883	0.0067	0.0004	0.0000	2598	62
751002 - 34	2	0.1530	0.0049	0.0091	0.0002	0.1914	0.0059	0.0003	0.0000	2380	54
751002 - 35	2	0.1671	0.0080	0.0124	0.0003	0.2853	0.0126	0.0004	0.0000	2529	79
751002 - 36	2	0.1718	0.0057	0.0076	0.0002	0.1787	0.0055	0.0003	0.0000	2575	54
751002 - 37	2	0.1553	0.0051	0.0127	0.0002	0.2712	0.0084	0.0005	0.0000	2405	54
751002 - 38	2	0.1403	0.0052	0.0108	0.0002	0.2091	0.0074	0.0003	0.0000	2231	63
751002 - 39	2	0.1204	0.0048	0.0225	0.0005	0.3744	0.0143	0.0004	0.0000	1963	70
751002 - 40	2	0.1615	0.0064	0.0138	0.0003	0.3061	0.0113	0.0003	0.0000	2471	65
751002 - 41	2	0.1696	0.0074	0.0294	0.0007	0.6880	0.0280	0.0015	0.0002	2554	71
751002 - 42	2	0.1949	0.0067	0.0466	0.0009	1.2512	0.0405	0.0017	0.0002	2784	55

Analysis_#	Ages (Ma) $^{206}Pb/^{238}U$	1σ	$^{207}Pb/^{235}U$	1σ	Ages (Ma) $^{208}Pb/^{232}Th$	1σ	^{204}Pb	^{206}Pb	Background subtracted CPS ^{207}Pb	^{208}Pb	^{232}Th	^{238}U
Sample 751003												
751003 - 01	388	5	849	11	45	2	172	28608	4319	98724	4.1E+07	556226
751003 - 02	696	9	1201	14	95	5	173	44190	6255	2E+05	3.2E+07	447919
751003 - 03	387	5	836	10	48	2	140	31483	4701	1E+05	4.4E+07	630566
751003 - 04	337	5	761	11	36	2	133	28315	4251	97519	5.2E+07	664183
751003 - 05	320	5	715	11	31	2	102	22852	3304	84441	5.1E+07	549788
751003 - 06	306	5	685	13	28	2	56	16297	2289	63874	4.1E+07	380483
751003 - 07	355	6	736	15	26	2	62	18819	2517	67527	4.6E+07	384132
751003 - 08	371	6	778	14	37	3	81	18843	2596	64267	3.2E+07	359721
751003 - 09	416	6	842	14	37	3	103	22960	3159	77157	3.7E+07	391393
751003 - 10	309	4	720	10	29	1	122	22910	3487	77695	4.8E+07	584696
751003 - 11	352	5	784	10	36	2	137	26348	3951	88023	4.4E+07	581013
751003 - 12	454	6	927	12	53	3	179	34345	5087	1E+05	4.2E+07	585884
751003 - 13	459	6	923	12	50	3	166	33497	4863	1E+05	4.3E+07	561910
751003 - 14	373	5	826	11	43	2	146	27543	4175	93050	4.2E+07	567699
751003 - 15	461	7	938	13	51	3	182	35450	5277	1E+05	4.6E+07	616241
751003 - 16	866	12	1402	17	17	1	220	35410	5328	84092	8.9E+07	318743
751003 - 17	645	9	1129	14	18	1	98	20761	2901	68547	7.4E+07	238781
751003 - 18	526	7	1003	14	14	1	73	14802	2121	53583	7.4E+07	215531
751003 - 19	883	12	1391	17	24	1	176	31952	4628	96941	7.4E+07	278444
751003 - 20	131	3	424	14	5	0	85	11008	2227	31902	5.2E+07	764339
751003 - 21	109	2	420	13	15	1	97	11503	2540	35736	4.5E+07	938515
751003 - 22	1344	20	1967	23	157	14	247	33805	6268	66643	8695793	187577
751003 - 23	225	4	660	16	33	3	58	10973	2045	31368	2E+07	393168
751003 - 24	148	3	461	11	14	1	69	9833	1754	24121	3.6E+07	532353
751003 - 25	200	3	568	12	16	1	86	12286	2104	27261	3.5E+07	487920
751003 - 26	163	4	460	15	3	0	147	14752	2859	25744	5.2E+07	831804
751003 - 27	636	10	1241	20	51	5	236	51378	8530	81753	3.1E+07	658238
Sample 751002												

751002 - 01	88	2	263	8	12	1	89	12813	1981	27591	4.9E+07	1251457
751002 - 02	1216	20	1820	22	168	11	136	20254	3536	40726	4435263	131622
751002 - 03	266	5	707	15	23	2	123	20170	3463	38743	3.6E+07	631970
751002 - 04	288	5	509	11	11	1	64	20213	2080	34437	6.5E+07	580718
751002 - 05	512	7	1056	13	29	2	196	39064	6218	61174	4.1E+07	568823
751002 - 06	164	3	372	8	9	1	48	12889	1593	24319	5.3E+07	604796
751002 - 07	192	3	438	8	14	1	72	19496	2520	39431	5.6E+07	807473
751002 - 08	233	3	515	8	13	1	81	20328	2651	38571	5.6E+07	692867
751002 - 09	291	4	501	9	12	1	38	23114	2316	39896	6.2E+07	636971
751002 - 10	548	9	1187	18	87	6	58	12026	2179	24739	5765036	168412
751002 - 11	263	4	603	10	16	1	147	27510	3869	49218	6.4E+07	855775
751002 - 12	256	4	529	9	15	1	72	18490	2264	35234	4.6E+07	549088
751002 - 13	265	4	513	11	13	1	87	25166	2838	46600	7.3E+07	801515
751002 - 14	229	4	455	10	15	1	96	23637	2690	49567	6.8E+07	859592
751002 - 15	182	3	392	8	11	1	71	18681	2224	37330	6.8E+07	846219
751002 - 16	222	4	568	14	9	1	108	11834	1867	20814	3.9E+07	461433
751002 - 17	120	2	348	8	10	1	49	9135	1457	17239	3.2E+07	641749
751002 - 18	245	4	535	12	11	1	114	24861	3303	49600	7.4E+07	880665
751002 - 19	389	6	634	12	18	1	75	31382	3178	59170	6.7E+07	656977
751002 - 20	301	5	569	11	11	1	79	25737	2952	41740	7.1E+07	710388
751002 - 21	310	6	536	13	7	0	97	28354	3129	52807	7.5E+07	811251
751002 - 22	98	2	256	6	10	1	84	15769	2155	33644	6.2E+07	1374480
751002 - 23	85	2	238	7	4	0	47	8602	1255	12224	6.8E+07	859387
751002 - 24	174	3	474	10	16	1	86	16029	2541	25924	3.4E+07	736632
751002 - 25	106	2	264	8	4	0	42	8958	1169	16026	7.5E+07	721382
751002 - 26	101	2	248	8	6	0	25	7801	989	14664	5.6E+07	617404
751002 - 27	152	3	372	10	9	1	51	13943	1878	27854	6.5E+07	762953
751002 - 28	109	2	294	8	6	0	39	9410	1344	17587	6.4E+07	725728
751002 - 29	68	2	210	7	4	0	17	6906	1095	10295	5.1E+07	875591
751002 - 30	87	2	251	9	4	0	51	11814	1873	20732	6.4E+07	1223052
751002 -	146	3	338	9	7	1	56	11677	1476	21634	6.4E+07	672965

31												
751002 - 32	216	3	412	10	14	1	63	18457	1966	35701	5.3E+07	673546
751002 - 33	50	1	175	6	8	1	79	10525	1891	24265	5.5E+07	1849133
751002 - 34	58	1	178	5	6	0	40	8827	1373	19390	5.7E+07	1296190
751002 - 35	79	2	255	10	7	1	54	5692	981	10920	2.7E+07	634160
751002 - 36	49	1	167	5	6	1	53	7031	1224	13424	4.3E+07	1215835
751002 - 37	81	2	244	7	9	1	80	10412	1635	22883	5E+07	1081543
751002 - 38	69	1	193	6	6	1	43	8543	1215	15294	4.9E+07	1056299
751002 - 39	144	3	323	11	8	1	52	16207	2055	32989	6E+07	1002522
751002 - 40	88	2	271	9	5	0	30	7880	1322	14260	4E+07	789931
751002 - 41	187	4	532	17	30	3	63	9668	1688	20306	1.3E+07	448526
751002 - 42	293	6	824	18	33	3	86	9669	1910	20653	1.1E+07	281007

APPENDIX B3: U-PB DATING OF HEMATITE

Analysis_#	Isotope Ratios								Ages (Ma)			
	$^{207}Pb/^{206}Pb$	1σ	$^{206}Pb/^{238}U$	1σ	$^{207}Pb/^{235}U$	1σ	$^{208}Pb/^{232}Th$	1σ	$^{207}Pb/^{206}Pb$	1σ	$^{206}Pb/^{238}U$	1σ
Sample 751003 and 751008												
751003 Early -01	0.2606	0.0055	0.6677	0.0102	23.9828	0.4742	1.1821	0.0503	3250	33	3297	40
751003 Early -02	0.1489	0.0023	1.8855	0.0233	38.7180	0.6003	5.6875	0.2143	2334	26	6831	52
751003 Early -03	0.3665	0.0104	0.7371	0.0164	37.2468	0.9369	3.7498	0.2086	3777	42	3560	61
751003 Early -04	0.3977	0.0128	0.9912	0.0262	54.3422	1.5747	22.2175	3.6475	3900	48	4440	85
751003 Early -05	0.5065	0.0065	1.7401	0.0198	121.5090	1.5572	16.2836	0.5122	4260	19	6498	47
751003 Early -06	0.1970	0.0063	1.2641	0.0275	34.3424	1.0541	17.8220	2.0551	2801	51	5268	78
751003 Early -07	0.1818	0.0025	5.0322	0.0652	126.1456	1.8892	59.2621	3.1831	2670	23	-	70
751003 Late - 01	0.2313	0.0062	0.3609	0.0067	11.5081	0.2854	0.1947	0.0086	3061	43	1986	32
751003 Late - 02	0.2221	0.0042	0.3795	0.0056	11.6206	0.2124	0.2286	0.0074	2996	30	2074	26
751003 Late - 03	0.2136	0.0033	0.4026	0.0049	11.8543	0.1734	0.2791	0.0063	2933	25	2181	23
751003 Late - 04	0.2495	0.0044	0.4950	0.0065	17.0296	0.2742	0.3290	0.0091	3182	27	2592	28
751003 Late - 05	0.2296	0.0044	0.4376	0.0064	13.8539	0.2501	0.2167	0.0058	3050	30	2340	29
751003 Late - 06	0.2437	0.0049	0.5119	0.0075	17.1995	0.3157	0.4272	0.0129	3144	32	2665	32
751003 Late - 07	0.2511	0.0042	0.3217	0.0042	11.1375	0.1733	0.2612	0.0064	3192	26	1798	20
751003 Late - 08	0.2860	0.0060	0.2518	0.0038	9.9305	0.1828	0.2675	0.0077	3396	32	1448	20
751003 Late - 09	0.2763	0.0085	0.2315	0.0048	8.8194	0.2348	0.3278	0.0135	3342	47	1343	25
751003 Late - 10	0.2068	0.0030	0.4310	0.0052	12.2900	0.1734	0.1675	0.0038	2881	23	2310	23
751003 Late - 11	0.2644	0.0056	0.4421	0.0070	16.1170	0.3296	0.3179	0.0153	3273	33	2360	31
751003 Late - 12	0.2676	0.0116	0.6094	0.0182	22.4908	0.8567	0.6330	0.0337	3292	66	3068	73
751003 Late - 13	0.2096	0.0027	0.3721	0.0042	10.7525	0.1374	0.2094	0.0049	2902	21	2039	20
751003 Late - 14	0.2135	0.0038	0.4310	0.0058	12.6859	0.2101	0.3006	0.0077	2932	28	2310	26
751003 Late - 15	0.2448	0.0031	0.2875	0.0033	9.7031	0.1273	0.2960	0.0082	3151	20	1629	16
751008 Early - 01	0.4078	0.0058	2.2256	0.0309	125.1315	1.8330	0.2582	0.0055	3938	21	7550	62
751008 Early - 02	0.3398	0.0121	0.9062	0.0245	42.4470	1.3635	0.1066	0.0060	3662	53	4159	83
751008 Early - 03	0.3465	0.0103	0.6292	0.0138	30.0619	0.8445	0.1861	0.0107	3692	45	3147	54
751008 Early - 04	0.3456	0.0083	0.7623	0.0141	36.3204	0.7809	0.1228	0.0045	3688	36	3653	52
751008 Early - 05	0.2975	0.0041	0.5707	0.0071	23.4066	0.3346	0.3316	0.0097	3457	21	2911	29
751008 Early - 06	0.3618	0.0122	1.1050	0.0295	55.1177	1.7244	2.1809	0.1533	3757	50	4798	90
751008 Early - 07	0.4518	0.0054	0.9922	0.0112	61.8126	0.7429	0.9193	0.0198	4091	18	4443	36
751008 Late - 01	0.5829	0.0338	0.4109	0.0193	33.0264	1.4462	0.5682	0.0333	4466	82	2219	88
751008 Late - 02	0.6269	0.0627	0.5880	0.0491	50.8366	3.9312	0.7461	0.0574	4572	138	2981	199
751008 Late - 03	0.5940	0.1465	1.5830	0.3599	129.6558	30.8760	2.8210	1.0970	4494	318	6117	898
751008 Late - 04	0.5620	0.0371	1.2704	0.0757	98.4554	5.6899	0.8661	0.0694	4413	93	5286	215
751008 Late - 05	0.3056	0.0397	0.4930	0.0397	20.7703	2.3379	0.3435	0.0417	3499	187	2584	171
751008 Late - 06	0.3312	0.0123	1.3543	0.0401	61.8500	2.1537	1.1528	0.0670	3623	56	5520	110
751008 Late - 07	0.4031	0.0109	0.9458	0.0208	52.5762	1.3035	1.0332	0.0497	3921	40	4291	69
751008 Late - 08	1.1018	0.2821	1.3814	0.3755	209.8560	47.6182	10.4197	12.1575	5373	317	5594	1016
751008 Late - 09	0.3721	0.0246	0.6835	0.0337	35.0711	1.9719	0.7209	0.0569	3800	96	3358	129
751008 Late - 10	0.3118	0.0080	0.7824	0.0154	33.6348	0.7884	0.7439	0.0303	3530	39	3726	56
751008 Late - 11	0.3472	0.0259	0.7062	0.0382	33.8162	2.1619	0.7017	0.0610	3695	109	3444	144
751008 Late - 12	0.3843	0.0169	2.1329	0.0841	113.0419	4.9046	1.4091	0.1036	3849	65	7362	173
751008 Late - 13	0.3325	0.0078	0.8077	0.0150	37.0328	0.7924	0.7581	0.0262	3629	36	3817	53
751008 Late - 14	0.5964	0.1475	0.4994	0.0942	41.0644	7.6486	226.5373	-	4499	319	2611	405
751008 Late - 15	0.2551	0.0161	0.9762	0.0418	34.3276	1.9709	0.2968	0.0185	3216	96	4391	136

Analysis_#	Ages (Ma)		Background subtracted CPS							
	$^{208}Pb/^{232}Th$	1σ	^{204}Pb	^{206}Pb	^{207}Pb	^{208}Pb	^{232}Th	^{238}U	204/206	Notes
Sample 751003 and 751008										
751003 Early -01	-	466	77	9484	2473	12761	7926	14756	0.01	Included for age
751003 Early -02	-	648	113	64925	9762	52207	6738	38085	0.00	Very reversely d
751003 Early -03	-	888	31	969	355	1055	207	1385	0.03	High comm Pb
751003 Early -04	-	3175	33	1056	422	1030	33	1170	0.03	High comm Pb
751003 Early -05	-	599	860	30691	15532	42695	1919	18208	0.03	High comm Pb
751003 Early -06	-	2207	7	7728	1533	6032	246	7082	0.00	Very reversely d
751003 Early -07	-	1068	90	17948	3271	15893	197	3799	0.01	Missed grain
751003 Late - 01	3596	146	120	10505	2483	9148	34233	34699	0.01	Included for age
751003 Late - 02	4161	121	173	15702	3547	12962	40660	48691	0.01	Included for age
751003 Late - 03	4975	99	110	8916	1903	7301	19090	22779	0.01	Included for age
751003 Late - 04	5749	138	106	7678	1905	6958	15498	15483	0.01	Included for age
751003 Late - 05	3964	96	69	6135	1424	5526	18438	15470	0.01	Included for age
751003 Late - 06	7190	183	65	5104	1236	4589	7867	9945	0.01	Included for age
751003 Late - 07	4691	102	99	5878	1475	4851	13606	18847	0.02	High comm Pb
751003 Late - 08	4791	122	42	3082	880	2541	6977	12464	0.01	Included for age
751003 Late - 09	5731	205	31	2445	681	1953	4313	11329	0.01	Included for age
751003 Late - 10	3131	65	121	10859	2251	9566	41760	26501	0.01	Included for age
751003 Late - 11	5579	234	332	23925	6450	19348	45247	65903	0.01	Included for age
751003 Late - 12	9913	417	12	1250	339	1159	1340	2284	0.01	Included for age
751003 Late - 13	3844	81	269	26523	5570	21313	74694	74941	0.01	Included for age
751003 Late - 14	5312	120	42	5075	1086	4050	9901	12432	0.01	Included for age
751003 Late - 15	5241	128	940	74388	18324	53942	132404	281575	0.01	Included for age
751008 Early - 01	4642	88	163	6763	2774	7429	23557	3160	0.02	High comm Pb
751008 Early - 02	2047	110	123	5732	1990	6080	47739	7481	0.02	High comm Pb
751008 Early - 03	3450	183	535	31700	12257	31305	78271	74059	0.02	High comm Pb
751008 Early - 04	2341	80	115	4102	1428	4314	27215	5239	0.03	High comm Pb
751008 Early - 05	5788	148	690	40077	11965	45240	115392	80142	0.02	High comm Pb
751008 Early - 06	-	974	118	7145	2672	6118	1981	8697	0.02	High comm Pb
751008 Early - 07	-	209	617	26793	12181	29991	26522	28298	0.02	High comm Pb
751008 Late - 01	9094	429	7	210	123	305	431	518	0.03	Low Uranium
751008 Late - 02	-	665	64	254	160	928	1061	483	0.25	Low Uranium
751008 Late - 03	-	5803	13	16	9	31	9	11	0.81	Low Uranium
751008 Late - 04	-	751	20	369	211	496	443	351	0.05	Low Uranium
751008 Late - 05	5968	628	29	65	20	51	121	139	0.45	Low Uranium
751008 Late - 06	-	629	65	2597	854	2947	2178	2058	0.03	High comm Pb
751008 Late - 07	-	494	106	3972	1616	4410	3622	4935	0.03	High comm Pb
751008 Late - 08	-	-	10	12	13	25	1	9	0.83	Low Uranium
751008 Late - 09	-	668	10	363	135	363	414	577	0.03	Low Uranium
751008 Late - 10	-	351	69	2696	844	2462	2692	3706	0.03	High comm Pb
751008 Late - 11	-	725	13	360	126	353	432	585	0.04	Low Uranium
751008 Late - 12	-	869	54	1674	653	1720	1047	954	0.03	Low Uranium
751008 Late - 13	-	301	42	1645	550	1586	1676	2157	0.03	High comm Pb
751008 Late - 14	-	-	0	17	10	16	0	36	0.00	Low Uranium
751008 Late - 15	5253	288	14	244	62	191	516	265	0.06	Low Uranium